

AD A 069385

DDC FILE COPY

RADC-TR-79-70
Final Technical Report
April 1979

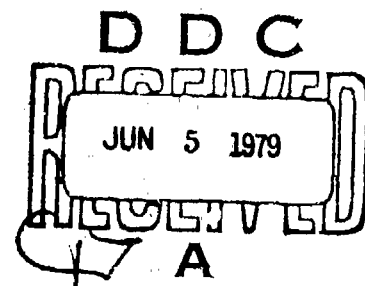
12
LEVEL



BISTATIC CLUTTER ANALYSIS

Decision-Science Applications, Inc.

Sponsored by
Defense Advanced Research Projects Agency (DoD)
ARPA Order No. 3071



APPROVED FOR PUBLIC RELEASE; DISTRIBUTION UNLIMITED

The views and conclusions contained in this document are those of the authors and should not be interpreted as necessarily representing the official policies, either expressed or implied, of the Defense Advanced Research Projects Agency or the U.S. Government.

ROME AIR DEVELOPMENT CENTER
Air Force Systems Command
Griffiss Air Force Base, New York 13441

79 06 01 006

This report has been reviewed by the RADC Information Office (OI) and is releasable to the National Technical Information Service (NTIS). At NTIS it will be releasable to the general public, including foreign nations.

RADC-TR-79-70 has been reviewed and is approved for publication.

APPROVED:

Robert G. Polce

ROBERT G. POLCE
Project Engineer

Exemption For	
GPO: 1979-0-281-101	
Unannounced Distribution	
By	
Distribution/	
Availability Codes	
Dist	Avail and/or special
A-	

If your address has changed or if you wish to be removed from the RADC mailing list, or if the addressee is no longer employed by your organization, please notify RADC (OCSA) Griffiss AFB NY 13441. This will assist us in maintaining a current mailing list.

Do not return this copy. Retain or destroy.

BISTATIC CLUTTER ANALYSIS

R. E. Vander Schuur
P. G. Tomlinson

Contractor: Decision-Science Applications, Inc.
Contract Number: F30602-77-C-0198
Effective Date of Contract: 5 September 1977
Contract Expiration Date: 31 May 1979
Short Title of Work: Bistatic Clutter Analysis
Program Code Number: 7E20
Period of Work Covered: Sep 1977 - Dec 1978

Principal Investigator: R. E. Vander Schuur
Phone: 703 243-2500

Project Enigneer: Robert G. Polce
Phone: 315 330-2814

Approved for public release; distribution unlimited.

This research was supported by the Defense Advanced Research Projects Agency of the Department of Defense and was monitored by Robert G. Polce (OCSA) Griffiss AFB NY 13441 under Contract F30602-77-C-0198.

UNCLASSIFIED

SECURITY CLASSIFICATION OF THIS PAGE (When Data Entered)

REPORT DOCUMENTATION PAGE		READ INSTRUCTIONS BEFORE COMPLETING FORM
1. REPORT NUMBER RADCTR-79-70	2. GOVT ACCESSION NO.	3. RECIPIENT'S CATALOG NUMBER
4. TITLE (and Subtitle) BISTATIC CLUTTER ANALYSIS.		5. TYPE OF REPORT & PERIOD COVERED Final Technical Report. 30 Sep 77 - 30 Nov 78
		6. PERFORMING ORG. REPORT NUMBER DSA-1067
7. AUTHOR(s) R. E. Vander Schuur P. G. Tomlinson		8. CONTRACT OR GRANT NUMBER(s) F30602-77-C-0198
9. PERFORMING ORGANIZATION NAME AND ADDRESS Decision-Science Applications, Inc. 1500 Wilson Blvd, Suite 810 Arlington VA, 22209		10. PROGRAM ELEMENT, PROJECT, TASK AREA & WORK UNIT NUMBERS 62301E C0710105
11. CONTROLLING OFFICE NAME AND ADDRESS Defense Advanced Research Projects Agency 1400 Wilson Blvd Arlington VA 22209		12. REPORT DATE April 1979
14. MONITORING AGENCY NAME & ADDRESS (if different from Controlling Office) Rome Air Development Center (OCSA) Griffiss AFB NY 13441		13. NUMBER OF PAGES 99
		15. SECURITY CLASS. (of this report) UNCLASSIFIED
		15a. DECLASSIFICATION/DOWNGRADING SCHEDULE N/A
16. DISTRIBUTION STATEMENT (of this Report) Approved for public release; distribution unlimited.		
17. DISTRIBUTION STATEMENT (of the abstract entered in Block 20, if different from Report) Same		
18. SUPPLEMENTARY NOTES RADC Project Engineer: Robert G. Polce (OCSA)		
19. KEY WORDS (Continue on reverse side if necessary and identify by block number) Bistatic Radar Bistatic Clutter		
20. ABSTRACT (Continue on reverse side if necessary and identify by block number) This report describes the analysis performed by Decision-Science Applications, Inc., (DSA) on bistatic clutter data collected by the Environmental Research Institute of Michigan (ERIM) during early 1978. This data consisted of measurements of bistatic radar cross section per unit (σ) of the terrain at two Michigan sites, using an airborne transmitter and a tower-mounted receiver. Reflectivity was measured (simultaneously) at L- and X-band, at both horizontal-horizontal (HH) and horizontal-vertical (HV) polarizations. The measurement objective was to obtain X- and L-band ground-clutter statistics (Cont'd)		

DD FORM 1 JAN 73 1473

UNCLASSIFIED

SECURITY CLASSIFICATION OF THIS PAGE (When Data Entered)

UNCLASSIFIED

SECURITY CLASSIFICATION OF THIS PAGE(When Data Entered)

Item 20 (Cont'd)

for large bistatic angles and out-of-plane geometries.

DSA received this calibrated bistatic data from ERIM in the form of calibrated magnetic tape recordings and analog plots; the data was extensively analyzed for internal consistency and correlated against other relevant and related data and theoretical models. This report presents the results and conclusions of these analyses. DSA found that the levels and trends exhibited by this data were quite different from previous data and models.

UNCLASSIFIED

SECURITY CLASSIFICATION OF THIS PAGE(When Data Entered)

CONTENTS

<u>SECTION</u>		<u>PAGE</u>
1.0	INTRODUCTION AND SUMMARY	7
2.0	BACKGROUND	8
3.0	DATA REDUCTION	19
3.1	Preprocessing Data Evaluation and Smoothing	19
3.2	Definition of σ_0 and Associated Parameters	20
3.3	Ensemble Statistics of a Set of Scattering Elements; Parameter Variation	24
3.4	Double-Valued Calibration Curve	39
3.5	Illumination Correction	45
3.6	Numerical Discrepancies	47
3.7	Noise Spikes	47
4.0	MOST RECENT ERIM DATA	53
4.1	Descriptions of Terrain, Weather Conditions, and Bistatic Geometry	53
4.2	Models of σ_0 Derived from Relevant Monostatic and Bistatic Data	53
4.3	Comparing the Data with Existing Models	62
4.4	Conclusions	80
<u>APPENDIX</u>		
A	TEST EQUIPMENT PARAMETERS	A-1
B	DATA OF 17 MARCH AND 18 MARCH PROCESSED BY DSA	B-1

LIST OF FIGURES

FIGURE		PAGE
2-1	Comparison of Clutter Model to ERIM L-Band Principal Polarization σ_0 Data Collected at Tall Vegetation Site	10
2-2	Basic Bistatic Geometry	12
2-3	L-Band Bistatic σ_0 Statistics. Second part of Pass 4, Site 2, HH Polarization, $0^\circ \phi_R$ 14° , compared to mono-static X-band σ_0 statistics collected over rural terrain with a 15° antenna depression angle.	13
2-4	L-Band Principal Polarization (HH) Bistatic σ_0 Data of 17 July 1976 (All Passes)	14
2-5	Comparison of ERIM and OSU Data	17
3-1	3-cm Wavelength Histograms, ERIM SAR Data (Ohio farmland, 10-ft resolution, single look)	25
3-2	Width of 95% Confidence Interval vs. Number of Samples	27
3-3	A_{gd} for SCAN = TRACK = 90° ($\phi_S = 0^\circ$)	31
3-4	A_{gd} for SCAN = TRACK = 120° ($\phi_S = 0^\circ$)	32
3-5	A_{gd} for SCAN = TRACK = 150° ($\phi_S = 0^\circ$)	33
3-6	A_{gd} for SCAN = TRACK = 60° ($\phi_S = 0^\circ$)	34
3-7	A_{gd} for SCAN = 90° , TRACK = 60° ($\phi_S = 30^\circ$)	35
3-8	A_{gd} for SCAN = 120° , TRACK = 60° ($\phi_S = 60^\circ$)	36
3-9	A_{gd} for SCAN = 60° (Back), TRACK = 60° ($\phi_S = 180^\circ$)	37
3-10	A_{gd} for SCAN = 120° (Back), TRACK = 60° ($\phi_S = 120^\circ$)	38
3-11	Double-Valued Calibration Curves	40
3-12	L-Band Principal Polarization (HH) Bistatic σ_0 Data of 17 March 1978, Passes 3 and 10, High Range	41
3-13	L-Band Principal Polarization (HH) Bistatic σ_0 Data of 17 March 1978, Passes 3 and 10, Low Range	42

LIST OF FIGURES (CONT'D.)

FIGURE		PAGE
3-14	X-Band Principal Polarization (HH) Bistatic σ_0 Data of 17 March 1978, Passes 3 and 10, High Range	43
3-15	X-Band Principal Polarization (HH) Bistatic σ_0 Data of 17 March 1978, Passes 3 and 10, Low Range	44
3-16	Time Histories of σ_0 and Illumination Correction Factor	46
3-17	L-Band Orthogonal Polarization (HV) Bistatic σ_0 Data Processed by ERIM, Passes 3 and 10 of 18 March 1978	48
3-18	L-Band Orthogonal Polarization (HV) Bistatic σ_0 Data Processed by DSA, Passes 3 and 10, 18 March 1978	49
3-19	L-Band Orthogonal Polarization (HV) Bistatic σ_0 Data Reprocessed by ERIM, Passes 3 and 10, 18 March 1978	50
3-20	Time History Showing Noise Spikes	51
4-1	Site II: 17, 18 and 19 February 1978: Snow Covered Flat Terrain With Weeds and Scrub Trees Extending Above the Snow Surface	54
4-2	Site III: 17 and 18 March 1978: Snow Covered Ground in Apple Orchard	56
4-3	Monostatic σ_0 Data for Snow, Dry Grass, and Weeds, X-Band HH Polarization	58
4-4	Bistatic σ_0 Data for Dry Grass and Site 2 Model for X-Band, HH Polarization	60
4-5	Site 2 L-Band Bistatic σ_0 Model for Principal and Orthogonal Polarizations	61
4-6	X-Band (HH) Monostatic σ_0 Data for Wooded Terrain and Bistatic σ_0 Model for Site 3	63
4-7	L-Band (HH Polarization) Monostatic σ_0 Data for Wooded Terrain and Bistatic σ_0 Model for Site 3	64
4-8	L-Band Principal Polarization (HH) Bistatic σ_0 Data of 17 February 1978 (All Passes) For a Snow Covered Field	65

LIST OF FIGURES (CONT'D.)

FIGURE		PAGE
4-9	L-Band Orthogonal Polarization (HV) Bistatic σ_0 Data of 17 February 1978 (All Passes) for a Snow Covered Field	66
4-10	L-Band Principal Polarization (HH) Bistatic σ_0 Data of 18 February 1978 (All Passes) for a Snow Covered Field	68
4-11	L-Band Orthogonal Polarization (HV) Bistatic σ_0 Data of 18 February 1978 (All Passes) for a Snow Covered Field	69
4-12	L-Band Principal Polarization (HH) Bistatic σ_0 Data of 19 February 1978 (All Passes) for a Snow Covered Field	70
4-13	L-Band Orthogonal Polarization (HV) Bistatic σ_0 Data of 19 February 1978 (All Passes) for a Snow Covered Field	71
4-14	L-Band Principal Polarization (HH) Bistatic σ_0 Data of 17 March 1978 (All Passes) for a Wooded Terrain	72
4-15	L-Band Orthogonal Polarization (HV) Bistatic σ_0 Data of 17 March 1978 (All Passes) for Wooded Terrain	73
4-16	X-Band Principal Polarization (HH) Bistatic σ_0 Data of 17 March 1978 (All Passes) for Wooded Terrain	74
4-17	X-Band Orthogonal Polarization (HV) Bistatic σ_0 Data of 17 March 1978 (All Passes) for Wooded Terrain	75
4-18	L-Band Principal Polarization (HH) Bistatic σ_0 Data of 18 March 1978 (All Passes) for Wooded Terrain	76
4-19	L-Band Orthogonal Polarization (HV) Bistatic σ_0 Data of 18 March 1978 (All Passes) for Wooded Terrain	77
4-20	X-Band Principal Polarization (HH) Bistatic σ_0 Data of 18 March 1978 (All Passes) for Wooded Terrain	78

LIST OF FIGURES (CONT'D.)

FIGURE		PAGE
4-21	X-Band Orthogonal Polarization (HV) Bistatic σ_0 Data of 18 March 1978 (All Passes) for Wooded Terrain	79
4-22	L-Band Principal Polarization (HH) Bistatic σ_0 Data of 18 March 1978 (All Passes)	83
B-1	L-Band Principal Polarization (HH) Bistatic σ_0 Data of 17 March 1978 (Passes 3 and 10, $\theta_s = 80^\circ$, $\theta_i = 60^\circ$) for Wooded Terrain	B-2
B-2	L-Band Orthogonal Polarization (HV) Bistatic σ_0 Data of 17 March 1978 (Passes 3 and 10, $\theta_s = 80^\circ$, $\theta_i = 60^\circ$) for Wooded Terrain	B-3
B-3	X-Band Principal Polarization (HH) Bistatic σ_0 Data of 17 March 1978 (Passes 3 and 10, $\theta_s = 80^\circ$, $\theta_i = 60^\circ$) for Wooded Terrain	B-4
B-4	X-Band Orthogonal Polarization (HV) Bistatic σ_0 Data of 17 March 1978 (Passes 3 and 10, $\theta_s = 80^\circ$, $\theta_i = 60^\circ$) for Wooded Terrain	B-5
B-5	L-Band Principal Polarization (HH) Bistatic σ_0 Data of 18 March 1978 (Passes 3 and 10, $\theta_s = 80^\circ$, $\theta_i = 70^\circ$) for Wooded Terrain	B-6
B-6	L-Band Orthogonal Polarization (HV) Bistatic σ_0 Data of 18 March 1978 (Passes 3 and 10, $\theta_s = 80^\circ$, $\theta_i = 70^\circ$) for Wooded Terrain	B-7

LIST OF TABLES

<u>TABLE</u>		<u>PAGE</u>
2-1	Comparison of ERIM and OSU Backscattering ($\phi_s = 180^\circ$) σ_o Data	16
3-1	Data Evaluation, 9 July 1976	21
3-2	Variations in A_{gd} and KI Values	30
3-3	Behavior of A_{gd} and KI for Forward and Backscattering Cases	30
4-1	Description of Test Areas and Bistatic Measurement Angles	55
A-1	Transmitter and Transmitting Antenna Characteristics	A-2
A-2	Receiver and Receiving Antenna Parameters	A-3

1.0 INTRODUCTION AND SUMMARY

This report describes the analysis performed by Decision-Science Applications, Inc., (DSA) on the bistatic clutter data collected by the Environmental Research Institute of Michigan (ERIM) on 17, 18, and 19 February and 17 and 18 March 1978.

The general scope of the ERIM effort called for measurements of bistatic radar cross section per unit area (σ_0) of the terrain at two Michigan sites, using an airborne transmitter and a tower-mounted receiver. Reflectivity was to be measured (simultaneously) at L- and X-band, at both horizontal-horizontal (HH) and horizontal-vertical (HV) polarizations. The overall objective was to obtain X- and L-band ground-clutter σ_0 statistics for large bistatic angles and out-of-plane geometries. The planned approach was to use dual-frequency pulsed transmitters in a fly-by aircraft to illuminate the test area at a constant antenna depression angle. The tower-mounted receivers then scan the test area in azimuth at a constant antenna depression angle, measuring the scattering from individual resolution cells at multiple bistatic angles.

DSA was assigned the task of interpreting the data and answering the question: How do these new data compare with data previously collected and to what extent has our general understanding of bistatic clutter been enhanced by the acquisition of this new data?

While this report was in preparation, ERIM reprocessed much of the data and supplied DSA with a new data set. It was not feasible for DSA to perform a complete evaluation of this newly submitted data; but, for the purpose of comparison, DSA generated a plot of the newly submitted L-band data of 18 March 1978. That comparison is discussed at the end of Sec. 4.4.

2.0 BACKGROUND

For downward-looking radars which are searching for aircraft, the earth's surface can be a source of very significant clutter echoes. This is particularly true for low-flying aircraft targets; with achievable antenna apertures and radar bandwidths, it is not always possible to resolve such targets from the clutter, and detection must often be performed in very high clutter environments. Clutter can be the dominant factor which limits detection performance, particularly for spaceborne radar platforms where beam spreading due to long ranges leads to very large clutter contributions. Consequently, clutter suppression approaches involving data processing (such as coherent cancellation and Doppler filtering) are normally required to enable look-down radars to function with acceptable probabilities of detection and false alarm. Quantitative statistical data on the clutter is required to assess the amount of suppression required and to select the appropriate data processing approach.

A great deal of quantitative data has been collected on monostatic radar clutter. However, for bistatic radar, a study revealed that almost no relevant clutter data existed, and that what little did exist had been collected under very limited and idealized conditions.¹⁻² It was apparent that more data was needed in order to be confident about bistatic radar clutter suppression requirements and approaches.

¹ V. W. Pidgeon, "Bistatic Cross Section of the Sea," IEEE Transactions on Antennas and Propagation, Vol. Ap-14, No. 3, May 1966, pp. 405-406.

² W. H. Peake and T. L. Oliver, The Response of Terrestrial Surfaces at Microwave Frequencies, OSU Electro Science Laboratory Report 2440-7, (AD 884 106), May 1971.

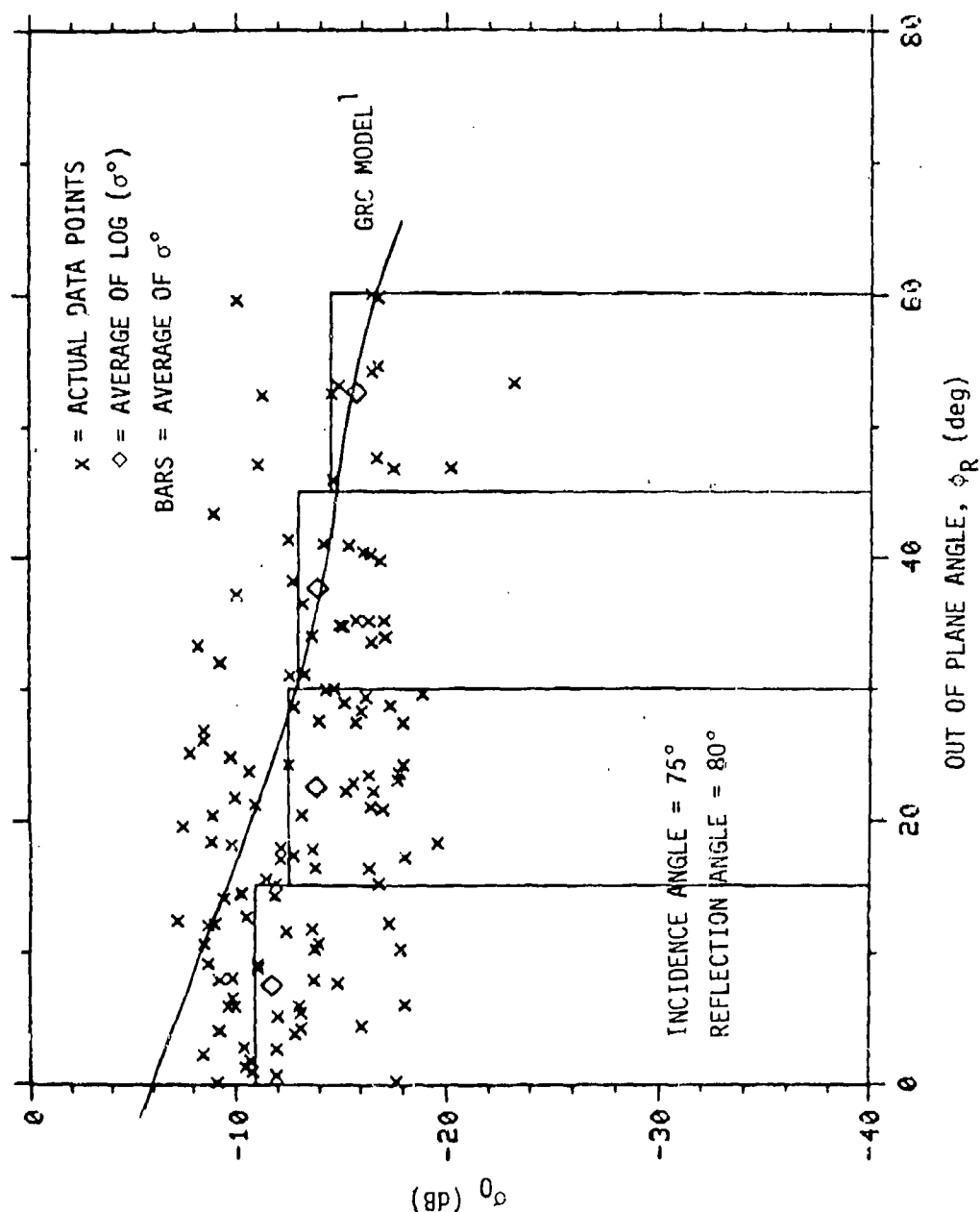
By studying the existing data base, it was shown that the bistatic theorem¹ provided an upper bound for bistatic clutter data. An interesting issue which was raised by some of this data² was a possible 20-dB reduction in the bistatic clutter reflectivity of vegetated terrain, for certain bistatic geometries. This phenomenon is believed to be due to Rayleigh criterion effects. However, the reliability of these conclusions needed to be explored for a wider variety of naturally occurring terrain samples. Also a greater volume of data was needed, so that the statistical properties of bistatic clutter could be accurately assessed. Consequently, DARPA initiated a bistatic clutter measurement program during FY 76. As a part of this program, ERIM developed a tower-mounted, two-frequency receiver system configured to operate in a bistatic mode, with an existing airborne L- and X-band radar acting as transmitter. This system is used to measure and record the calibrated radar energy scattered bistatically from resolved portions of the surrounding terrain; subsequent analysis derives the σ_0 from this data.

ERIM performed data-taking flights with this equipment on 2, 9, and 17 July 1976, which resulted in bistatic clutter data on (1) a level area comprised of a concrete parking ramp for aircraft and mowed grass, and (2) a level area covered with waist-high grass and weeds. These data showed that the bistatic theorem provided an upper bound for the tall vegetation data. In these flights low grazing angles were used, but no sign of the Rayleigh criterion effects found in the previous data was noted.

Figure 2-1 shows L-band principal polarization σ_0 data from the tall vegetation site, taken during the aircraft pass 4 on 17 July. During this

¹J. W. Crispin, Jr., and K. M. Kiegel, Methods of Radar Cross Section Analysis, Academic Press, New York, 1968, p. 158.

²W. H. Peak et al., op. cit.



G. A. Ackerson et al., op. cit., p. 59.

Figure 2-1. Comparison of Clutter Model to ERIM L-Band Principal Polarization σ_0 Data Collected at Tall Vegetation Site

pass the incidence angle $\theta_s = 75^\circ$ and the reflection angle $\theta_r = 80^\circ$. σ_0 is plotted as a function of the out-of-plane angle, ϕ_R (see Fig. 2-2 for a definition of the experiment coordinate system). Figure 2-1 compares this ERIM data to the predictions of the preliminary clutter algorithm which GRC devised using the bistatic theorem.¹ The ERIM data agrees quite well with this algorithm.

Figure 2-3 shows the cumulative probability distribution of the same bistatic σ_0 data, plotted on probability paper. This is compared to the distribution of X-band monostatic σ_0 data, collected with the same airborne radar used as a transmitter in the present experiment, operated at a 15° antenna depression angle.¹ The two distributions fall within 2 dB of each other between the 10% and 90% points. However, the distribution of the monostatic data shows dramatically higher tails rising to $\sigma_0 = +10$ dB at the 99.9% level. The bistatic data does not appear to share this tendency and in fact seems to have leveled off at -8 dB. If this apparent trend is substantiated at other test sites, it would indicate a significant reduction in the expected clutter false alarms that could result from bistatic operation.

Figure 2-4 shows the ERIM σ_0 data taken on all passes occurring on 17 July 1976 plotted against inclination of the bistatic bisector. Shown for comparison is the model derived using L-band data, which Ament et al.² collected on wooded terrain, and the bistatic theorem. Except for a few points the agreement is quite good.

Comparisons can also be made between the 17 July 1976 ERIM data and data recorded some years ago by Ohio State University (OSU) researchers. Conditions are by no means the same for the two sets of data, yet it may be

¹G. A. Ackerson et al., op. cit., p. 58ff.

²W. S. Ament, F. C. Macdonald, and R. D. Shewbride, "Radar Terrain Reflections for Several Polarizations and Frequencies," Transactions of the 1959 Symposium of Radar Return, University of New Mexico, May 11-12, 1959.

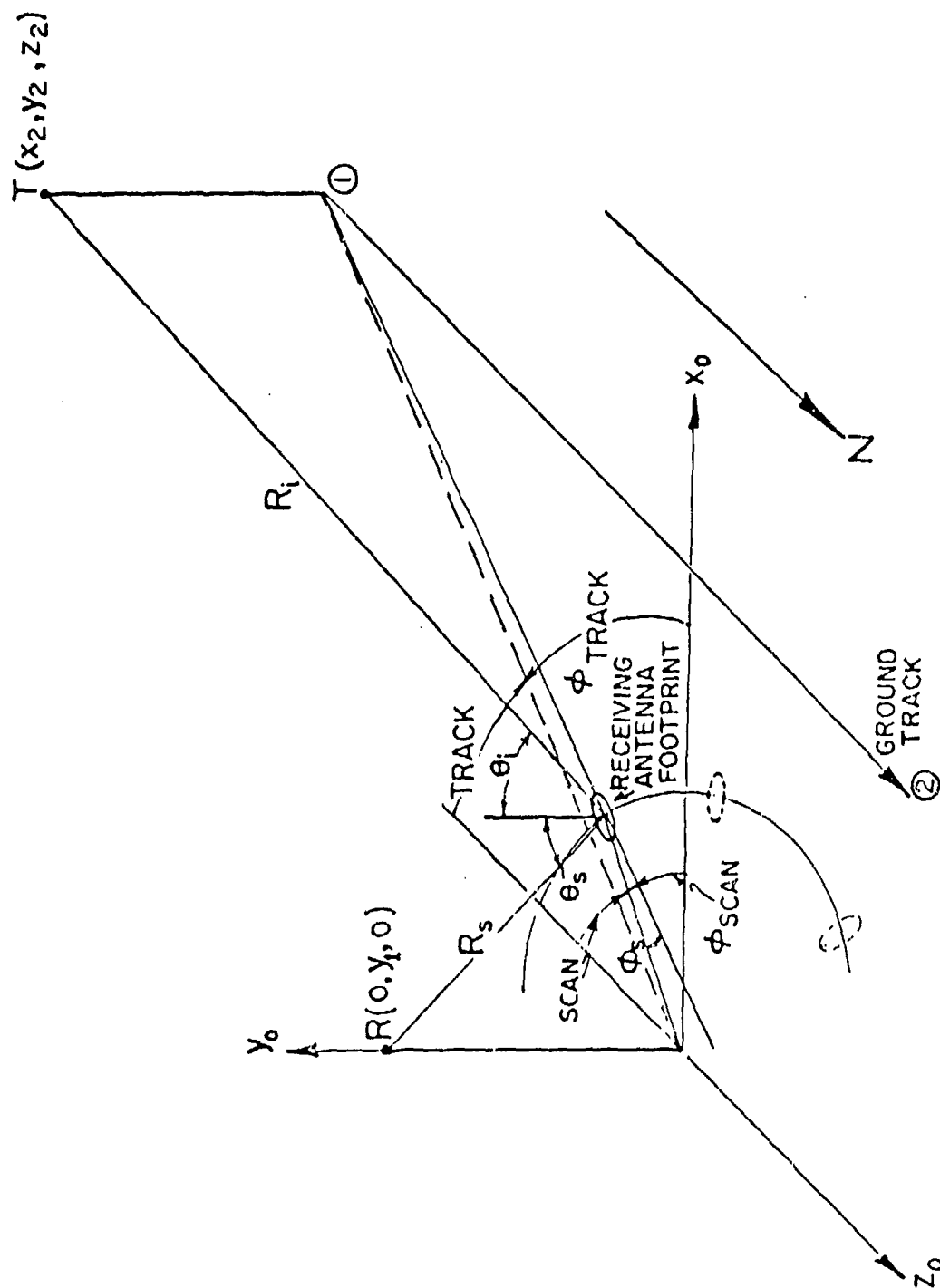


Figure 2-2. Basic Bistatic Geometry¹

¹This figure was drawn from Bistatic Clutter Data Measurements Program, RADC-TR-389, Environmental Research Institute of Michigan, November 1977.

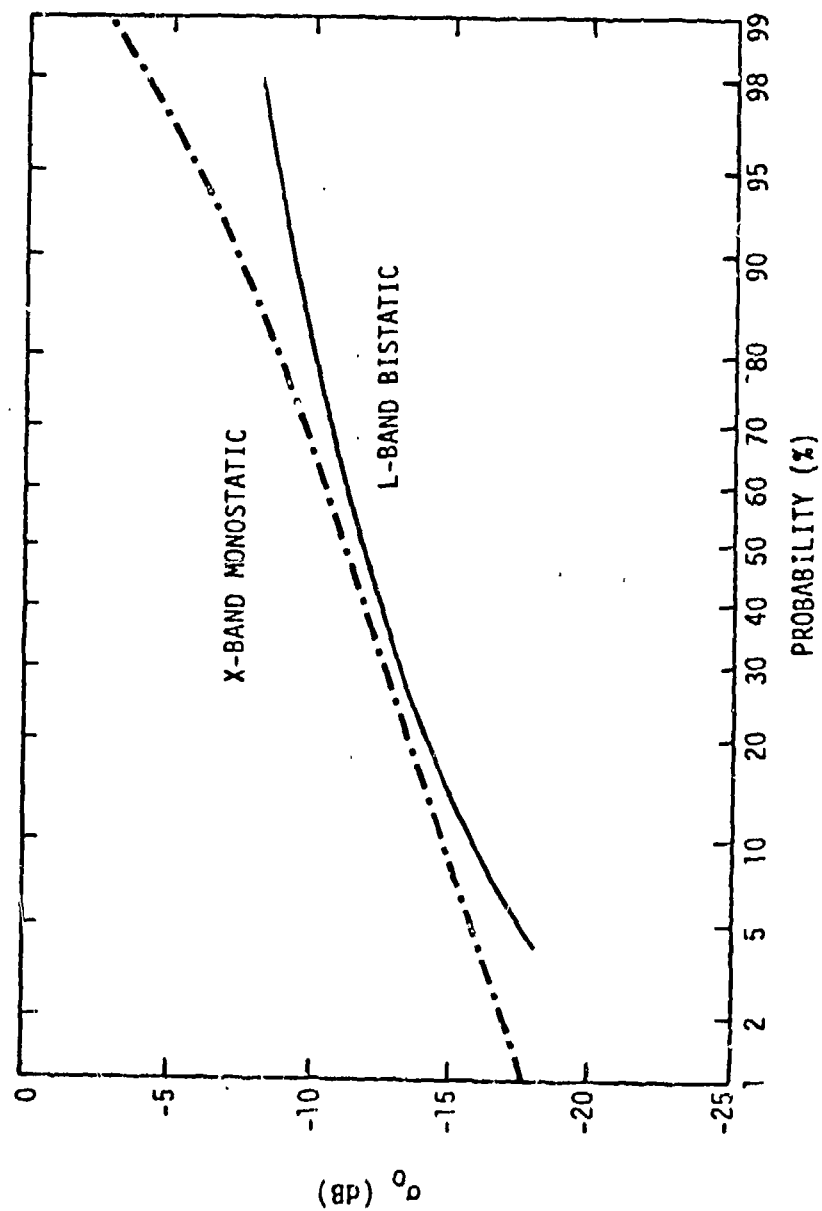


Figure 2-3. L-Band Bistatic σ_0 Statistics. Second part of Pass 4, Site 2, HH Polarization, $\theta \leq \phi_R \leq 14^\circ$, compared to monostatic X-band σ_0 statistics collected over rural terrain with a 15° antenna depression angle.

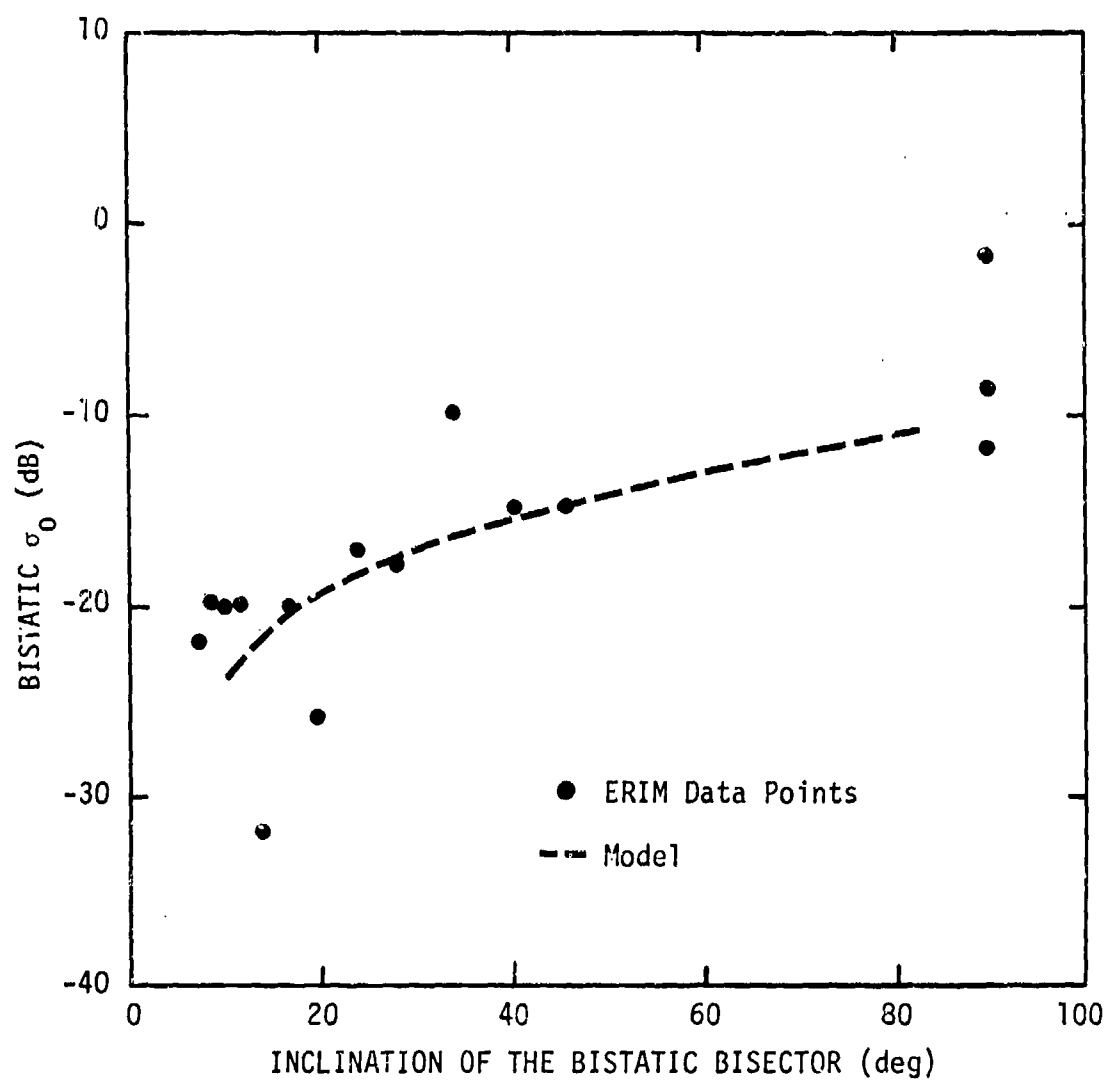


Figure 2-4. L-Band Principal Polarization (HH) Bistatic σ_0
Data of 17 July 1976 (All Passes)

appropriate to compare those terrain conditions for which the ratio of vegetation size to wavelength is similar. For example, the ERIM L-band data from passes 3 and 12 of 17 July 1976 were recorded for terrain covered with 4-ft weeds and brush. On the other hand, some of the OSU data¹ were recorded for 3-in. green soybeans and 4-in. oats in head (July) at a 3-cm wavelength. Table 2-1 shows a comparison of these data for $\theta_i = \theta_s = 70^\circ$ (pass 12) and $\theta_i = \theta_s = 80^\circ$ (pass 3) and $\phi_s = 180^\circ$ (the backscatter case). Note that the σ_0 values are in good agreement.²

A second comparison with the Ohio State data is possible for a forward scattering situation. In Fig. 2-5, the incidence and scattering angles are both 80° for both sets of data. The ERIM data in this figure were collected on 17 July 1976 and are for terrain covered with 4-ft weeds and brush at L-band (23-cm wavelength). The OSU data shown³ are for 4-in. soybean foliage at X-band (3-cm wavelength). Both data sets were collected with horizontal-horizontal polarization. Although the data themselves differ markedly at some out-of-plane angles, the trends for the two data sets are quite similar. Shown also is the GRC model which represents well the ERIM data but exhibits a trend with out-of-plane angle that is much too slow to represent the Ohio State data.²

These comparisons lead us to conclude that the model derived from the bistatic theorem agrees quite well with the ERIM data of 17 July 1976, but neither agree very well with the OSU data for small out-of-plane angles ($\phi_s < 50^\circ$). However, agreement between the OSU and ERIM data is good for large out-of-plane angles.

¹R. L. Cosgriff, W. H. Peake, and R. C. Taylor, Terrain Scattering Properties for Sensor System Design (Terrain Handbook II), Engineering Experiment Station Bulletin No. 181, Ohio State University, Columbus, May 1960.

²This material abstracted from Bistatic Clutter Data Measurements Program, RADC-TR-77-389, Environmental Research Institute of Michigan, November 1977. A050125.

³S. T. Cost, Measurements of the Bistatic Echo Area of Terrain at X-Band, Report No. 1822-2, Ohio State University Research Foundation, Columbus, May 1965.

TABLE 2-1
COMPARISON OF ERIM AND OSU BACKSCATTERING ($\phi_s = 180^\circ$) σ_o DATA

$\theta_i = \theta_s$	Description	Passes	σ_o (dB)
70	ERIM 23-cm data: 4-ft weeds and brush, 17 July 1976	12	-18
70	OSU 3-cm data: 3-in. green soybeans		-22
70	OSU 3-cm data: 4-in. oats in head (July)		-20
80	ERIM 23-cm data: 4-ft weeds and brush, 17 July 1976	3	-20
80	OSU 3-cm data: 3-in. green soybeans		-26
80	OSU 3-cm data: 4-in. oats in head (July)		-21

x OSU X-Band Data. 4-in. soybean foliage,
 $\theta_i = \theta_s = 80^\circ$, horizontal polarization on transmit
 and receive.
 • ERM L-Band Data of 7/17/76, 4-ft weeds and brush
 $\theta_i = \theta_s = 80^\circ$, horizontal polarization on transmit
 and receive.

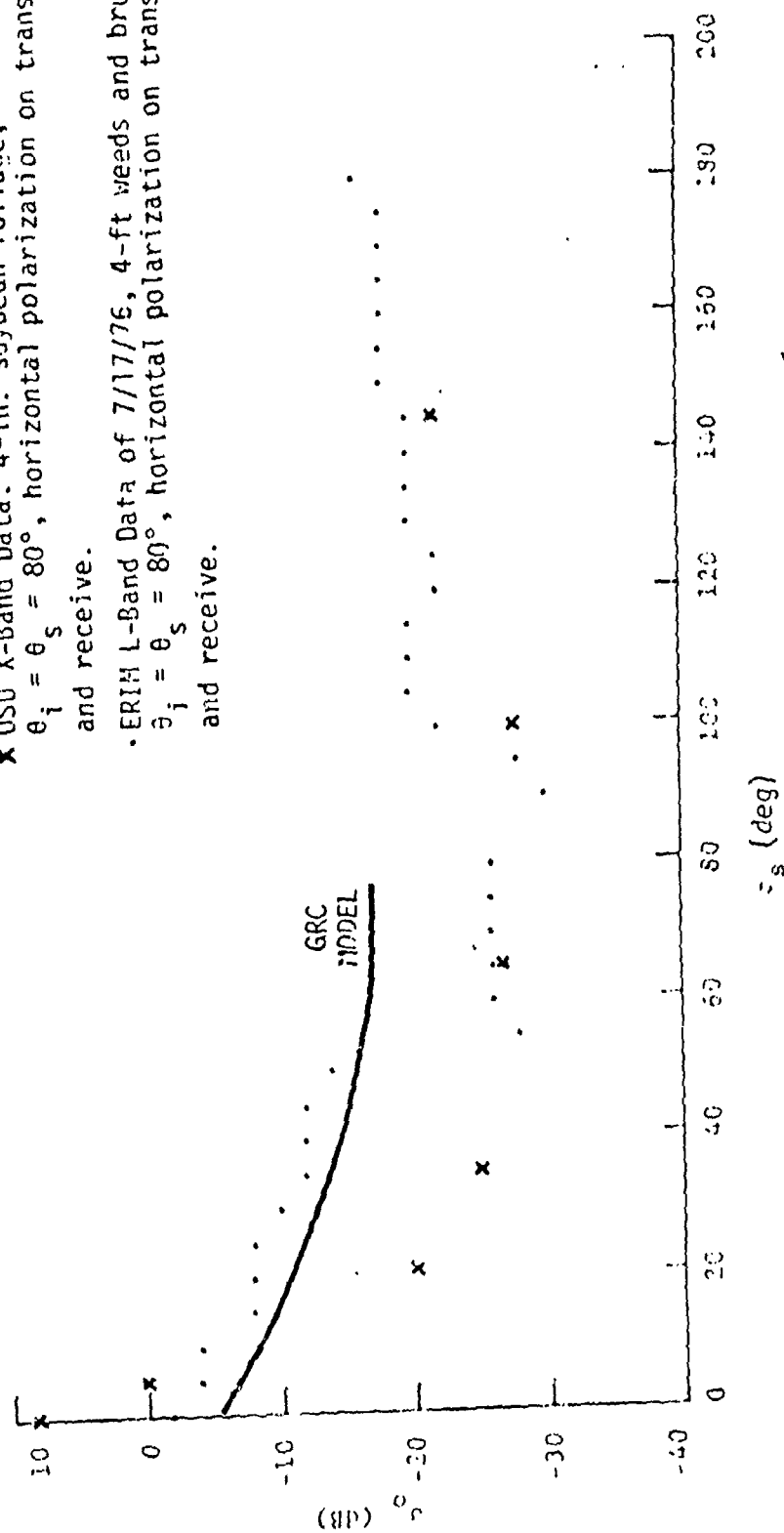


Figure 2-5. Comparison of ERM and OSU Data¹

¹This figure was drawn from Bistatic Clutter Data Measurements Program, RADG-TR-389, Environmental Research Institute of Michigan, November 1977.

The most recent ERIM tests, the subject of this report, were conducted in February and March 1978 for the purpose of obtaining data on terrain types different from those investigated in the earlier ERIM tests.

The 1976 series of ERIM measurements occurred at two sites. Site 1 was comprised of a concrete parking ramp for aircraft and mowed grass. The roughness scale was less than 4-in. rms for this site. Site 2 was a level area covered with waist-high grass and weeds and scrub trees 6 ft to 8 ft tall. The ground surface had a roughness scale of less than 6-in. rms and 12-in. peak-to-peak. This series of tests occurred in the summer when the grass, weeds and trees were alive and growing.

The most recent series of tests took place in the winter when the ground was snow covered and the grass, weeds, and trees were dead or dormant. The sites for these tests are described in Sec. 4.1.

3.0 DATA REDUCTION

This section describes the processing ERIM used to derive the bistatic scattering coefficient, σ_0 , from the recorded data and discusses the difficulties DSA encountered in their analysis and interpretation of the data. Subsection 3.1 describes a visual evaluation to sort out the good from the bad data and a data smoothing operation. Subsection 3.2 defines and describes the parameters on which the scattering coefficient depends. Because σ_0 is a random variable, some consideration must be given to insuring that an adequate and independent sample set from the terrain region is examined. This aspect of the data acquisition and reduction is considered in Subsection 3.3.¹

Subsection 3.4 discusses the ambiguity produced by the double-valued calibration function and the resolution of that ambiguity. The transmitter illumination correction factor appears to be valid only as long as it is smaller than 10 dB. Data associated with larger corrections appear to be invalid as discussed in Subsection 3.5. Subsection 3.6 discusses some of the numerical discrepancies found in the data. Noise spikes found in the data and their effect on the data are discussed in Subsection 3.7; and, finally, in 3.8 the level of confidence in the calibration is discussed.

3.1 PREPROCESSING DATA EVALUATION AND SMOOTHING

ERIM's data reduction process begins with a visual evaluation of the chart recordings obtained during the data gathering operation, wherein the received signal level, local oscillator power level, track angle, receiver antenna scan angle, and aircraft operating parameters are evaluated to determine whether the equipment operation was satisfactory during each individual pass of the transmitter aircraft. The data evaluations for the flight of 9 July 1976 are summarized in Table 3-1, which indicates the passes that will provide acceptable data for computing σ_0 values. Following this initial evaluation, the analog data are converted to a digital format and recorded on a 9-track tape to facilitate the processing to follow.

¹The material in Subsections 3.1 through 3.3 was abstracted from Bistatic Clutter Data Measurements Program, RADC-TR-77-389, Environmental Research Institute of Michigan, November 1977.

TABLE 3-1
DATA EVALUATION, 9 JULY 1976

Pass	S/N	L.O. Power	ΔR	Signal Level		Antenna		Transmitter Antenna Weighing, $\lambda = 23$ cm			Evaluation
				$\lambda = 3$ cm	$\lambda = 23$ cm	TRACK	SCAN	Start	Mid	End	
1	---	Low	---	Marginal	---	Manual	---	---	---	---	Low signals
2*		Last half	Partially	Last half of pass moderate strong TRACK = $55^\circ - 110^\circ$		Manual	Last half	-4 -1	-3 0	-6 -3	Good last half pass
3	---	Low	---	---	---	No track	---	---	---	---	Nothing
4	---	None	---	---	---	---	---	---	---	---	Nothing
5*	---	Adequate	Good	Good last half of pass	Good last half of pass	No track	Scan	---	---	---	Last half OK
6*	---	Good	Good	Good Low in first half of pass TRACK = $74^\circ - 130^\circ$	Good	Track	Scan	-5 -2	-6 -3	-3 0	Good all passes
7*	---	Adequate	Good	Good last third of pass TRACK = $60^\circ - 130^\circ$	Good	Track	Scan	-9 -6	-3 0	-3 0	Acceptable last half

* Usable for computing G_0 .

The data on the digital tape include measures of received power on a pulse-by-pulse basis, while the data analysis is performed on received power values averaged over the 5° beamwidth of the receiver (as will be discussed in Sec. 3.3). The next data preparation step is the averaging operation described by the relation

$$S_n = \frac{1}{N} \sum_{i=1}^N X_i^2$$

where X_i is the voltage amplitude received from the i^{th} transmission and N is the number of transmissions occurring during 5° of receive antenna scan.

3.2 DEFINITION OF σ_o AND ASSOCIATED PARAMETERS

The terrain scattering cross section per unit area, σ_o , is defined^{1,2} as

$$\sigma_o = \frac{4\pi r^2 dS_s}{S_i dA} \quad (1)$$

The incident power density S_i is expressible in terms of transmitted power P_i , transmitting antenna maximum gain, G_{OT} , and normalized power pattern function f_T as

$$S_i = \frac{1}{4\pi r_i^2} P_i G_{OT} f_T \quad (2)$$

¹D. E. Barrick, Normalization of Bistatic Radar Return, Report No. 1388-13, Ohio State University Research Foundation, Columbus, January 1964.

²W. H. Peake and T. L. Oliver, The Response of Terrestrial Surfaces at Microwave Frequencies, Report No. AFAL-TR-70-301, Electrosience Laboratory, Ohio State University, Columbus, May 1971.

(Since G_{0T} is constant, and f_T is a normalized function of aspect, the product $G_{0T}f_T$ represents the antenna gain as a function of aspect.) The scattered power density dS_s may be written in terms of the incremental power dP_r received by an antenna of aperture A_R , which in turn is expressible in terms of receiving antenna gain G_{0R} and power pattern function f_R . The result is

$$dS_s = \frac{dP_r}{A_R} = dP_r \frac{\lambda^2 G_{0R} f_R}{4\pi} \quad (3)$$

Equations 1, 2, and 3 may be assembled to yield the increment of received power dP_r as

$$dP_r = \frac{P_i \lambda^2 G_{0T} G_{0R} L}{(4\pi)^3} \cdot \frac{f_T f_R \sigma_o dA}{r_i^2 r_s^2} \quad (4)$$

The total power received from the entire illuminated surface A_{gd} is then

$$P_r = P_i K \int_{A_{gd}} \frac{f_T f_R \sigma_o dA}{r_i^2 r_s^2} \quad (5)$$

where constant terms have been collected as

$$K = \frac{\lambda^2 G_{0T} G_{0R} L}{(4\pi)^3} \quad (6)$$

The region on the ground denoted by A_{gd} is defined by:

1. the receiver antenna footprint
2. the transmitter antenna footprint
3. the range ellipses defined by the transmitter pulse interval and the receiver sampling interval

A weighting is applied over this region to reflect the response of the receiver to the transmitted pulse shape. That weighting is denoted as $h[t(A)]$. The integral

$$I = \int_{A_{gd}} \frac{f_T f_R \sigma_0 dA}{r_i^2 r_s^2} \quad (7)$$

is evaluated with the aid of approximation in which:

1. σ_0 is assumed constant over the region A_{gd} and brought outside of the integral
2. the transmit antenna gain function is rotationally symmetric and $f_T = 1$ in the area A_{gd} since the footprint of the transmit beam is much larger than that of the receive beam
3. the receive antenna gain function is rotationally symmetric and is approximated by the function,^{1, 2}

$$f_R = \left[\frac{8J_2(u)}{u^2} \right] = \left[\Lambda_2(u)^2 \right] \quad (8)$$

the integral I' becomes one that can be readily evaluated

$$I' = \frac{I}{\sigma_0} = \frac{(f_T = 1) f_R = [\Lambda(u)]^2 j[t(A)] dA}{r_i^2 r_s^2} \quad (9)$$

¹ S. Silver, Microwave Antenna Theory and Design, MIT Radiation Laboratory Series, No. 12, Boston Technical Lithographers, Inc., Lexington, Mass., 1963.

² E. Jahnke and F. Emde, Tables of Functions with Formulae and Curves, Dover Publications, New York, 1945.

and the final expression for σ_0 becomes

$$\sigma_0 = \frac{Pr}{P_j KI} \quad (10)$$

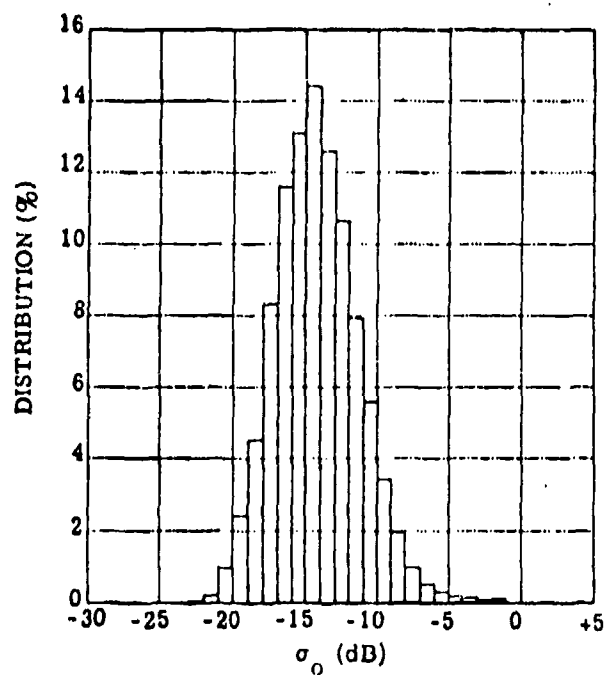
3.3 ENSEMBLE STATISTICS OF A SET OF SCATTERING ELEMENTS; PARAMETER VARIATION

The quantity σ_0 is a random variable whose distribution is governed by the type and condition of the terrain it describes. Thus, in order to estimate the statistics of the terrain being measured, the number of samples taken at a fixed set of parameters must be sufficiently large. Unfortunately, the number of samples required is based on the distribution of the terrain clutter σ_0 that must be approximated with the sample statistics. Since such distributions are unavailable, estimates must be made.

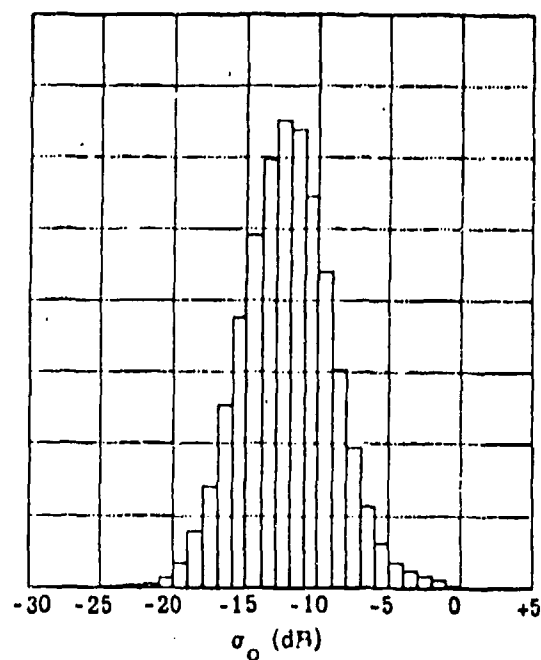
Long¹ gives the probability distribution for monostatic backscattering σ_0 from terrain. For homogeneous terrain, the distribution tends to be Rayleigh, while those for urban and mountainous areas have long tails typical of log-normal distributions. Figure 3-1 shows histograms of monostatic σ_0 data taken with the ERIM synthetic aperture radar. These distributions are approximately log-normal. Since the distribution of clutter return often becomes log-normal as the area of the resolution cell decreases, fine-resolution SARs are more likely to measure log-normal distributions than are conventional radars.

For the data of Fig. 3-1, the standard deviation, s , of $\log \sigma_0$ is on the order of 3 or 4 dB. For a Rayleigh distribution, the standard deviation is 5.6 dB, so that the log-normal distribution makes a fair approximation to the distribution for ground clutter no matter whether these are actually log-normal or Rayleigh distributed. So it is assumed here, for

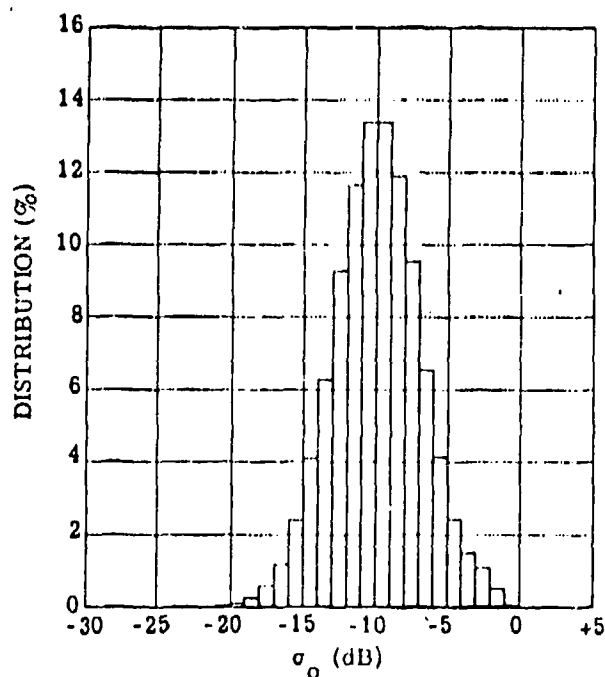
¹M. W. Long, Radar Reflectivity of Land and Sea, Lexington Books, Lexington, Mass., 1975, page 156.



(a) Grazing Angle 11°
 $(\bar{\sigma}_0 = 0.048 = -13.2 \text{ dB})$



(b) Grazing Angle 15°
 $(\bar{\sigma}_0 = 0.079 = -11.0 \text{ dB})$



(c) Grazing Angle 19°
 $(\bar{\sigma}_0 = 0.128 = -8.9 \text{ dB})$

Figure 3-1. 3-cm Wavelength Histograms, ERIM SAR Data
 (Ohio farmland, 10-ft resolution, single look)

purposes of estimating desired sample size, that terrain clutter, both monostatic and bistatic, is log-normal distributed.

From standard statistical theory, the 95% confidence interval for the population mean is given by

$$\sigma_0 - \frac{1.96s}{n} < \mu < \sigma_0 + \frac{1.96s}{n}$$

where σ_0 is the mean of n samples, while μ and s are the mean and standard deviation of the terrain clutter population. The 95% confidence interval for μ is therefore $3.92s/\sqrt{n}$ dB in width. Figure 3-2 shows plots of $3.96s/\sqrt{n}$ for s equal to 3 and 5 dB for sample numbers n ranging from 4 to 20 (which is representative of the range of σ_0 samples obtained in this program).

To achieve the desired number of samples, the receiving antenna is made to rotate from side to side as the transmitting antenna travels along a straight-line course. The angles defining the direction of look of the receiving antenna and the direction of the transmitter from the receiver are each measured clockwise from the negative z_0 -axis of Fig. 2-2; they are called SCAN and TRACK respectively.

For the forward scattering case (scattering area between transmitter and receiver), the azimuth angle ϕ_s is given approximately¹ by

¹The precise value is

$$\phi_s = |\text{SCAN} - \text{TRACK}| + \arcsin \frac{y_1 \tan \theta_s \sin |\text{SCAN} - \text{TRACK}|}{y_2 \tan \theta_i}$$

However, since the denominator is much larger than the numerator in the arcsine argument, the arcsine value is close to zero.

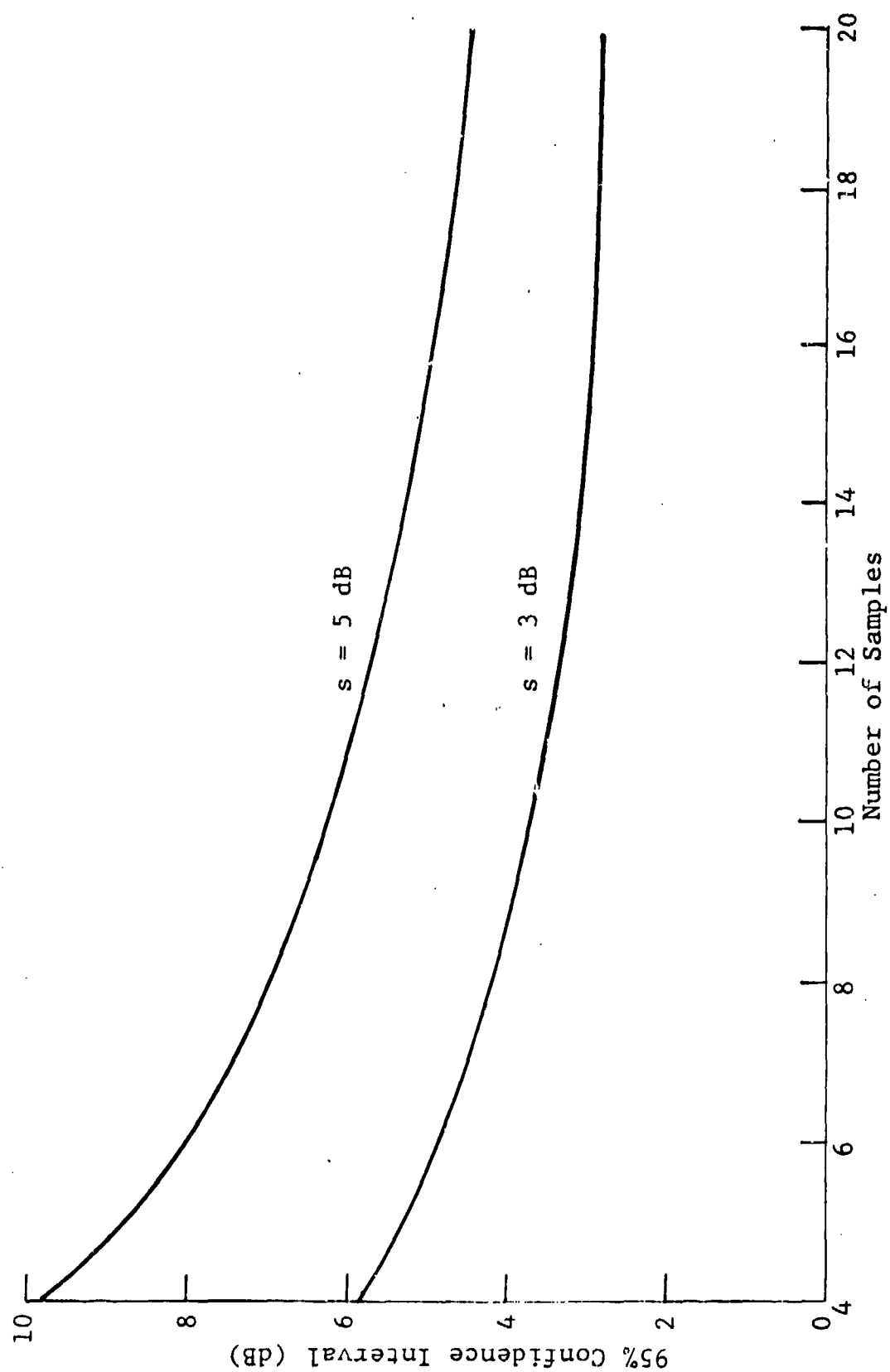


Figure 3-2. Width of 95% Confidence Interval vs. Number of Samples

$$\phi_s = |\text{SCAN} - \text{TRACK}|.$$

Since SCAN moves through its range (typically 65° through 155°) many times (typically 20) during a pass of the transmitter (TRACK range typically 45° through 135°), ϕ_s takes on the same (largely acute) value many times. Each of these ϕ_s values occurs for a different terrain scattering element in an essentially homogeneous field or region of terrain, in this way, the sought-after set of scattering element (or σ_0) samples is obtained. If values of SCAN and TRACK are approximated to the nearest multiple of 5° , then a typical sample number range of 4 to 20 can be expected.

For the backscattering case (receiver between scattering area and transmitter), the azimuth angle ϕ_s is given approximately by

$$\phi_s = ||\text{SCAN} - \text{TRACK}| - 180^\circ|$$

Since, in this case, SCAN is measured clockwise from the positive z_0 -axis while TRACK is measured clockwise from the negative z_0 -axis as above. Once again, each ϕ_s value is repeated many times, each time for a different terrain scattering element. Typical numbers of samples are in the same range as for the forward scattering case.

To insure that a given value of ϕ_s is repeated many times in the data, an average is derived of all σ_0 values over a range of ϕ_s values within $2\frac{1}{2}$ on either side of integer multiples of 5° . In this interval of ϕ_s , samples may come from any portion of the pass and so the incidence angle θ_i may vary by the maximum amount possible in the total pass. The incidence angle is given approximately* by

*The exact expression is

$$\theta_i = \sqrt{\frac{1}{y_2^2} + x_2^2 \csc^2(\text{TRACK}) - 2x_2y_1 \tan \theta_s [1 + \cos(\text{SCAN})] + y_1^2 \tan^2 \theta_s [1 + \cos^2(\text{SCAN})]}$$

$$\theta_i = \arctan \frac{x_2 \csc (\text{TRACK})}{y_2}$$

and so varies directly as $\csc (\text{TRACK})$. In a pass with, say, $x_2 = 18,000$ ft, $y_2 = 6000$ ft, and TRACK between 65° and 155° , the incidence angle θ_i may change by as much as 9° for samples at the beginning and end of the pass. This is the most serious change in any parameter over any set of samples; it may or may not occur in any particular sample set depending on the portions of the pass for which SCAN and TRACK combine to give a particular ϕ_s value. The scattering angle θ_s , of course, remains fixed throughout a given pass.

Since σ_0 samples may come from any part of a pass, the sizes of A_{gd} and values of KI may vary correspondingly. Consider an L-Band (23-cm wavelength) example for which $y_1 = 100$ ft, $\theta_s = 80^\circ$, $x_2 = 20,000$ ft, and $y_2 = 6000$ ft. Then, for all of the (SCAN, TRACK) pairs $(90^\circ, 90^\circ)$, $(120^\circ, 120^\circ)$, and $(150^\circ, 150^\circ)$, ϕ_s is 0° . Assuming that the first limiting range ellipse passes through the intersection of the receiver antenna beam axis with the earth and the second limiting range ellipse occurs 90 nanoseconds later, there are pronounced differences in A_{gd} and KI values because of the range changes involved. Table 3-2 illustrates these differences. Graphs of A_{gd} for the three sets of conditions covered in the table are shown in Figs. 3-3, 3-4, and 3-5, respectively.

As the values ϕ_s change, A_{gd} can vary over a much wider range; but, due again to the changing ranges from A_{gd} to transmitter and receiver, the values of KI seldom suffer more than 4 to 6 dB excursions. Illustrations of this behavior of A_{gd} and KI are afforded by the five illustrations (using the above values of y_1 , θ_s , x_2 , and y_2), three for forward and two for back-scattering, given in Table 3-3. The areas A_{gd} corresponding, respectively, to the five sets of conditions covered in the table are shown in Figs. 3-6, 3-7, 3-8, 3-9, and 3-10.

TABLE 3-2. VARIATIONS IN A_{gd} AND K_I VALUES

$\frac{\text{SCAN}}{(\text{deg})}$	$\frac{\text{TRACK}}{(\text{deg})}$	$\frac{\phi_s}{(\text{deg})}$	$\frac{A_{gd}}{(\text{m}^2)}$	$\frac{K_I}{(\text{dB})}$
90	90	0	4387	-97.6
120	120	0	4475	-99.2
150	150	0	4855	-103.0

TABLE 3-3. BEHAVIOR OF A_{gd} AND K_I FOR FORWARD AND BACKSCATTERING CASES

$\frac{\text{SCAN}}{(\text{deg})}$	$\frac{\text{TRACK}}{(\text{deg})}$	$\frac{\phi_s}{(\text{deg})}$	$\frac{A_{gd}}{(\text{m}^2)}$	$\frac{K_I}{(\text{dB})}$
60	60	0	4475	-99.2
90	60	30	4065	-95.2
120	60	60	1579	-96.5
60 (back)	60	180	468	-101.1
120 (back)	60	120	614	-100.2

AREA = 4386.8

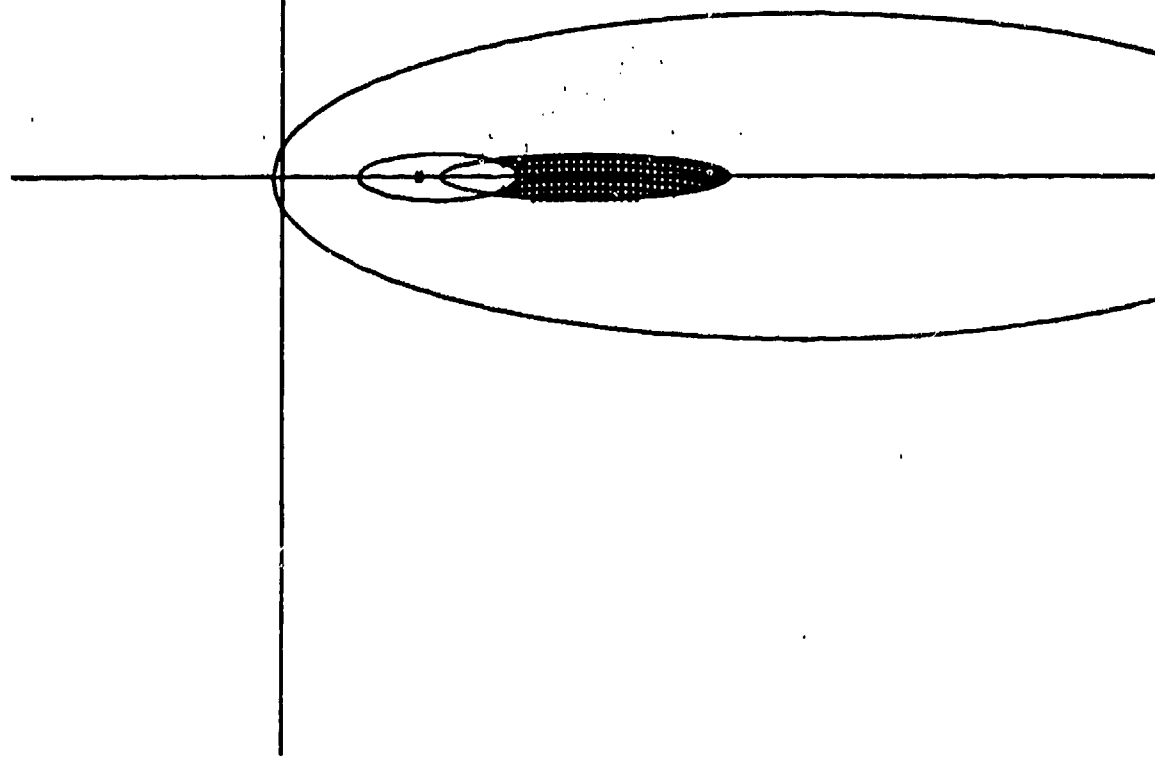


Figure 3-3. A_{gd} for SCAN = TRACK = 90° ($\phi_s = 0^\circ$)

AREA = 4474.5

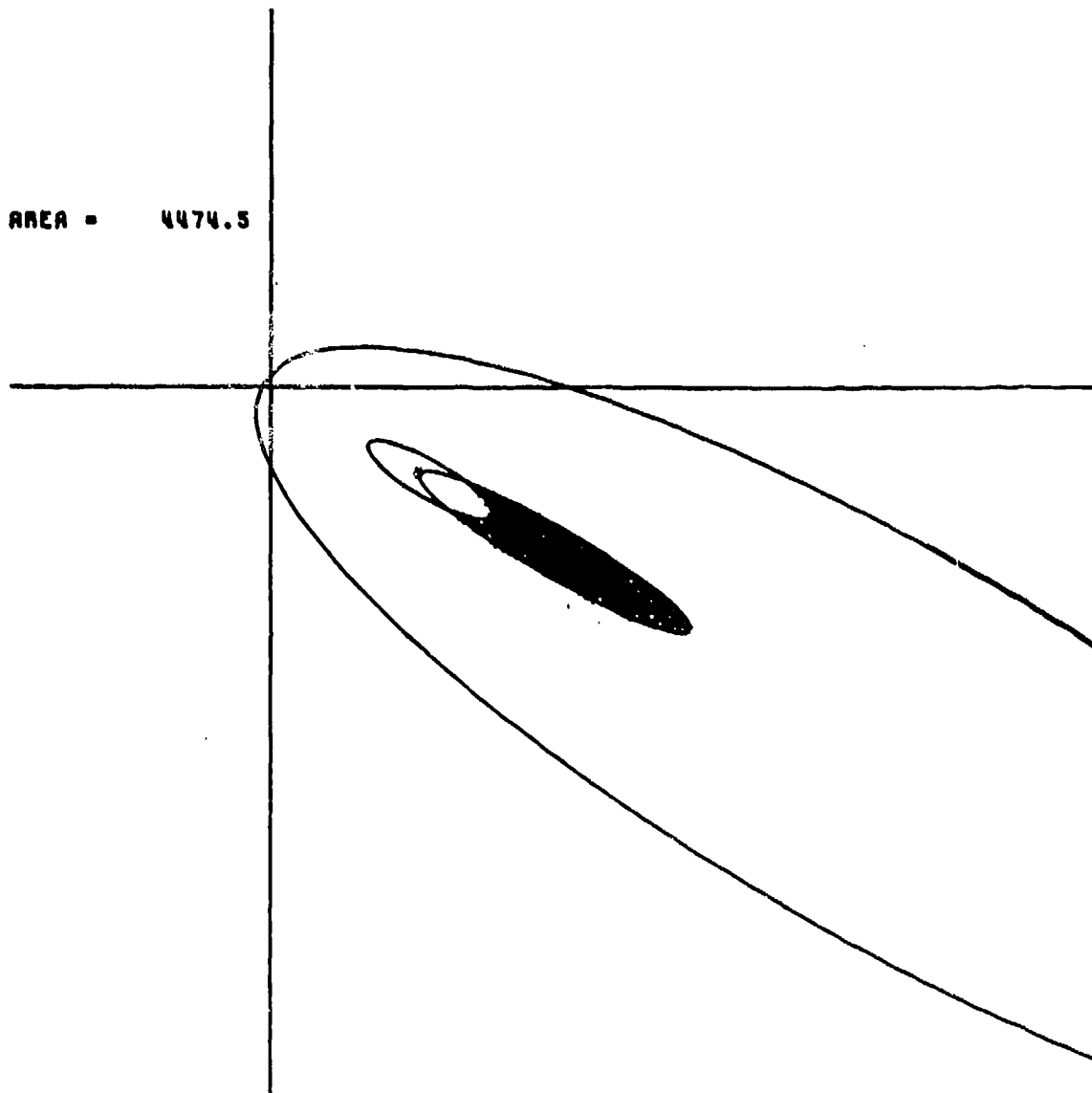


Figure 3-4. A_{gd} for SCAN = TRACK = 120° ($\phi_s = 0^\circ$)

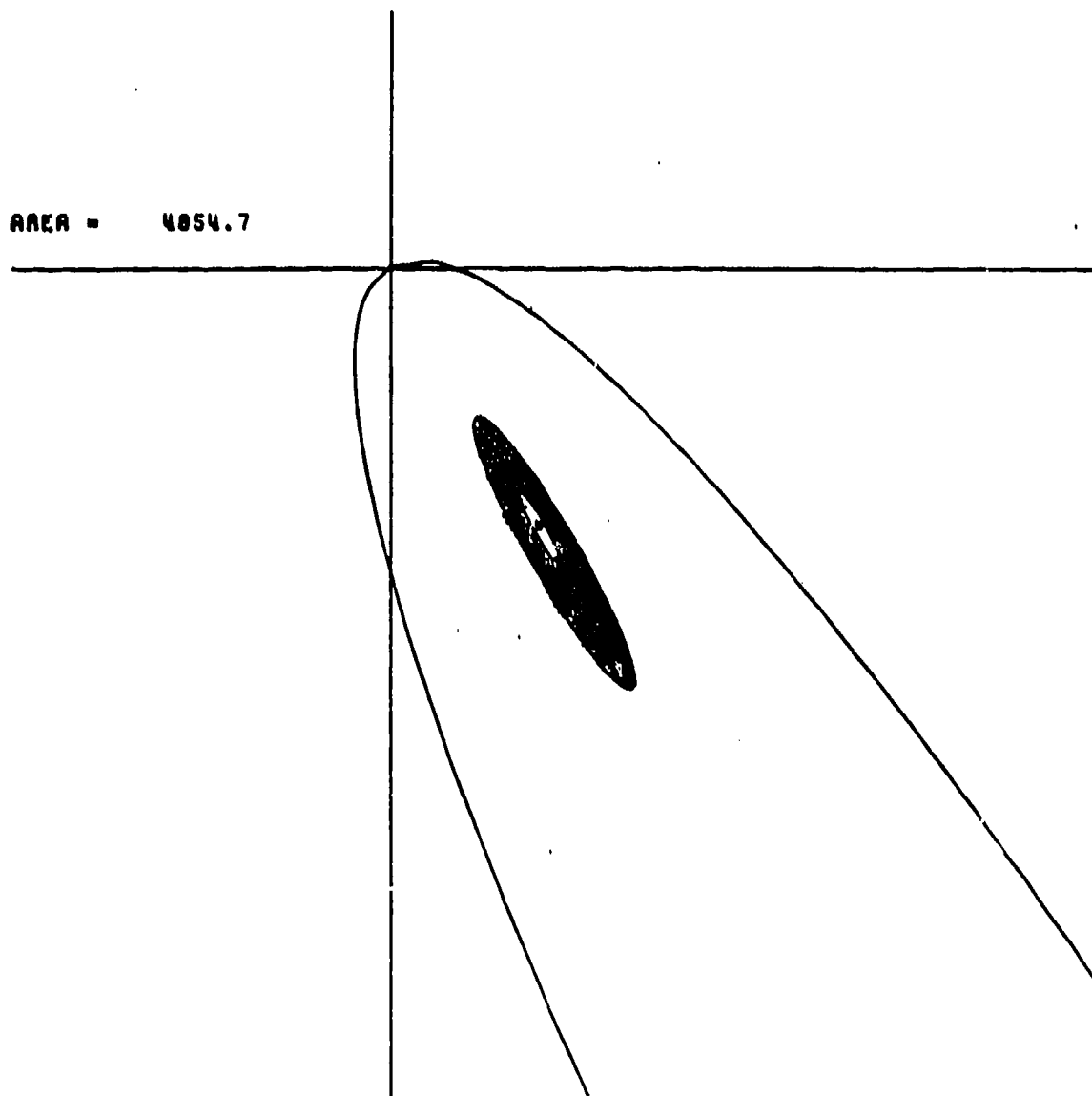


Figure 3-5. A_{gd} for SCAN = TRACK = 150° ($\phi_s = 0^\circ$)

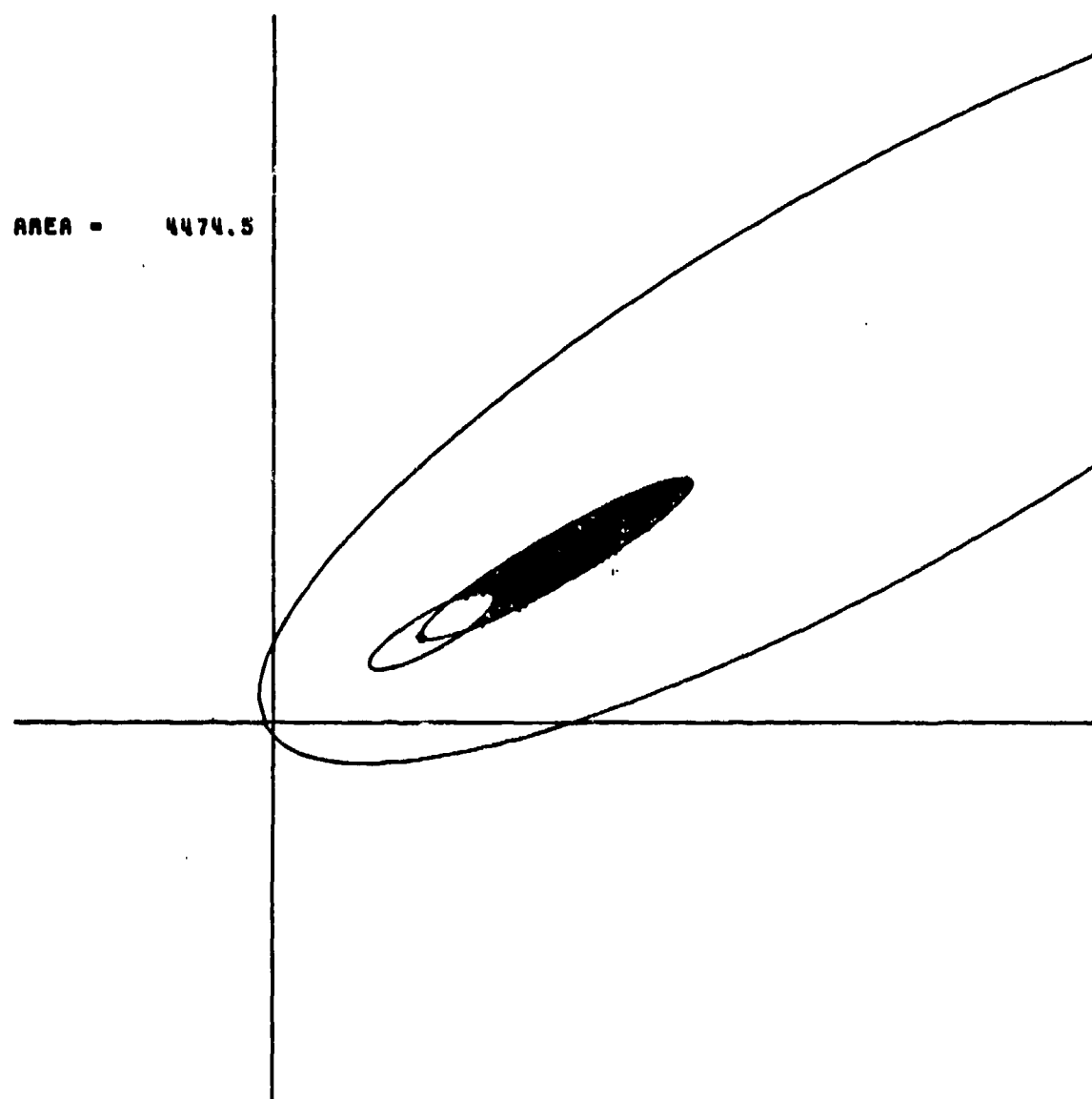


Figure 3-6. A_{gd} for SCAN = TRACK = 60° ($\phi_s = 0^\circ$)

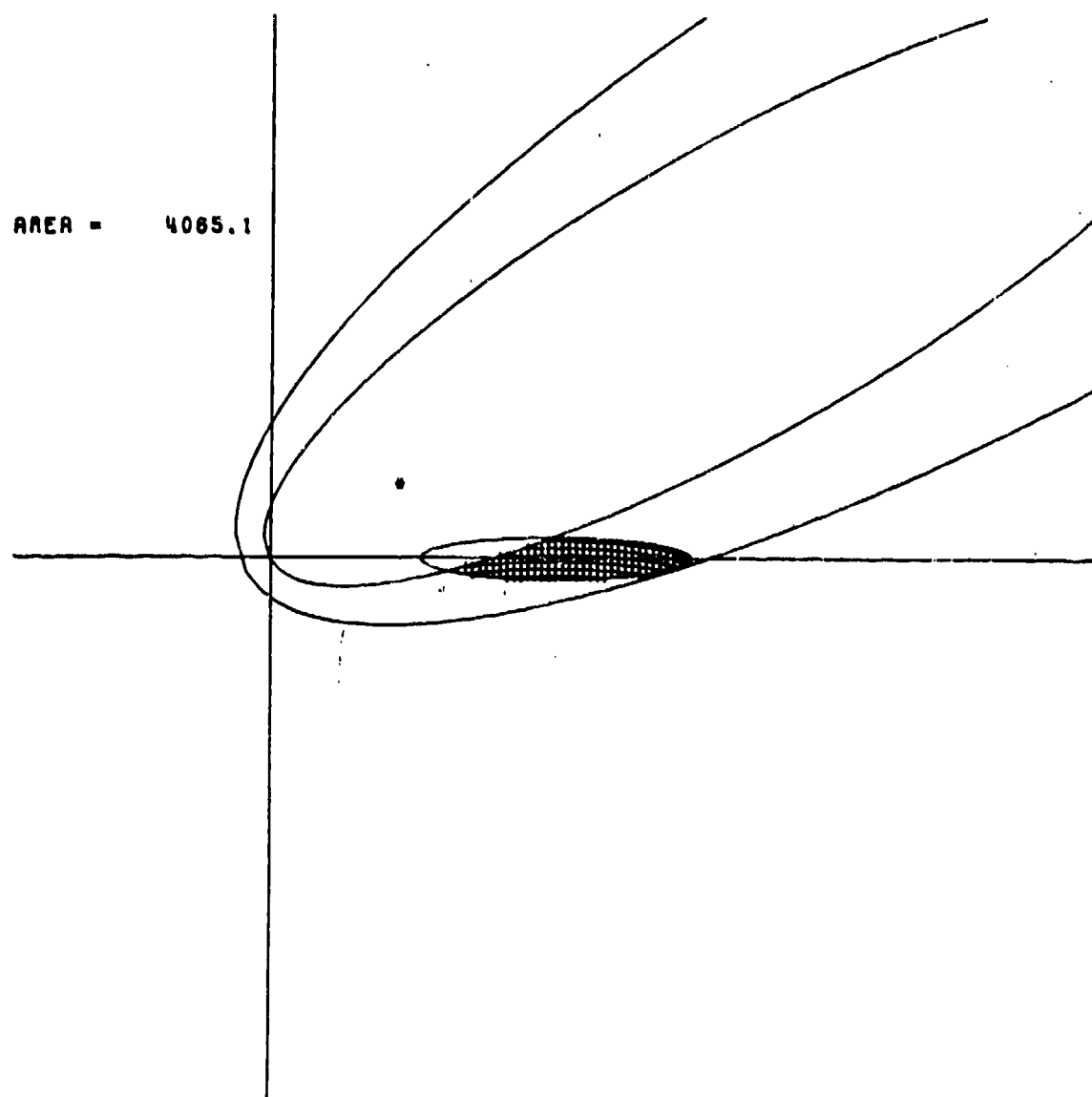


Figure 3-7. A_{gd} for SCAN = 90° , TRACK = 60° ($\phi_s = 30^\circ$)

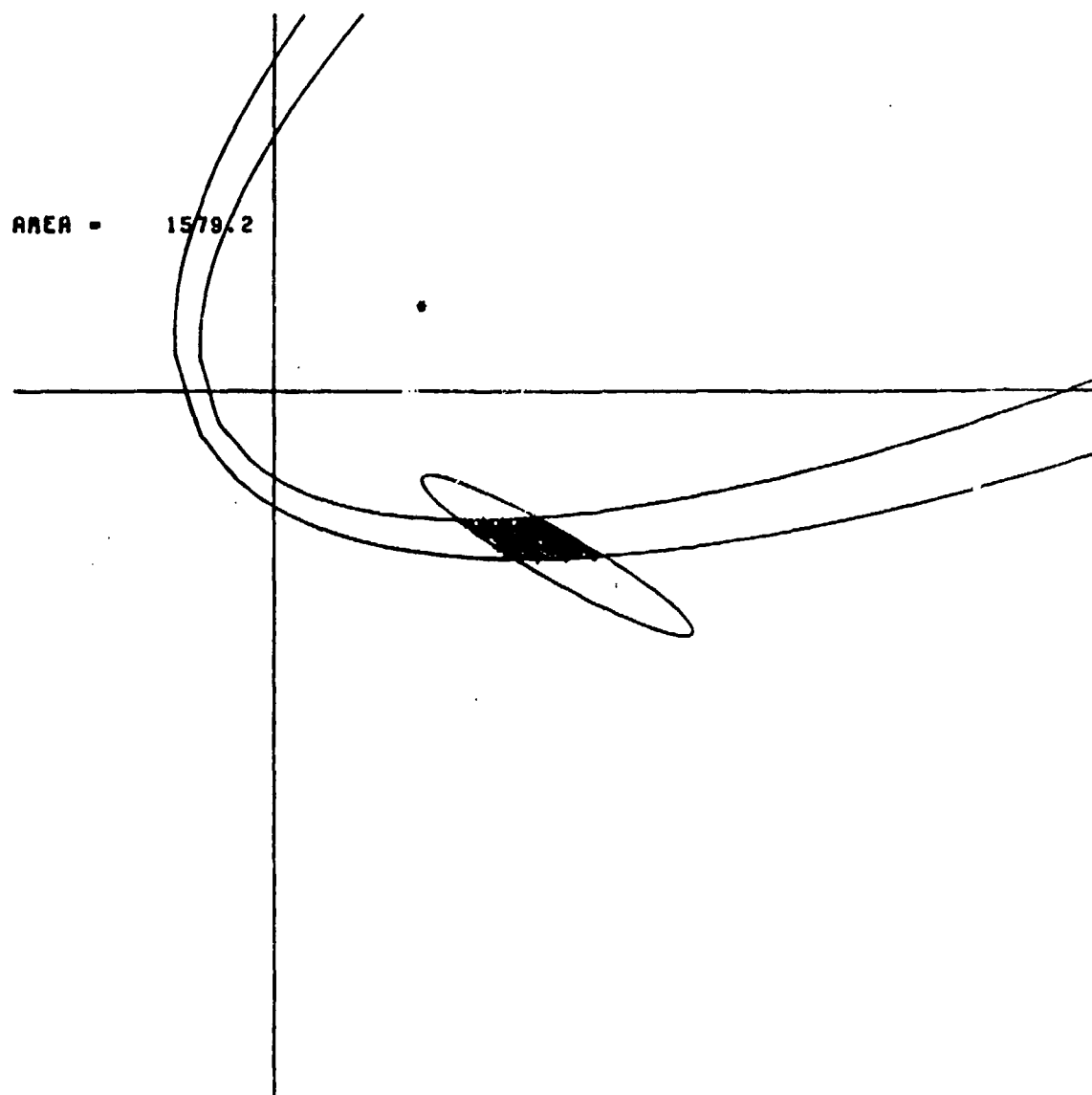


Figure 3-8. A_{gd} for SCAN = 120° , TRACK = 60° ($\phi_s = 60^\circ$)

AREA = 467.9

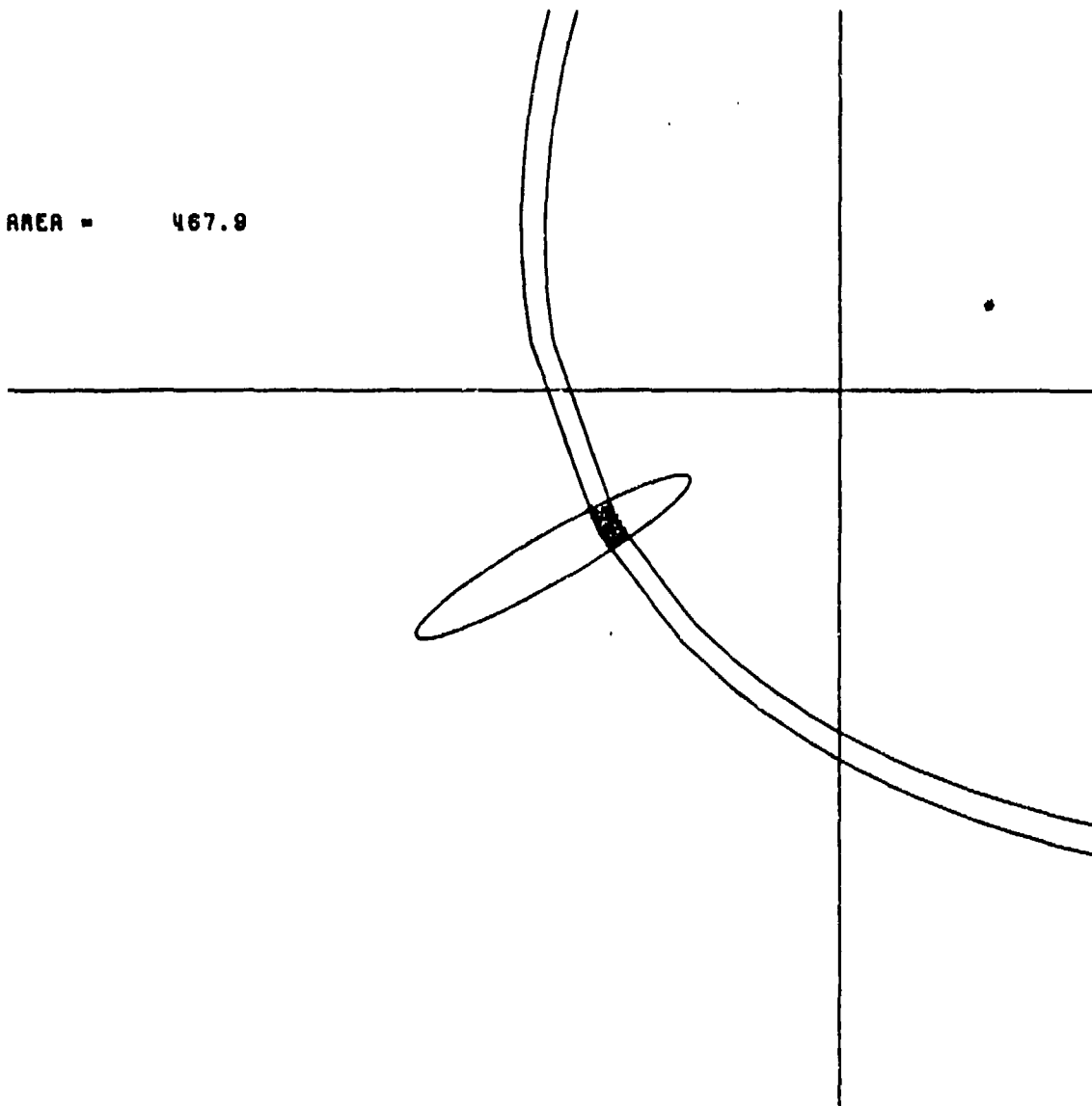


Figure 3-9. A_{gd} for SCAN = 60° (Back), TRACK = 60°
($\phi_s = 180^\circ$).

AREA = 814.2

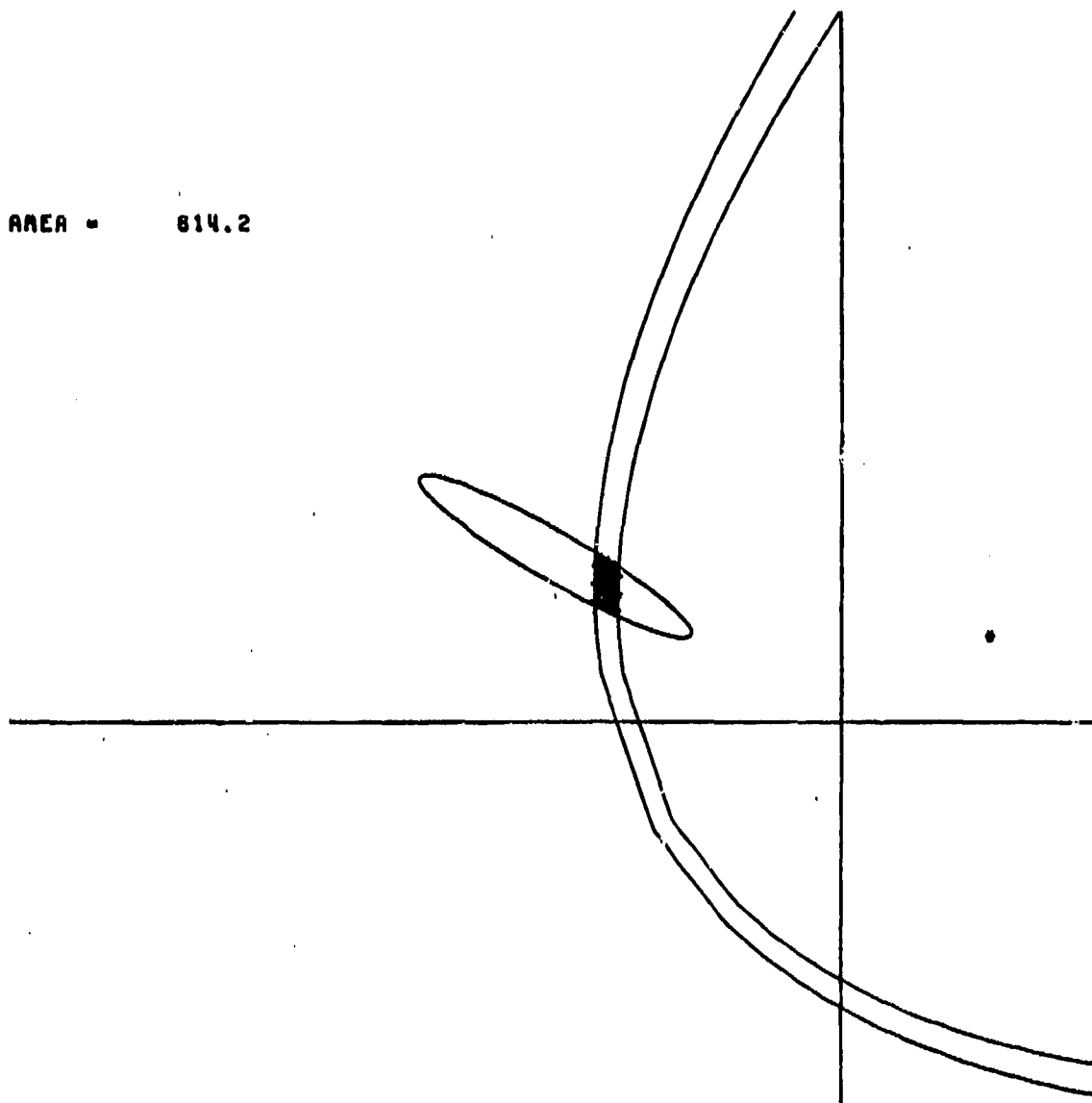


Figure 3-10. A_{gd} for SCAN = 120° (Back), TRACK = 60°
($\phi_s = 120^\circ$)

3.4 DOUBLE-VALUED CALIBRATION CURVE

Perhaps the most serious problem DSA encountered in analyzing the ERIM data is the double-valued nature of the video calibration. That is, two grossly different values of received power can produce the same value of recorded video, (see Fig. 3-11). For this reason, most of the data can be interpreted as either of two different values of σ_0 . While this ambiguity cannot be removed with certainty, its effects can be minimized.

ERIM's solution to this problem was the application of the following "correction":

L-Band

Use the higher value.

X-Band

Try the higher value first; if $\sigma_0 > 0$ dB, use the lower value; if not, use the higher value.

DSA noted that the X-band σ_0 as derived by ERIM was unusually high, and the following procedure was used to interpret the data:

1. Interpret both L and X-band data using first the higher, then, the lower of the possible values.
2. Based on previous ground clutter experience, choose that which seems more reasonable.

Some examples are shown in Figs. 3-12 and 3-13 for the L-band and Figs. 3-14 and 3-15 for the X-band data of 17 March 1978.

It appears that the most reasonable assignment results if the low range is used for X-band and the high range is used for L-band. Unfortunately, in the case of X-band data, this choice greatly restricts the range of values which may be attributed to a given data point. Note in Fig. 3-11 for example,

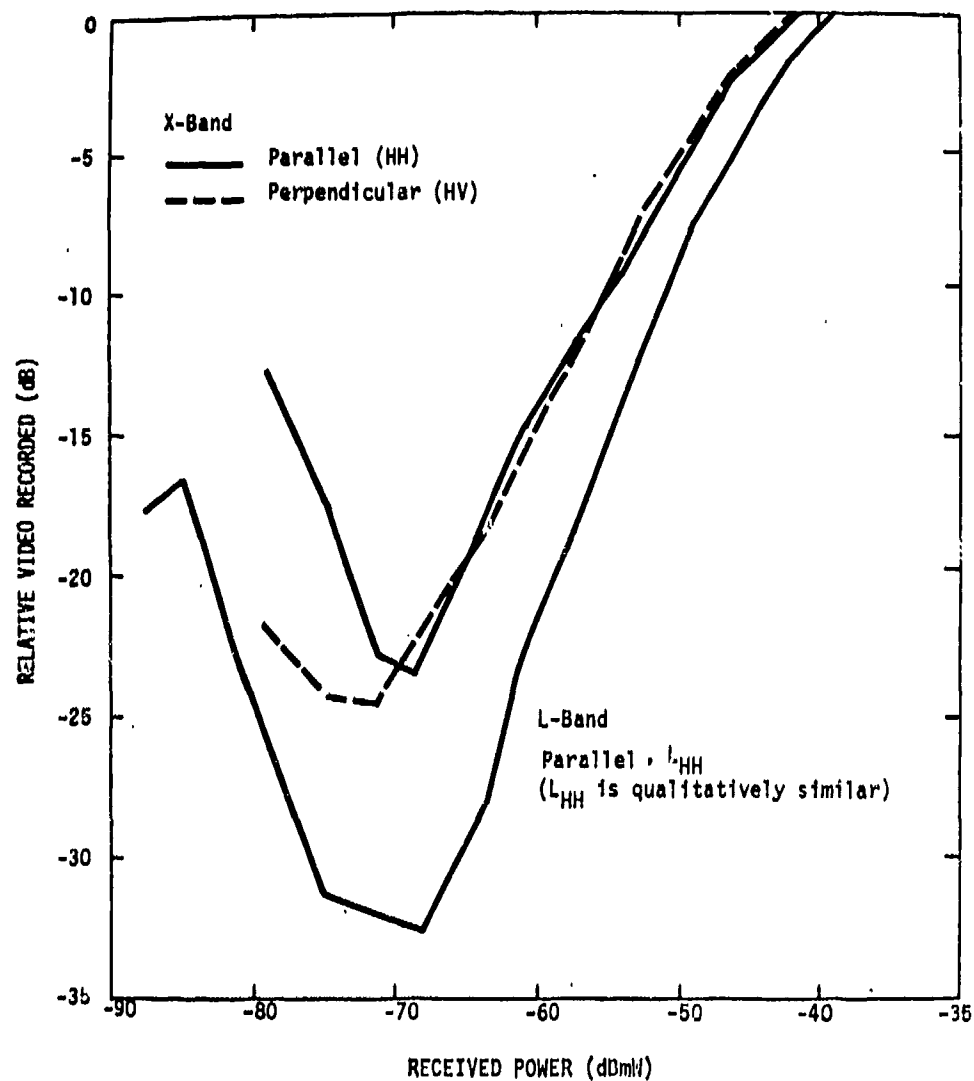
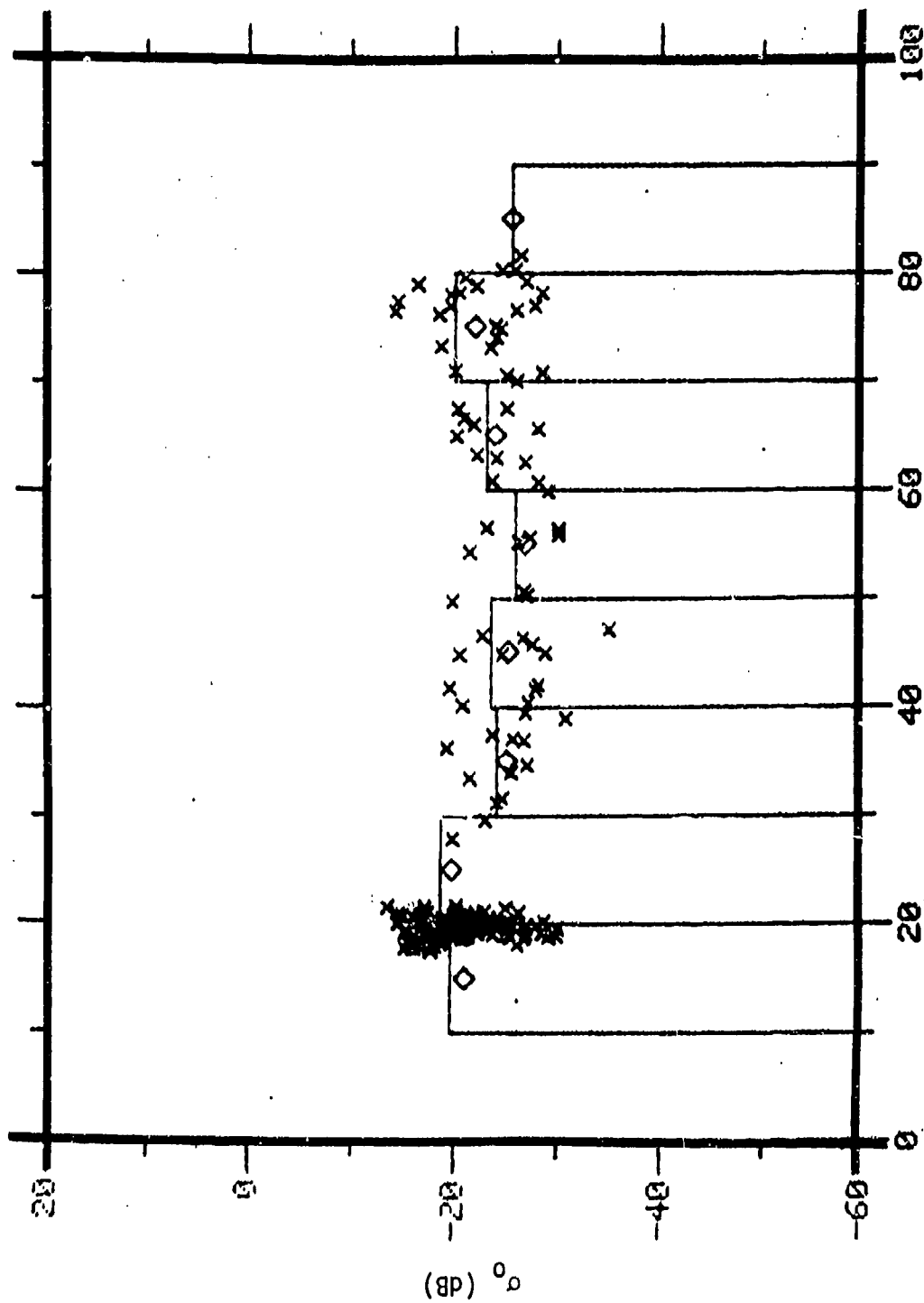
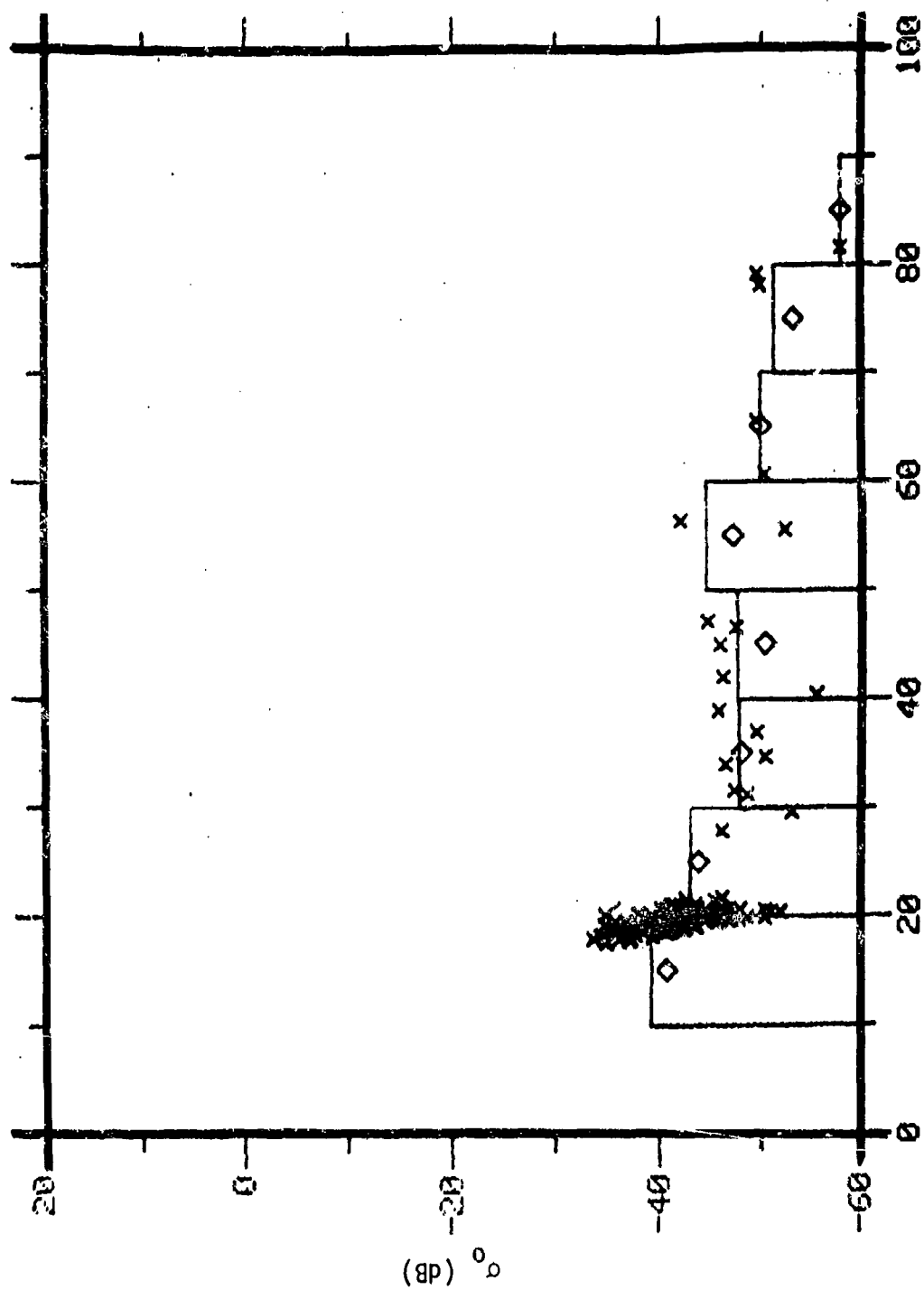


Figure 3-11. Double-Valued Calibration Curves



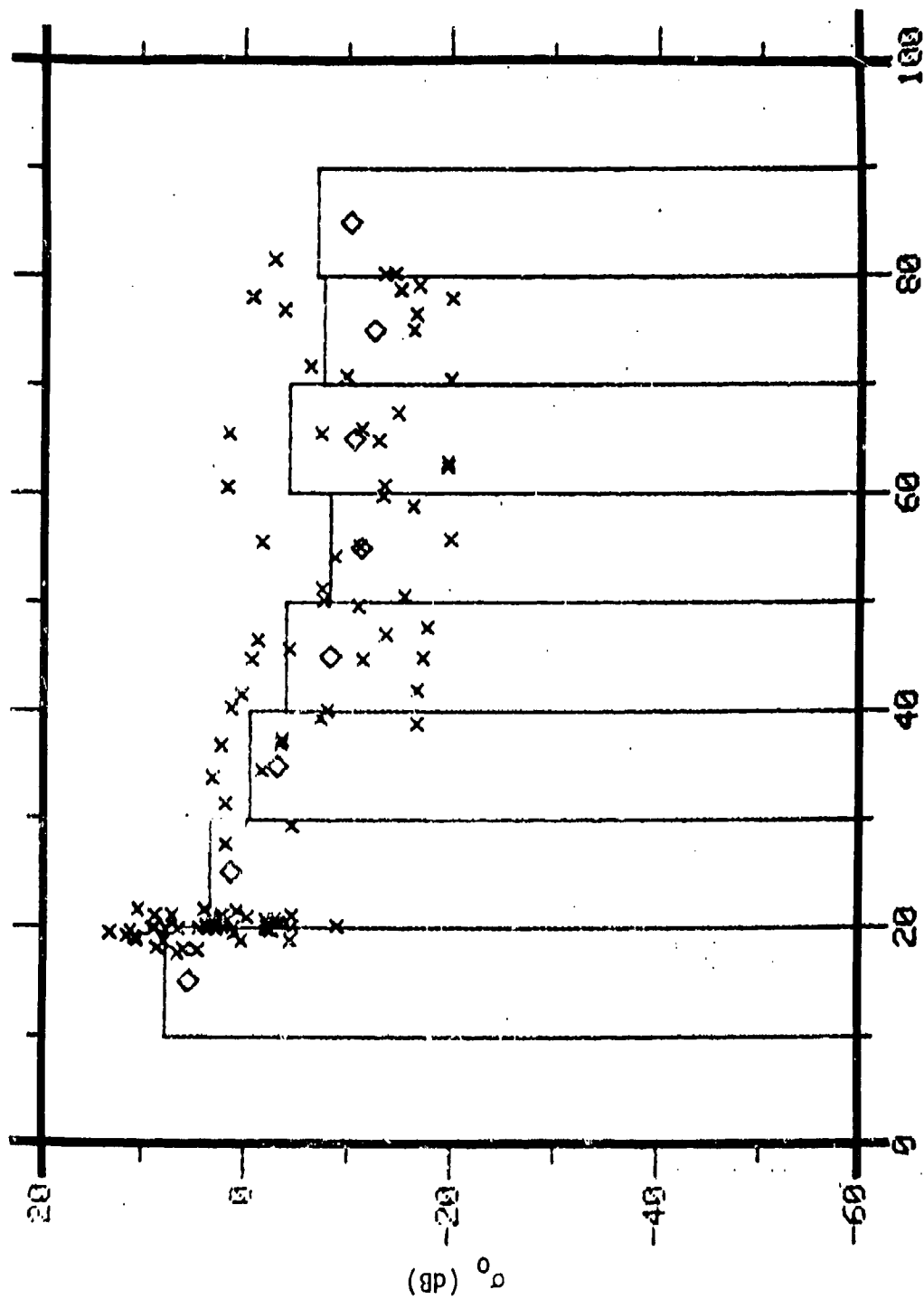
INCLINATION OF THE BISTATIC BISECTOR (deg)

Figure 3-12. L-Band Principal Polarization (HH) Bistatic σ_0 Data
of 17 March 1978, Passes 3 and 10, High Range



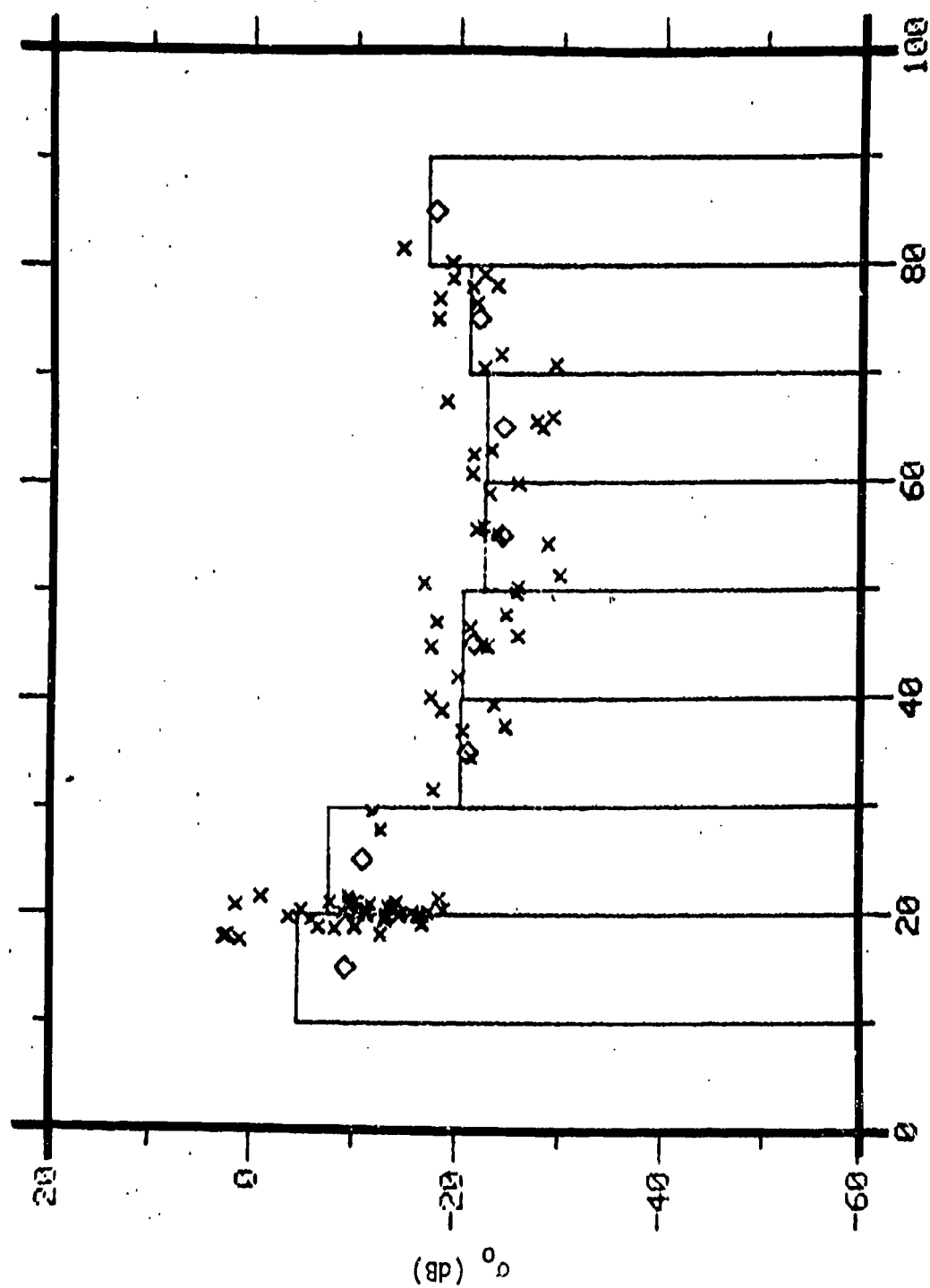
INCLINATION OF THE BISTATIC BISECTOR (deg)

Figure 3-13. L-Band Principal Polarization (HH) Bistatic σ_0 Data
of 17 March 1978, Passes 3 and 10, Low Range



INCLINATION OF THE BISTATIC BISECTOR (deg)

Figure 3-14. X-Band Principal Polarization (HH) Bistatic σ_0 Data
of 17 March 1978, Passes 3 and 10, High Range



INCLINATION OF THE BISTATIC BISECTOR (deg)

Figure 3-15. X-Band Principal Polarization (HH) Bistatic σ_0 Data of 17 March 1978, Passes 3 and 10, Low Range

the lower range of the calibration curve spans only 10.3 dB for X_{HH} and 7.5 dB for X_{HH} , while the upper range spans nearly 25 dB.

3.5 ILLUMINATION CORRECTION

Because of the difficulty in keeping the transmit beam always pointed at the base of the receiver tower, the illumination of the receiver footprint is nonuniform with time. To correct for this nonuniformity, ERIM measured and recorded the illumination at the base of the receiver tower. When DSA first analyzed the data there was 20 to 30 dB spread in the σ_0 values for similar geometries. This was consistent with the spread in the data processed by ERIM. However, when the data are displayed as a function of time, it is clear that perhaps 10 dB of spread is caused by static factors and the remainder is caused by a long-term drift in the measurement system. Furthermore, this drift is correlated with the illumination correction factor. Figure 3-16 shows for pass 3 of 17 March 1978, the time histories of the σ_0 data and the illumination correction factor.

The rapid rise in σ_0 that accompanies the rapid drop in the illumination suggests that when the base of the tower is on the edge of the transmit beam where antenna gain (and, consequently, the spacial variation of the ground illumination) is varying rapidly, a measurement of the illumination at the tower base is not at all indicative of the illumination on the receiver footprint. As a consequence, proper calibration of the data having a large correction factor is not possible, and for that reason DSA edited out the data having an illumination correction factor greater than 10 dB. This at L-band at least, greatly reduced the spread in the σ_0 values.

In some cases, the illumination correction factors are positive which implies that the power incident on the ground in front of the receiver is higher than theoretically possible. In fact, for passes 3 and 10 of 18 March 1978 the values are all positive, reaching as high as 6 dB. This, according to ERIM, was an error that has been corrected.

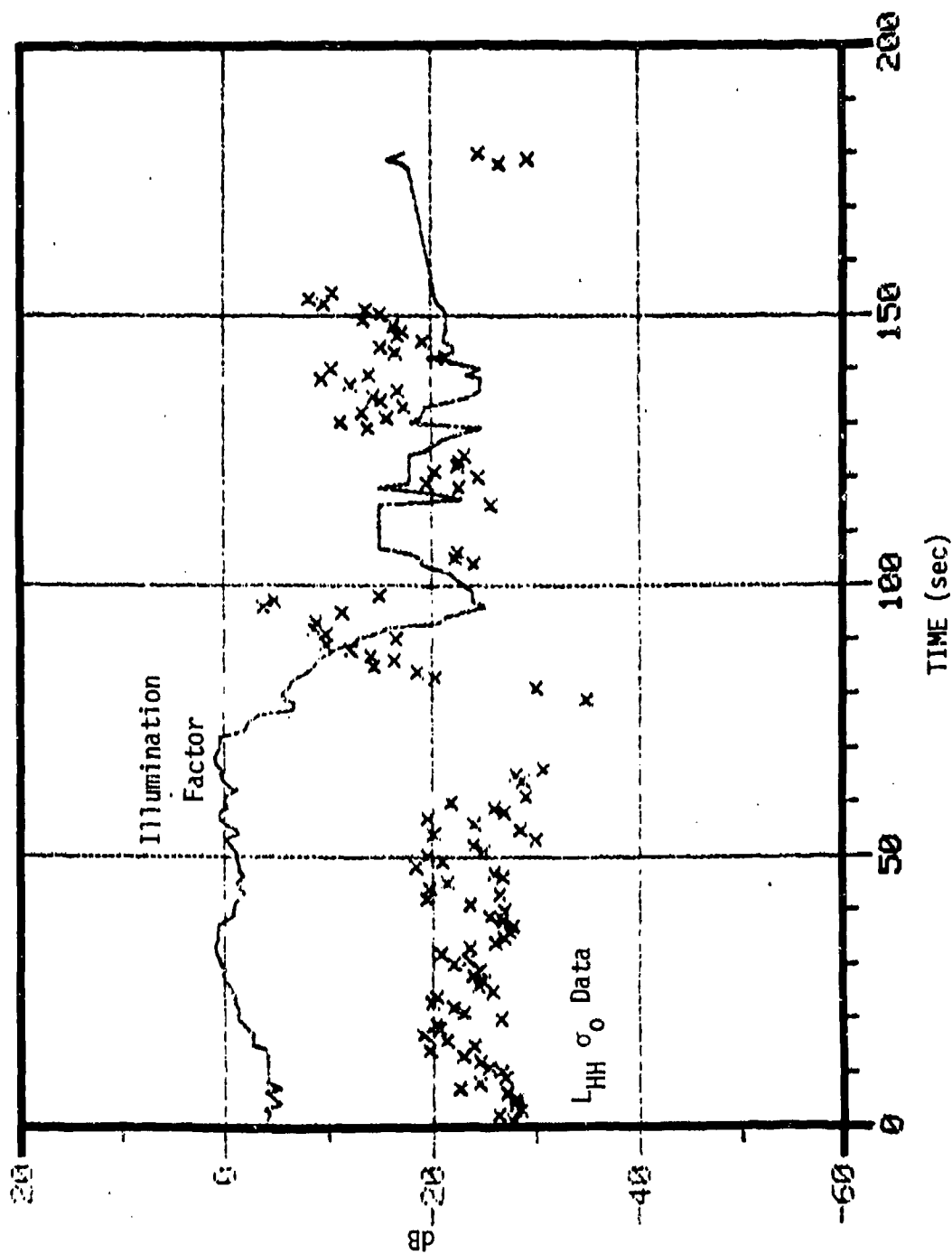


Figure 3-16. Time Histories of σ_o and Illumination Correction Factor

3.6 NUMERICAL DISCREPANCIES

For the most part, the values of σ_0 derived by ERIM and DSA using the same raw data are consistent. That is, most discrepancies can be explained by a different interpretation of the double-valued calibration curve, or DSA's editing of data which required large illumination corrections, etc. However, there is one glaring exception.

Before attempting to process the raw data, DSA noticed apparent anomalies in the processed data ERIM supplied. One of these occurred in the 18 March 1978 data and involved a huge discontinuity in going from a predominantly forward to a predominantly backward scattering geometry. For intermediate geometries where $\phi_s = 90^\circ$, the data for the two passes should match up. However at $\phi_s = 90^\circ$ on passes 3 and 10, there is a 30 dB discrepancy in both the L-band (HH) and HV data.

This anomaly was among those which DSA decided to attempt to resolve by performing the complete data processing cycle. When this was done the anomaly was not observed. There is a discrepancy of about 25 dB between the L-band σ_0 values obtained by DSA and ERIM on pass 10 and there is substantial agreement on pass 3. These are plotted in Figs. 3-17 and 3-18. The discrepancy cannot be explained by the double-valued calibration curve because both ERIM and DSA used the high range for L-band data. Neither can it be caused by the illumination correction factor since for this pass, the illumination was always high. When alerted to this problem, ERIM reprocessed the data of 17 and 18 March and the results show the discrepancy at $\phi_s = 90^\circ$ to be 20 dB rather 30 dB (see Fig. 3-19), the pass 10 data of ERIM being in excess of 10 dB higher than that of DSA.

3.7 NOISE SPIKES

One of the first problems encountered in the DSA analysis effort was the presence of huge noise spikes in both parallel polarization channels of the first file of tape BISTATF. This file was labeled "Calibration #1 (video)." An example of these noise spikes is shown in Fig. 3-20. They are characterized by a sudden increase in the video output and a trail-off

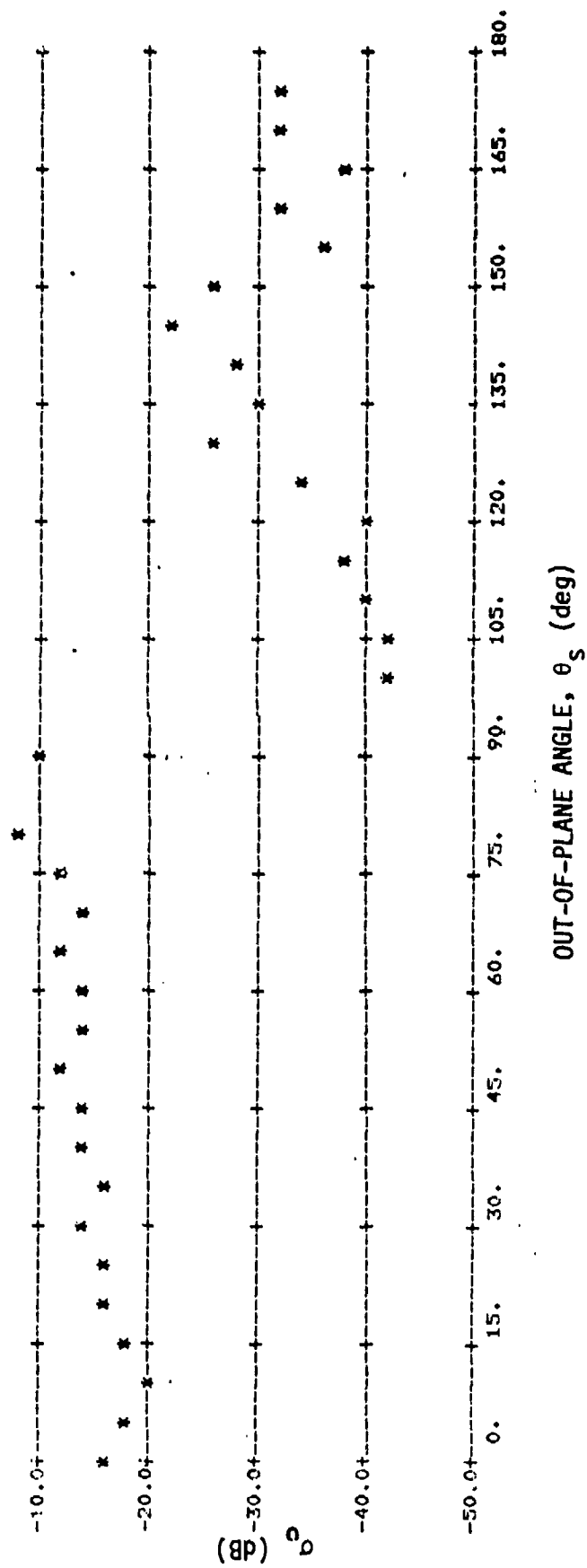


Figure 3-17. L-Band Orthogonal Polarization (HV) Bistatic σ_o Data Processed by ERIM,
 Passes 3 and 10 of 18 March 1978

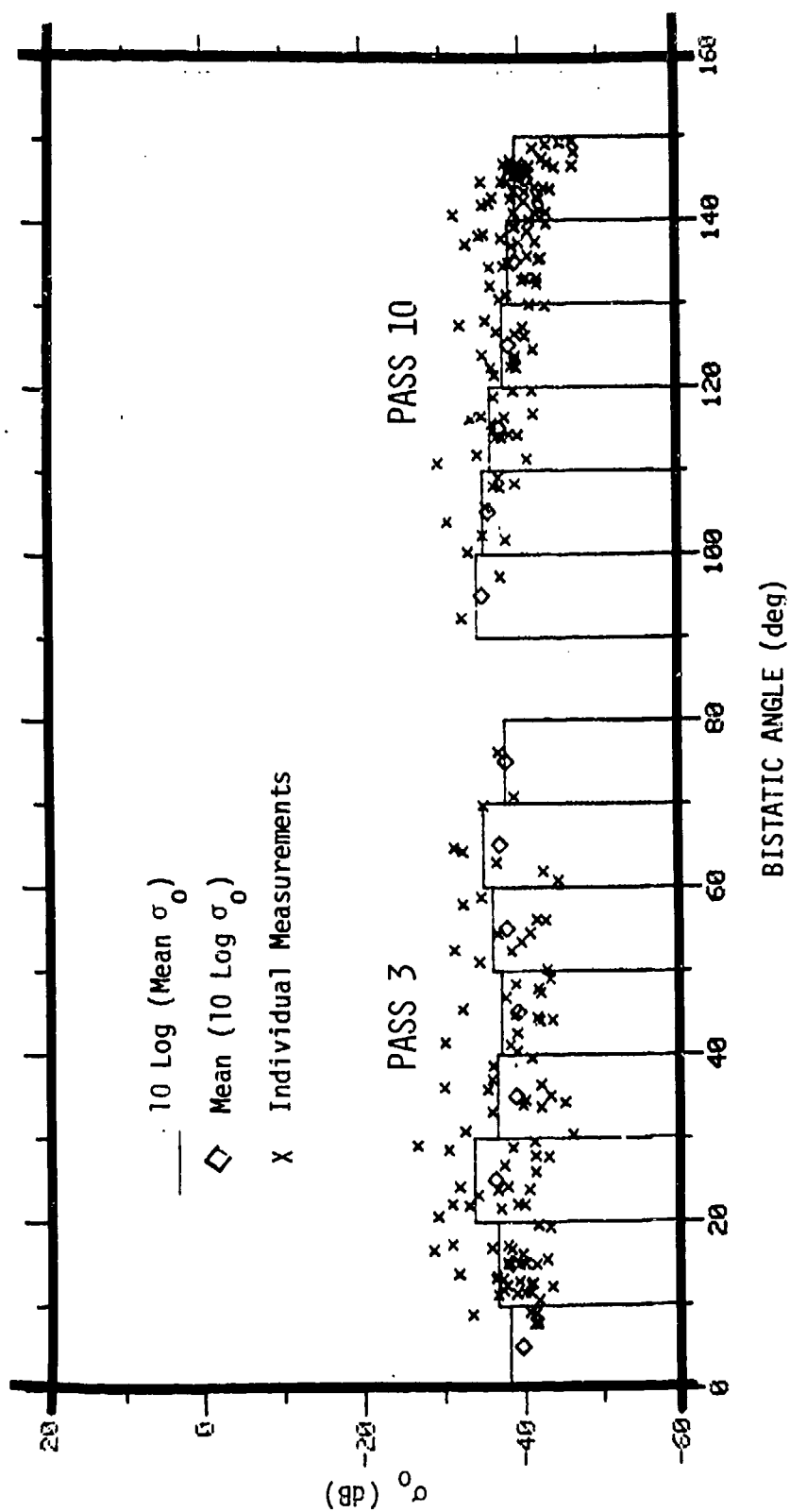


Figure 3-18. L-Band Orthogonal Polarization (HV) Bistatic σ_0 Data
Processed by DSA, Passes 3 and 10, 18 March 1978

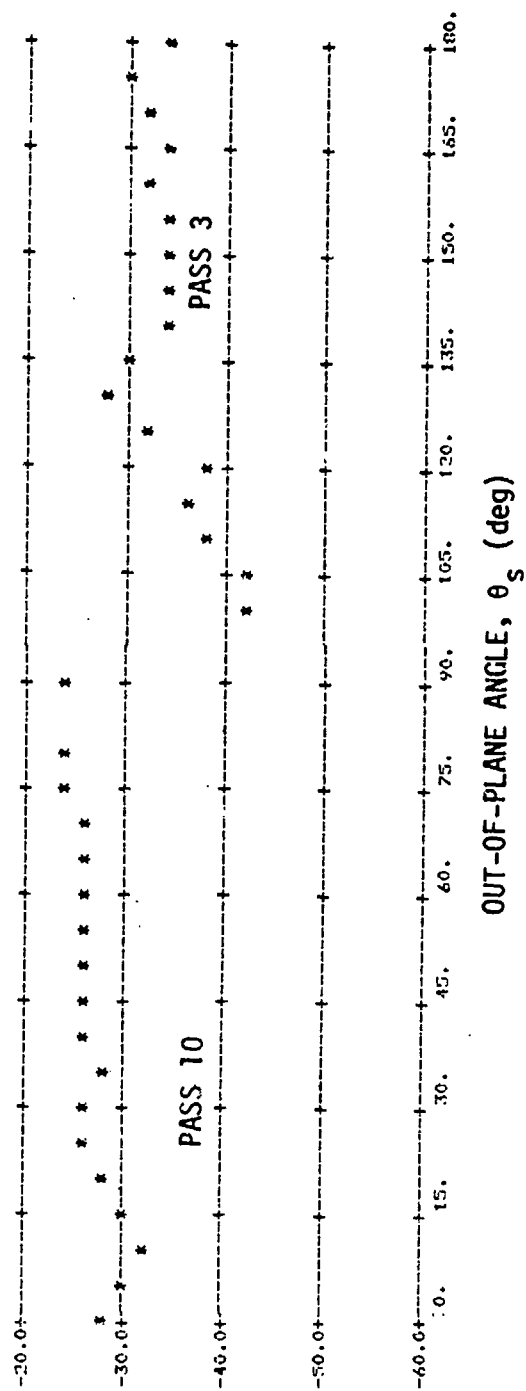


Figure 3-19. L-Band Orthogonal Polarization (HV) Bistatic σ_0 Data Reprocessed by ERIM, Passes 3 and 10, 18 March 1978

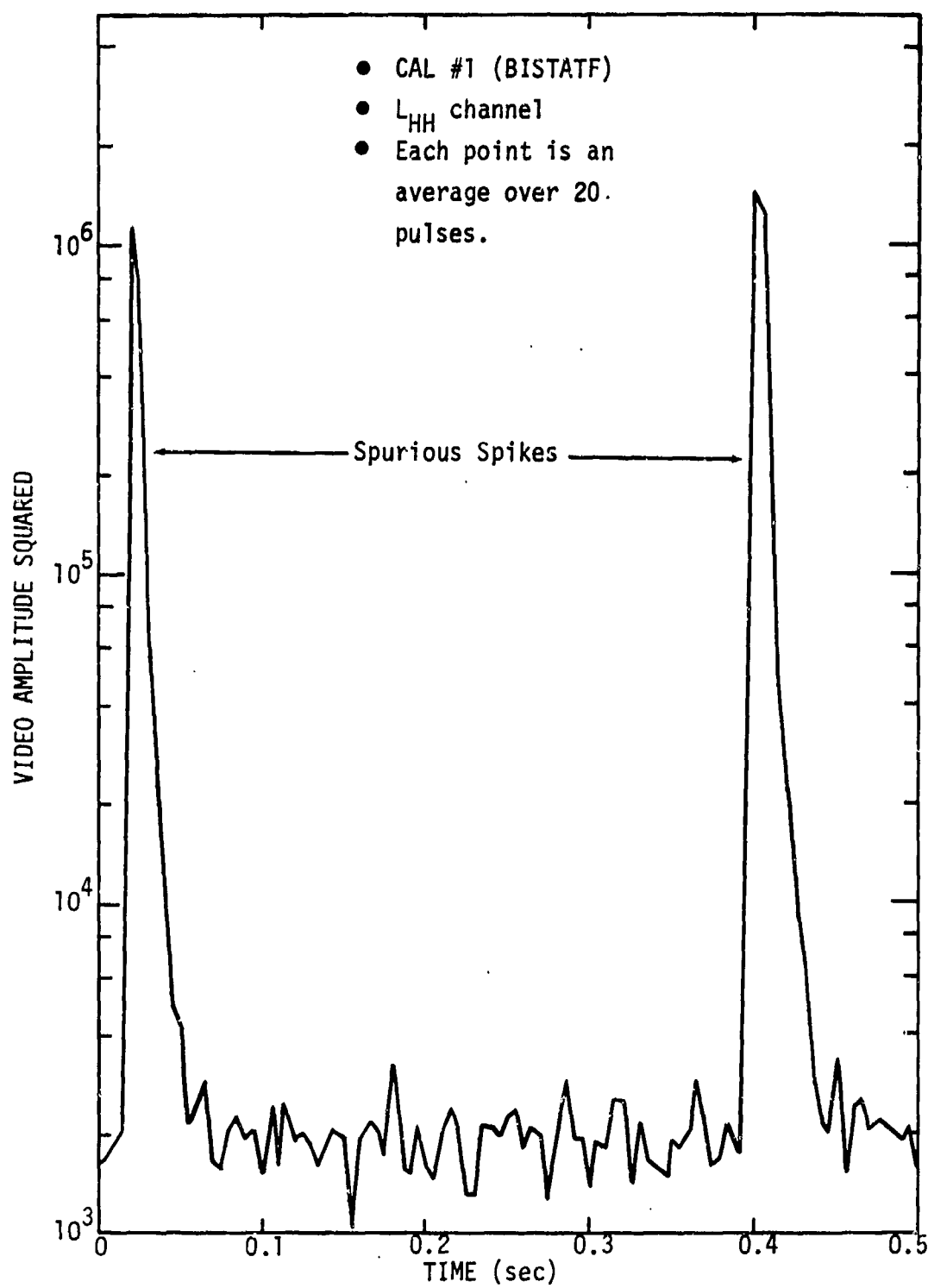


Figure 3-20. Time History Showing Noise Spikes

within about 300 samples or 75 msec. We soon learned that ERIM did not use these calibration values to process the data, but used instead calibration runs from another tape.

Further investigation showed that the spikes were not nearly so numerous in the actual clutter video data but were nevertheless present in both passes (3 and 10) which DSA analyzed for the 17 March 1978 date.

Partially because of the noise spike problem, DSA edited the video data in batches of 300 samples rather than the number in one beam scan (~ 2000). This apparently removed most if not all noise spikes, and DSA concluded that the problem did not seriously affect the results.

4.0 MOST RECENT ERIM DATA

4.1 DESCRIPTIONS OF TERRAIN, WEATHER CONDITIONS, AND BISTATIC GEOMETRY

Two test sites were employed for this series of bistatic terrain scattering measurements. Those occurring on 17, 18, and 19 February 1978, employed Site II located at the Willow Run Airport outside of Ypsilanti, Michigan. This site was completely snow covered with an average snow depth of 12 in to 20 in. The dielectric constant of the snow varied from 1.71 to 1.95 over the 3 days. The snow surface was very smooth with respect to X-band (3-cm wavelength) with gradual slopes. There were scattered regions throughout the site area where dry weeds were visible, some extending 1 or 2 ft above the snow surface. A photograph of Site II appears in Fig. 4-1. Table 4-1 summarizes these site characteristics as well as the weather conditions that existed during the three days of measurements and the bistatic measurement angles for which data were collected.

The measurements occurring on 17 and 18 March 1978 employed Site III consisting of an apple orchard located northwest of Ann Arbor, Michigan. The average height of the trees was 25 ft. The ground was completely snow covered with wet snow having a dielectric constant of greater than 3.15. The snow depth was 6 to 10 in. The trees' branches were free of snow. A photograph of Site III appears in Fig. 4-2. Table 4-1 summarizes the site characteristics as well as the weather conditions that existed during the measurement period and the bistatic measurement angles for which data were collected.

4.2 MODELS OF σ_0 DERIVED FROM RELEVANT MONOSTATIC AND BISTATIC DATA

As a part of the task of evaluating and interpreting the ERIM data, DSA has brought together the relevant monostatic and bistatic clutter data for the purpose of deriving a best estimate of what the new data should look like. Because no bistatic data are available to represent the terrain type found at Site III and only a limited amount of bistatic data are available that represent Site II, monostatic data and use of the

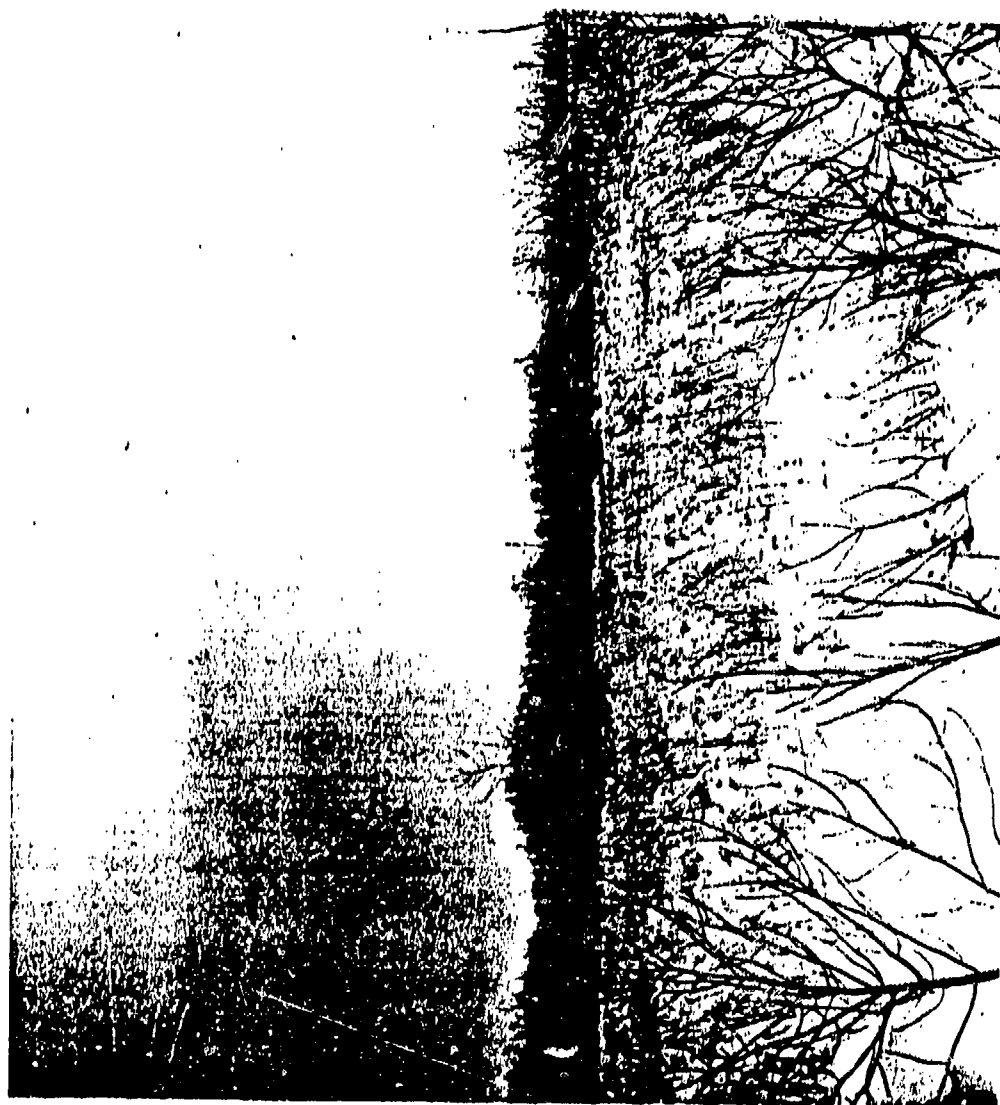


Figure 4-1. Site II: 17, 18 and 19 February 1978: Snow Covered Flat Terrain
With Weeds and Scrub Trees Extending Above the Snow Surface

TABLE 4-1
DESCRIPTION OF TEST AREAS AND BISTATIC MEASUREMENT ANGLES

Date	Site Terrain	Weather	Wind	θ_s	θ_i	ϕ_s
2/17/78	Site II Snow covered with weeds extending 1 to 2 ft above snow. Snow surface was smooth with respect to X-band. Snow depth 12" to 20".	20° F, sky clear to 2000'	5-10 knots from West	30° 70°	70° 70°	0-180° 0-180°
2/18/78		18° F, sky clear	5-10 knots from West	60° 70°	80° 80°	0-180° 0-180°
2/19/78		20° F, sky clear	Calm	60° 70° 80°	60° 60° 65°	0-180° 90-180° 0-90°
3/17/78	Site III tree orchard average height = 25'. Snow covered surface. 6" to 10" depth. Wet snow.	20° F, sky clear	Light	60° 60° 60° 60°	60° 70° 80° 84°	0-180° 0-180° 0-180° 0-180°
3/18/78		20° - 30° F, sky high overcast	15-20 knots gusts to 35 knots	60° 60° 70° 70° 80° 80° 84° 84°	70° 80° 70° 80° 70° 80° 70° 80°	0-180° 0-180° 0-180° 0-180° 0-180° 0-180° 0-180° 0-180°



Figure 4-2. Site III: 17 and 18 March 1978: Snow Covered
Ground in Apple Orchard

bistatic theorem¹ will supplement the available bistatic data. The bistatic theorem says, in effect, that the bistatic cross section of an object when observed with a bistatic system having a bistatic angle, β , (the angle formed by the transmitter-target-receiver) is, under the appropriate conditions, equal to the monostatic cross section of that target when viewed from a point on the line bisecting the angle β . The conditions under which this theorem is valid are: (1) the target must be sufficiently smooth, and (2) the wavelength is small in comparison to the body dimensions.

The terrain at Site II is a smooth (at X-band) snow-covered field with dry weeds, grass, and small trees protruding from the surface of the snow. The terrain surface appears to meet the requirements for bistatic theorem validity, and Fig. 4-3 shows the available X-band, monostatic data for dry weeds and grass with snow cover plus a single data point for dry weeds without snow. The σ_0 data are plotted against the grazing angle or equivalently (through the bistatic theorem) the inclination of the bistatic bisector. The dotted lines in the figure will be discussed later.

The available bistatic data on terrain similar to that at Site II were taken by Peak and Cost² and Peak and Oliver³ for dry grass with 1/2 in of nonuniform snow cover. Their experimental equipment consisted of a nonrange gated, stationary receiver and transmitter observing terrain samples on railroad flat cars which moved slowly past the radar. Their data showed anomalous behavior when the transmitter and receiver were essentially collocated, i.e., near monostatic operation, and viewing the terrain samples at very low grazing angles (10°). The very large σ_0 values (typically -20 dB to -10 dB) can be attributed to the sidelobes of the transmitter and receiver beams illuminating the edges and undercarriage of the flat car and perhaps the railroad tracks. For this reason, the low

¹J. W. Crispin, Jr., and K. M. Siegel, op. cit., page 158.

²R. L. Cosgriff, W. H. Peake, and R. C. Taylor, "Terrain Return Measurements and Applications," Transactions of the 1959 Symposium on Radar Return, University of New Mexico, May 11-12, 1959.

³R. L. Cosgriff, W. H. Peake, and R. C. Taylor, op. cit.

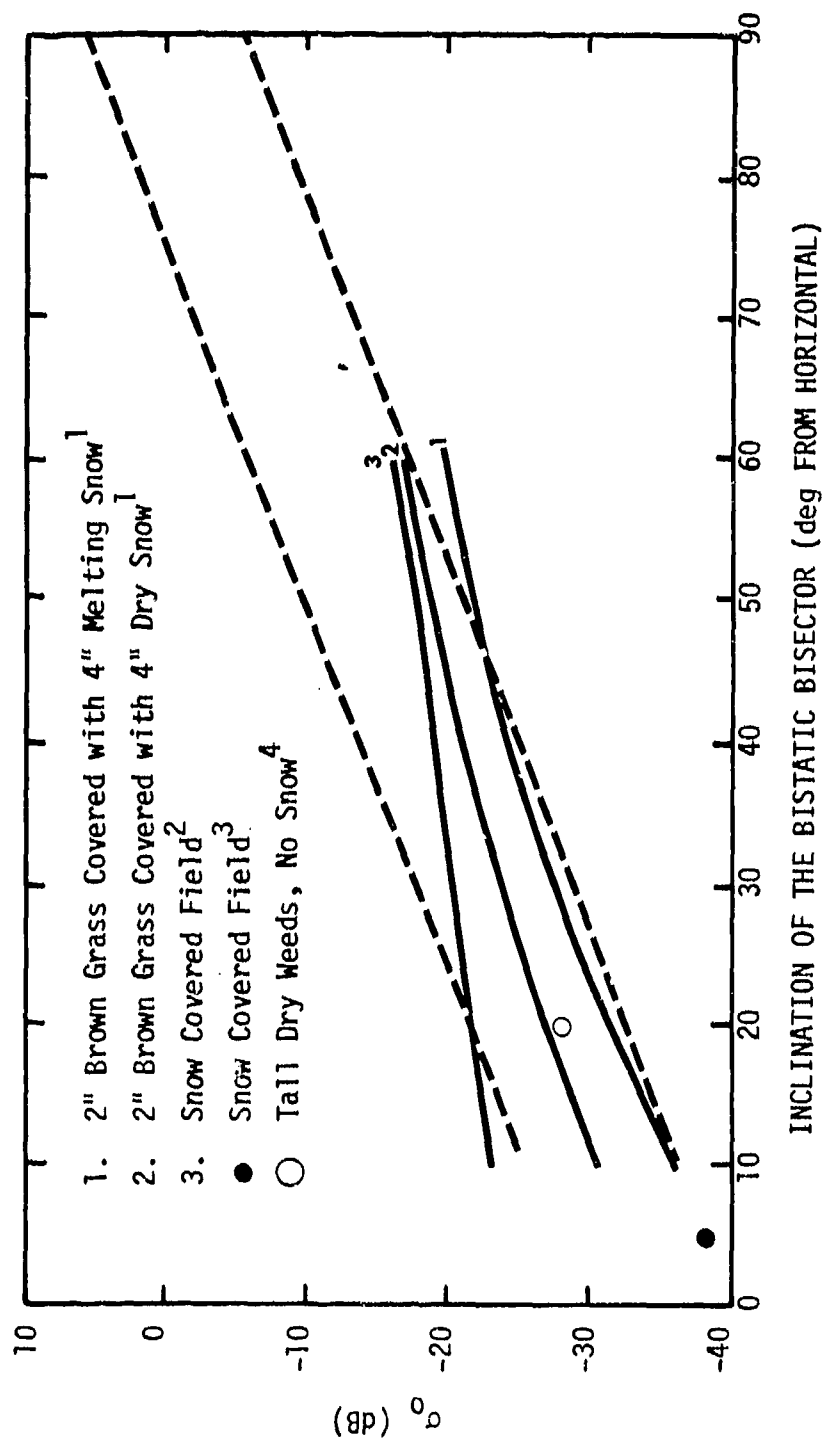


Figure 4-3. Monostatic σ_0 Data for Snow, Dry Grass, and Weeds, X-Band HH Polarization

¹R. L. Cosgriff, W. H. Peake, and R. C. Taylor, op. cit.

²K. Soofi, Clutter Model for Land, Forest, Snow, Seaice, and Ocean, Remote Sensing Laboratory. University of Kansas, RSL Technical Report TR2923-2, July 1978.

³T. Linell, An Experimental Investigation of the Amplitude Distribution of Radar Terrain Return, Sixth Conference of the Swedish National Committee on Scientific Radio, March 13, 1963.

⁴C. R. Grant and B. S. Yaplee, Back Scattering from Water and Land at cm and mm Wavelength, Proceedings of the IRE, Vol. 45, pp. 976-82, July 1957.

grazing angle data were deleted from this bistatic data; and, for the reason of a direct path link through transmitter and receiver sidelobes, the data having bistatic angles greater than 155° were deleted. The remaining bistatic data appearing in Fig. 4-4 fall into a band 11 dB wide shown with dotted lines. When this band is placed on the graph of monostatic data, (Fig. 4-3), we find good agreement between the monostatic data and the bistatic data when the bistatic theorem is used. The X-band bistatic σ_0 model for Site II data comparison will be the 11 dB band containing the bistatic data shown in Fig. 4-4.

Bistatic L-band data for dry grass with or without snow cover are not available; however, some L-band monostatic data on a snow-covered field of grass and weeds exists.¹ That data with the application of the bistatic theorem form the basis for the L-band principal polarization bistatic σ_0 model for Site II shown in Fig. 4-5.

Both Hayes et al.² and Ament et al.³ have taken cross polarized monostatic data on tree-covered terrain. Ament's data show the ratio of HH return to HV return to vary with grazing angle in a range of 8 dB to 12 dB, where HH refers to horizontal polarization or transmission and horizontal polarization on reception, and HV refers to horizontal polarization on transmission and vertical polarization on reception. These are referred to as principal and orthogonal polarizations in the discussion of the ERIM data, and the orthogonal polarization data should be expected to be 10 dB lower than the principal polarization data at both Sites II and III.

¹R. K. Moore, "Radar Return from the Ground," Bulletin of Engineering No. 59, University of Kansas, 1969.

²R. D. Hayes, J. R. Walsh, D. F. Eagle, H. A. Ecker, M. W. Long, J. G. B. Rivers, and C. W. Stuckey, Study of Polarization Characteristics of Radar Targets, Engineering Experiment Station, Georgia Institute of Technology, Final Report, Contract DA-36-039-sc-64713, October 1958.

³W. S. Ament, et al., op. cit.

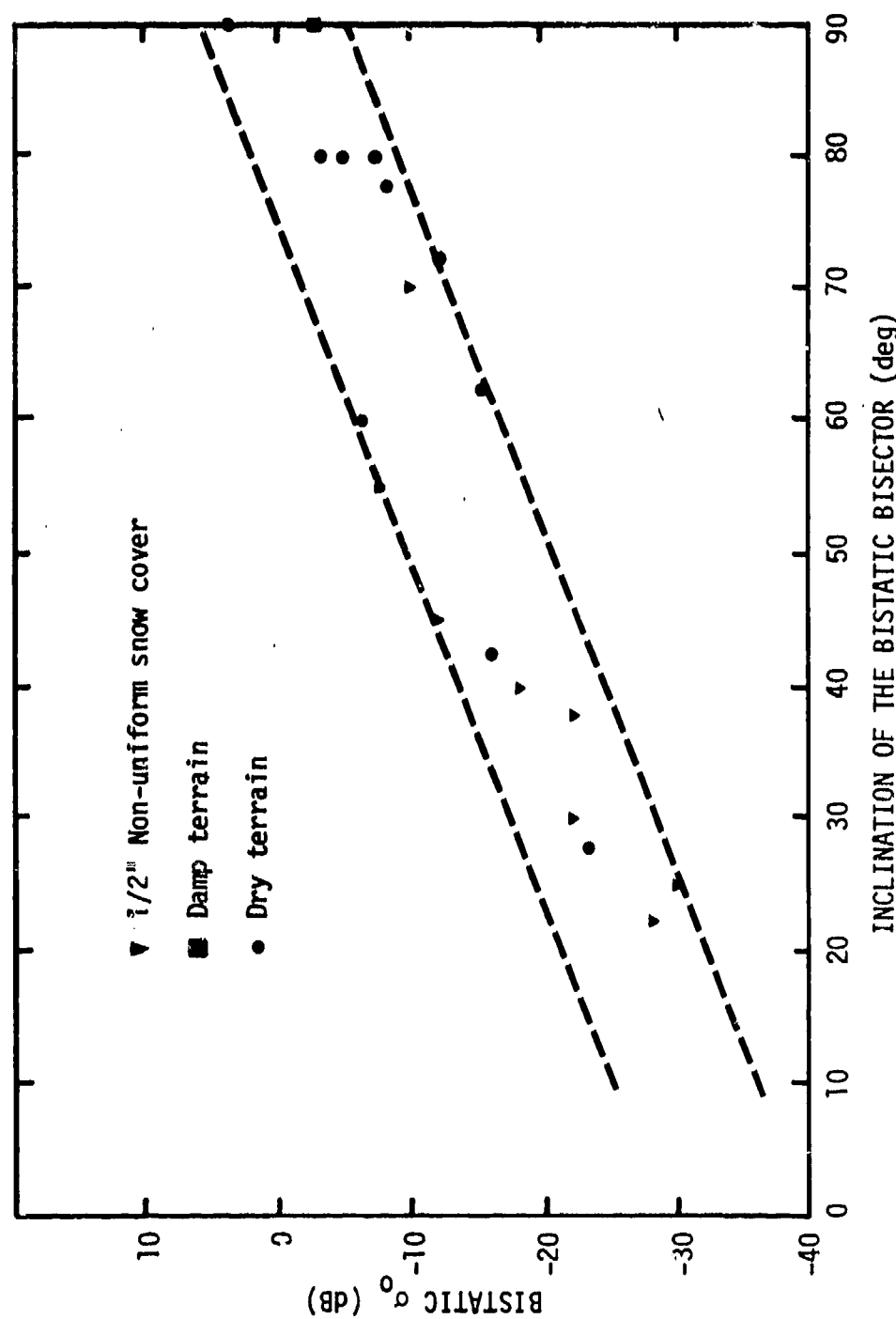
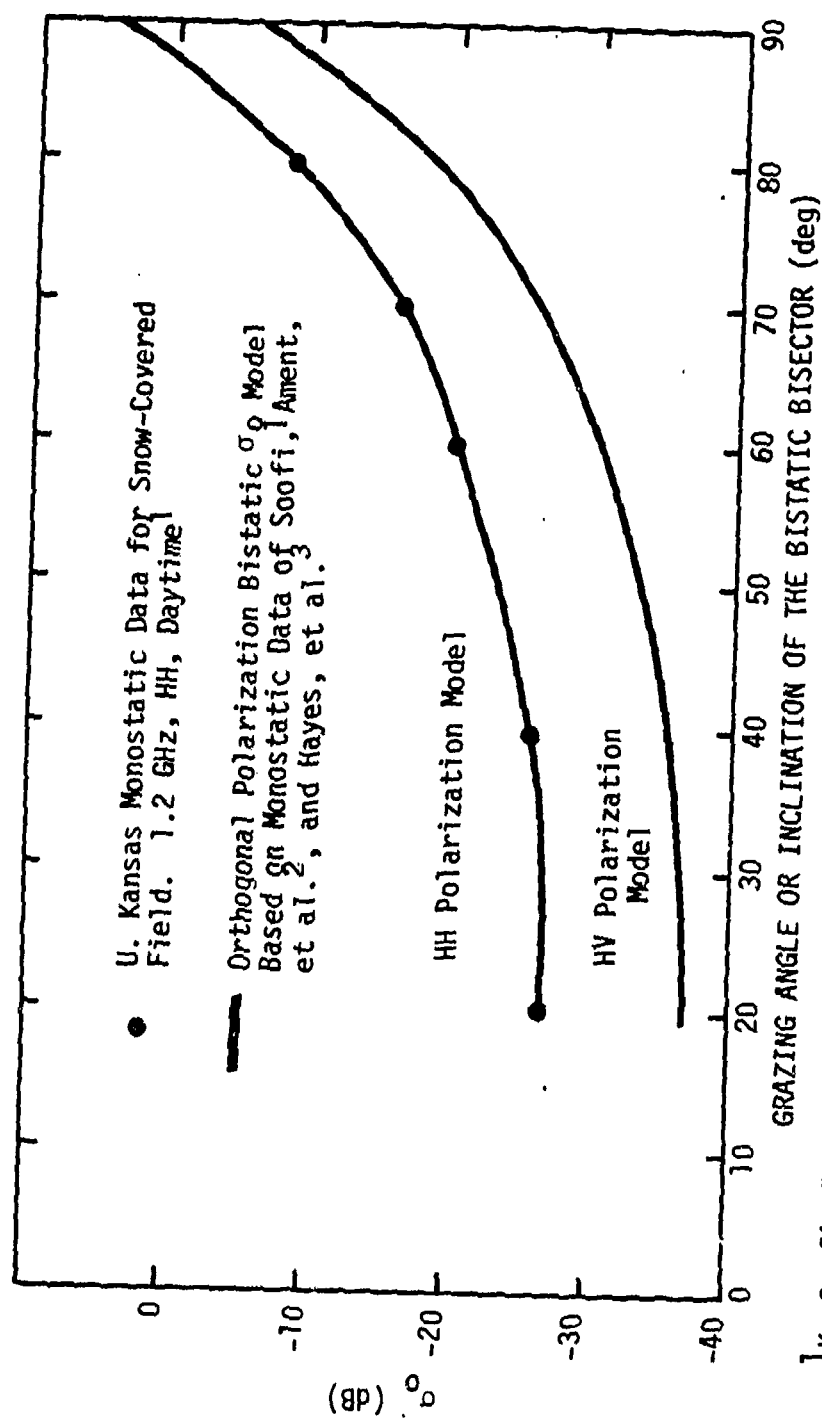


Figure 4-4. Bistatic σ_0 Data for Dry Grass and Site 2 Model for X-Band, HH Polarization^{1,2}

¹W. H. Peake and T. L. Oliver, op. cit.

²W. H. Peake and S. T. Cost, The Bistatic Echo Area of Terrain at 10 GHz, Performed under Subcontract No. 1 to Contract AF33(615)-1153.



¹K. Soofi, "Clutter Model for Land, Forest, Snow, Seaice, and Ocean," Remote Sensing Laboratory, University of Kansas, RSL Technical Report TR 2923-2, July 1978.

²W. S. Ament, et al, op. cit.

³R. D. Hayes, J. R. Walsh, D. F. Eagle, H. A. Ecker, M. W. Long, J. G. B. Rivers, and C. W. Stuckey, "Study of Polarization Characteristics of Radar Targets," Engineering Experiment Station, Georgia Institute of Technology, Final Report, Contract DA-36-039-sc-64713, October 1958

Figure 4-5. Site 2 L-Band Bistatic σ_0 Model for Principal and Orthogonal Polarizations

The only available data on terrain typical of Site III is that attributed to Ament et al.,¹ which are X-band monostatic measurements of pine forest with heavy undergrowth and patches of snow on the ground. Although this terrain does not meet the requirements for smoothness required for invoking the bistatic theorem, these being the best available data will constitute the basis for the L- and X-band bistatic σ_0 model for Site III. These data and the X-band model for principal and orthogonal polarizations are shown in Fig. 4-6.

The above mentioned X-band data and some L-band data of Ament et al.¹ form the basis for the L-band bistatic σ_0 model for Site III. These are shown in Fig. 4-7. The data points for L-band being on the average 8 dB below those for X-band, the L-band model is simply 8 dB below that at X-band.

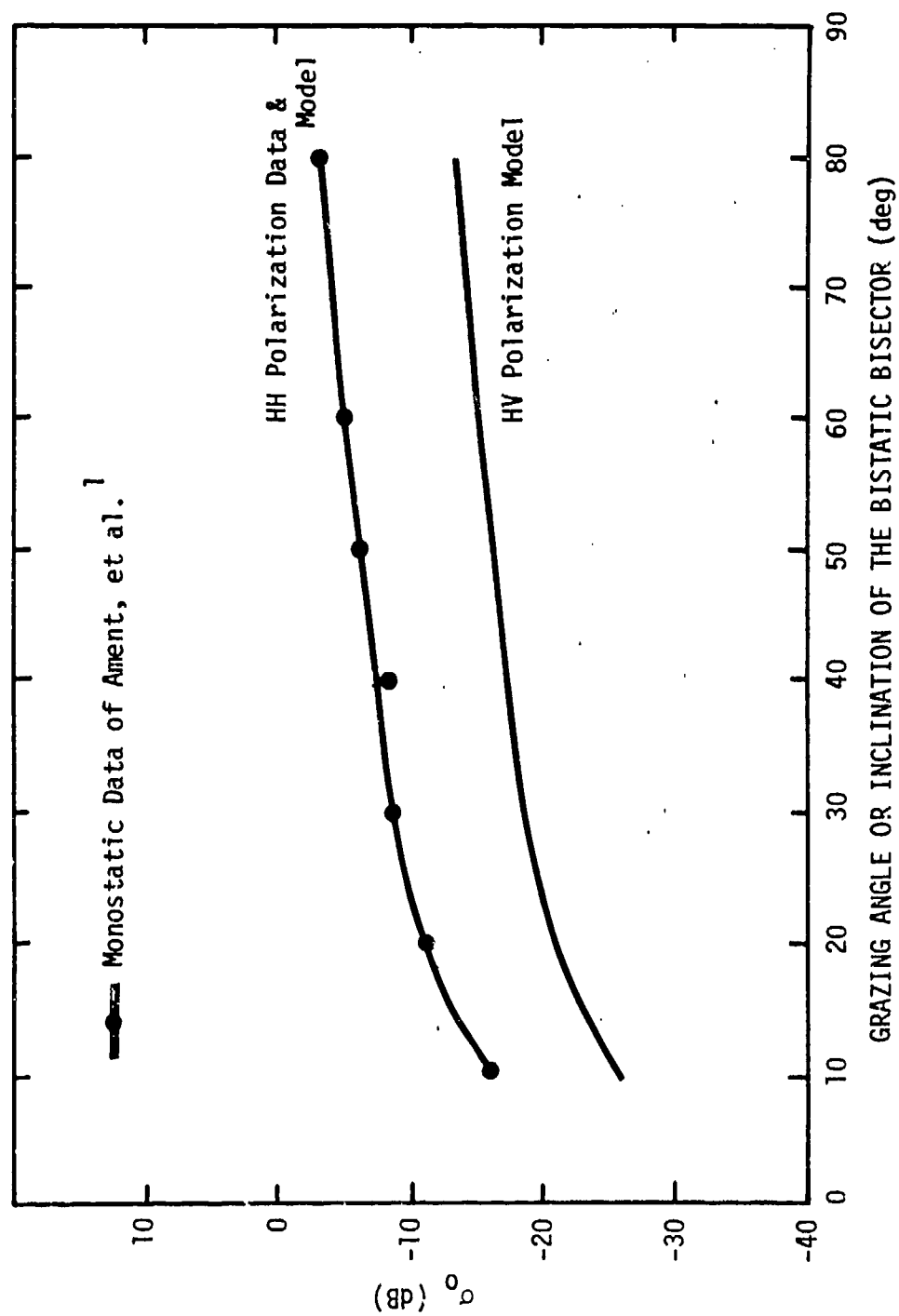
4.3 COMPARING THE DATA WITH EXISTING MODELS

A representative sampling of the L-band principal polarization data collected on all passes made on 17 February 1978 is shown in Fig. 4-8, wherein each point represents an average σ_0 taken over a 15° interval of the out-of-plane angle. This figure and the ones to follow are, then, summaries of all of the data collected on that date. Appendix B includes a discussion of the data collected on individual passes of 17 and 18 March 1978. The independent variable in these figures is the inclination of the bistatic bisector for which 90° represents a line perpendicular to the earth's surface. The data in Fig. 4-8 show a spread of about 10 dB and a trend that is not nearly as steep as that of the model derived from previous monostatic data.

The L-band orthogonal polarization data of 17 February shown in Fig. 4-9 is similar in spread and trend and is a few dB lower than the principal polarization data of that date. Much of the data falls above the model.

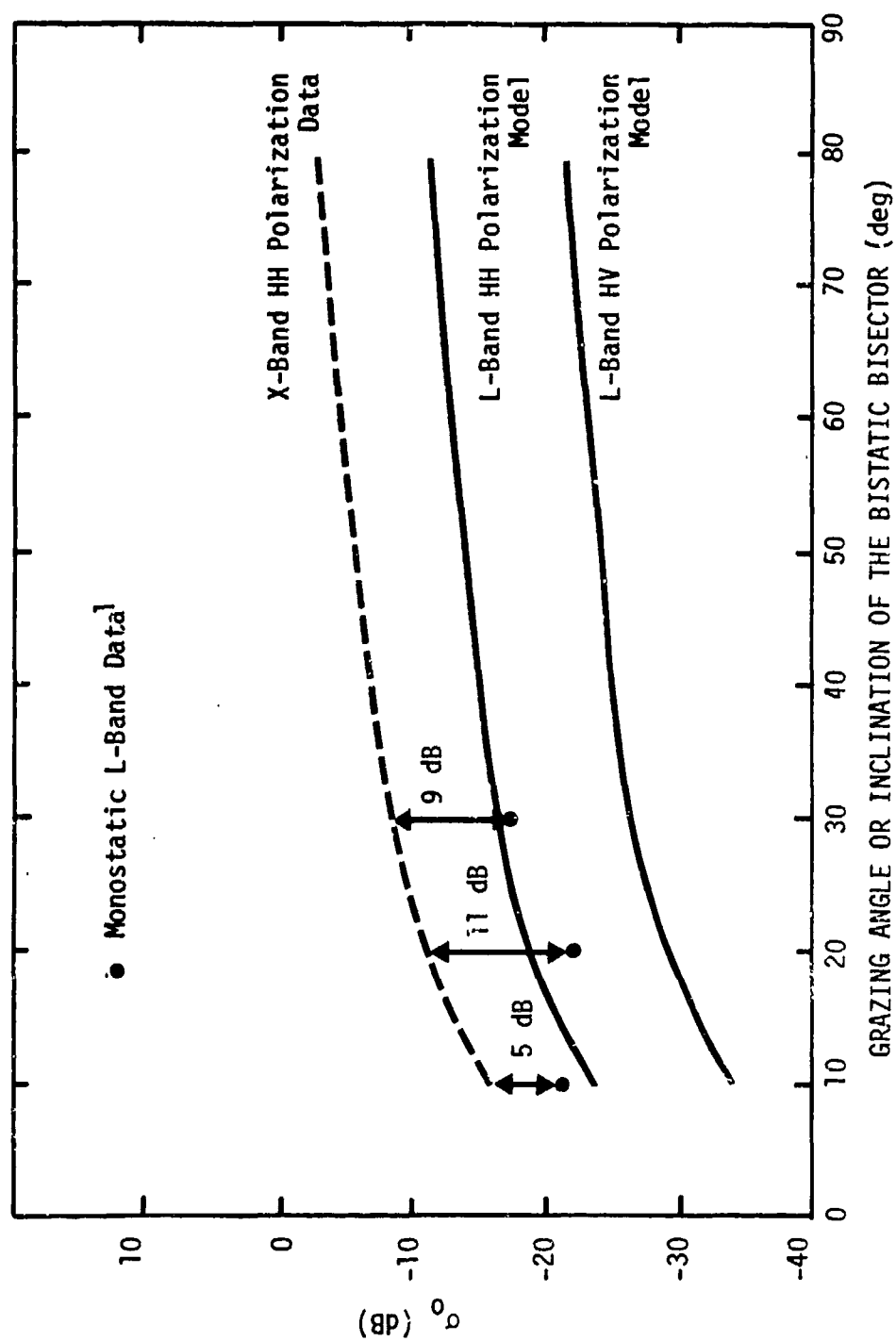
Turning now to the data of 18 February 1978, we find that the principal polarization data has a character considerably different from that of

¹W. S. Ament, F. C. Macdonald, and R. D. Shewbridge, op. cit.



W. S. Ament, et al., op. cit.

Figure 4-6. X-Band (HH) Monostatic σ_0 Data for Wooded Terrain and Bistatic σ_0 Model for Site 3



W. S. Ament, et al., op. cit.
 Figure 4-7. L-Band (HH Polarization) Monostatic σ_0 Data for Wooded Terrain
 and Bistatic σ_0 Model for Site 3

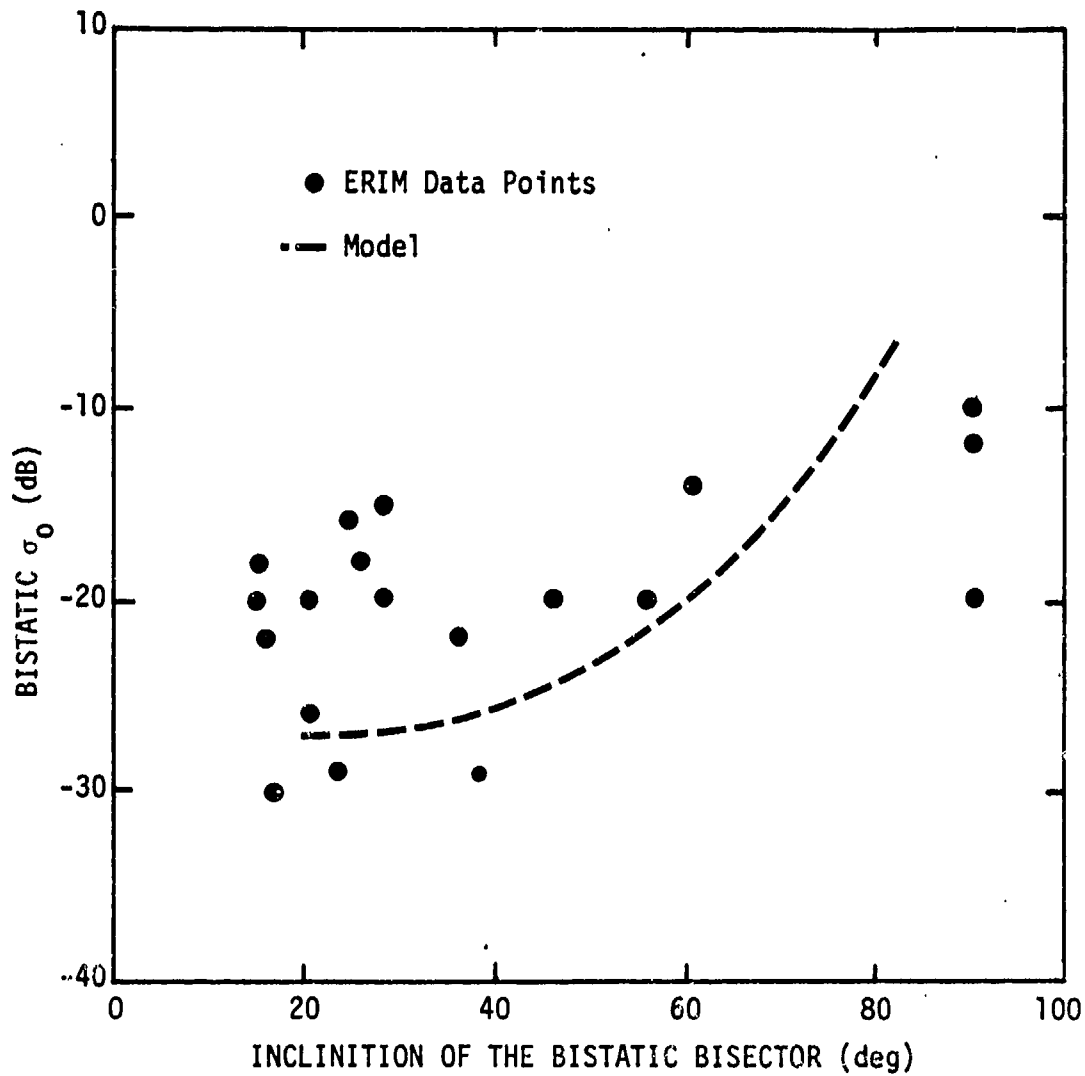


Figure 4-8. L-Band Principal Polarization (HH) Bistatic σ_0 Data of 17 February 1978 (All Passes) for a Snow Covered Field

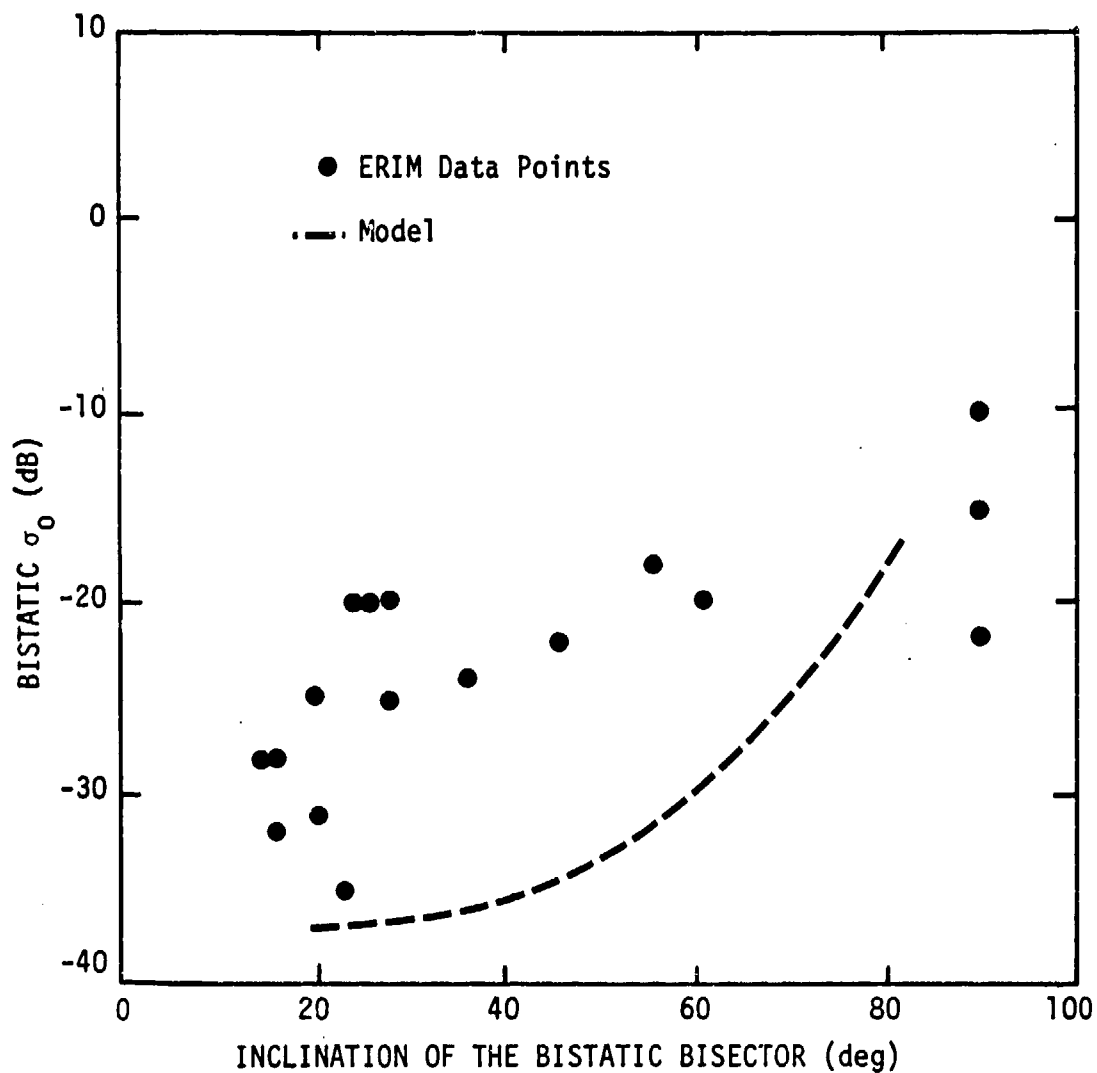


Figure 4-9. L-Band Orthogonal Polarization (HV) Bistatic σ_0 Data of 17 February 1978 (All Passes) for a Snow Covered Field

the previous day. The 18 February data, shown in Fig. 4-10, has a spread of 20 to 30 dB, more than twice as large as that for the data of 17 February 1978. The average trend of the data is approximately the same as that of the model. Primarily it is the great increase in the spread in the data that differentiates the 17 February from the 18 February principal polarization data. The L-band orthogonal polarization data of 18 February (shown in Fig. 4-11) is similar in both spread and trend but is somewhat higher when compared with the orthogonal polarization data of the previous day.

The L-band principal polarization data of 19 February 1978 (shown in Fig. 4-12) has a 10 dB to 15 dB spread and is essentially trendless, as is the orthogonal data of 19 February shown in Fig. 4-13.

DSA received no X-band data from the 17, 18, and 19 February 1978 flights, as ERIM has yet to process the data.

The L-band principal and orthogonal polarization data of 17 March 1978 (shown in Figs. 4-14 and 4-15) exhibit a relationship with the inclination angle that can be characterized as U-shaped and that is quite different from the model. The X-band data of the date (shown in Fig. 4-16 and 4-17) have a trend that runs counter to the model and is in most cases higher than the model.

All of the data of 18 March 1978 (shown in Figs. 4-18 through 4-21) are essentially trendless, exhibit 20 dB spreads, and in most cases fall above the models. (The X-band data for both polarizations fall into the range, 0 dB to -10 dB, and the L-band data for both polarizations fall into the range, -10 dB to -20 dB.)

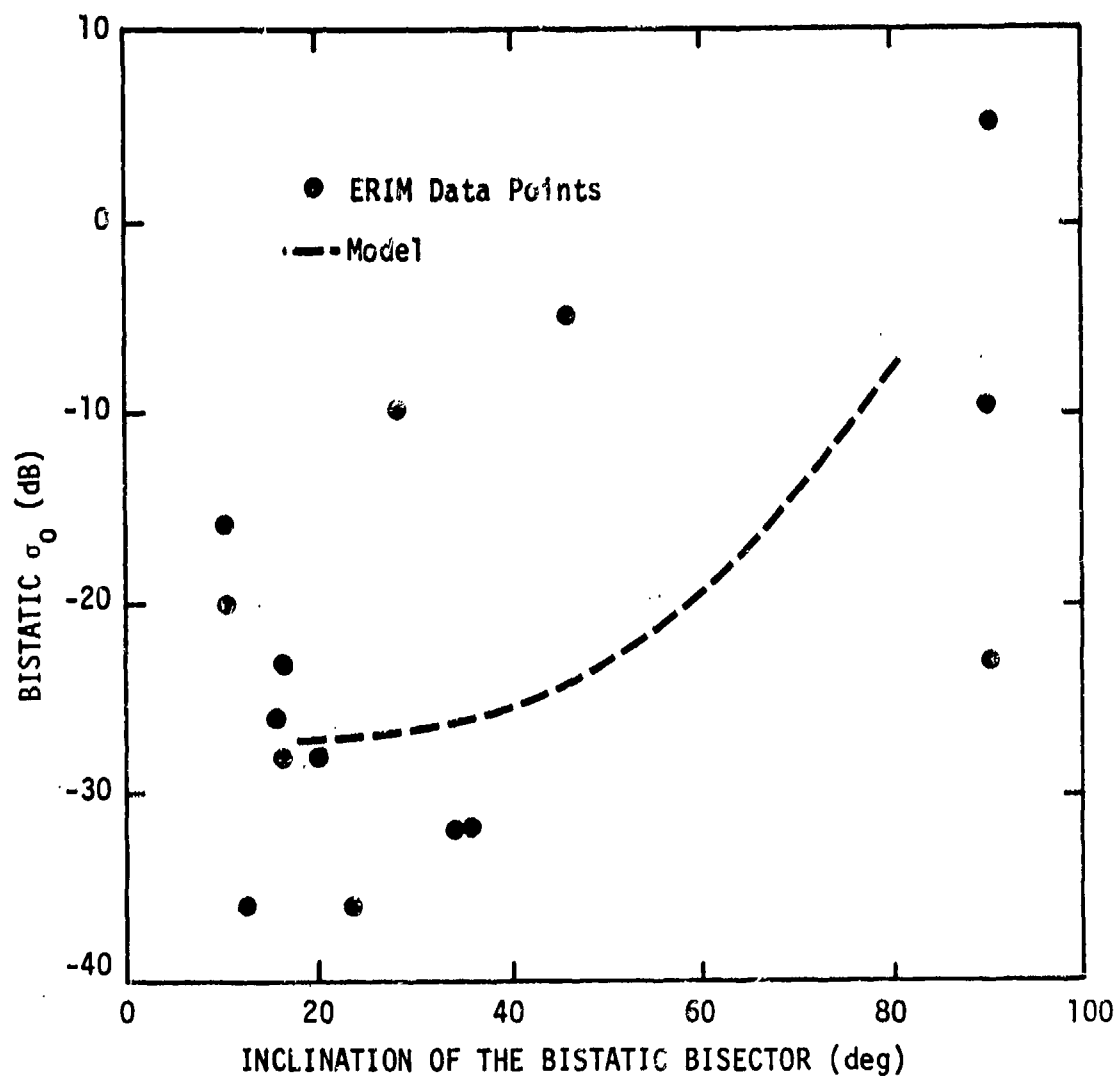


Figure 4-10. L-Band Principal Polarization (HH) Bistatic σ_0
Data of 18 February 1978 (All Passes) for a
Snow Covered Field

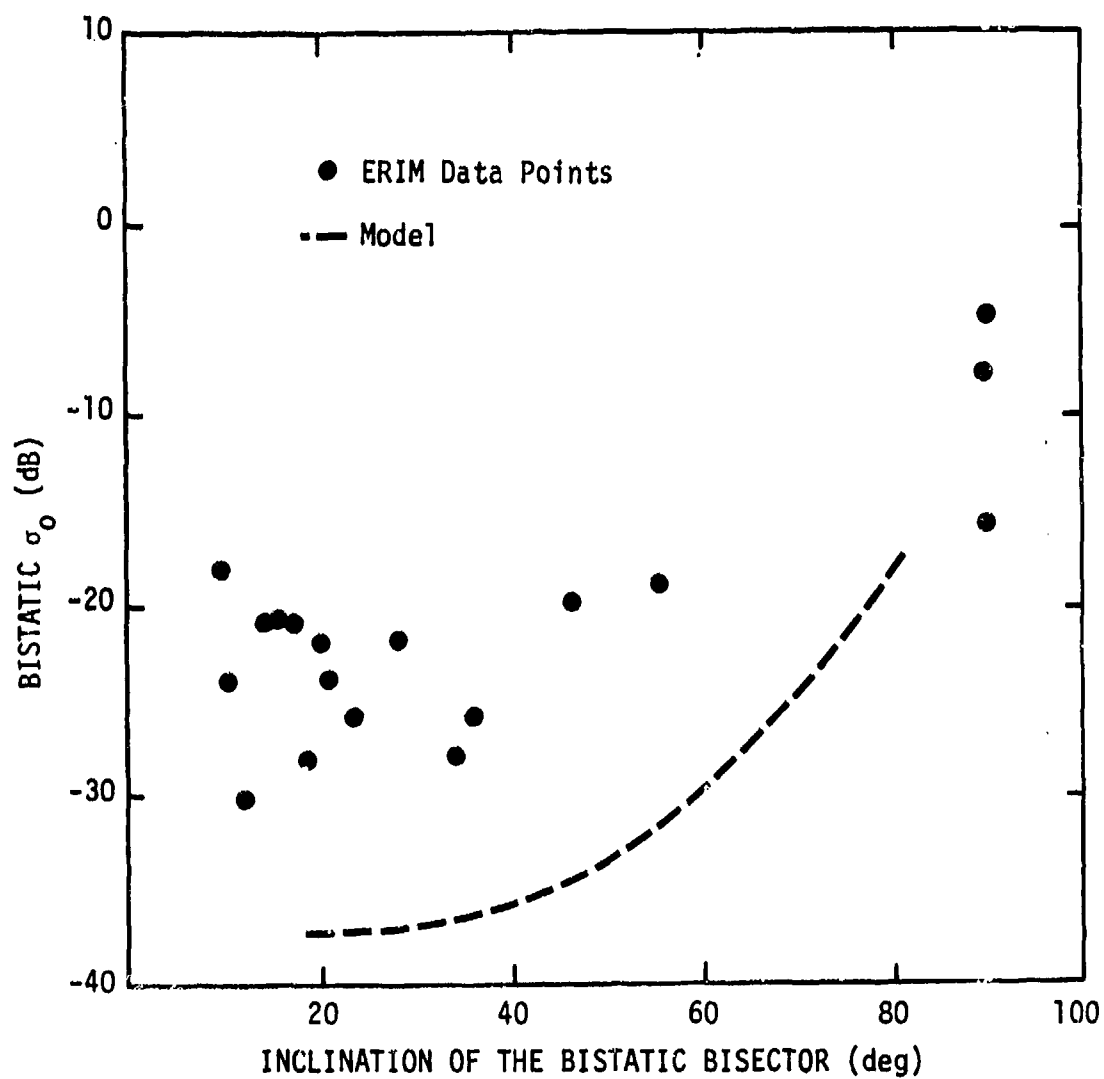


Figure 4-11. L-Band Orthogonal Polarization (HV) Bistatic σ_0
Data of 18 February 1978 (All Passes) for a
Snow Covered Field

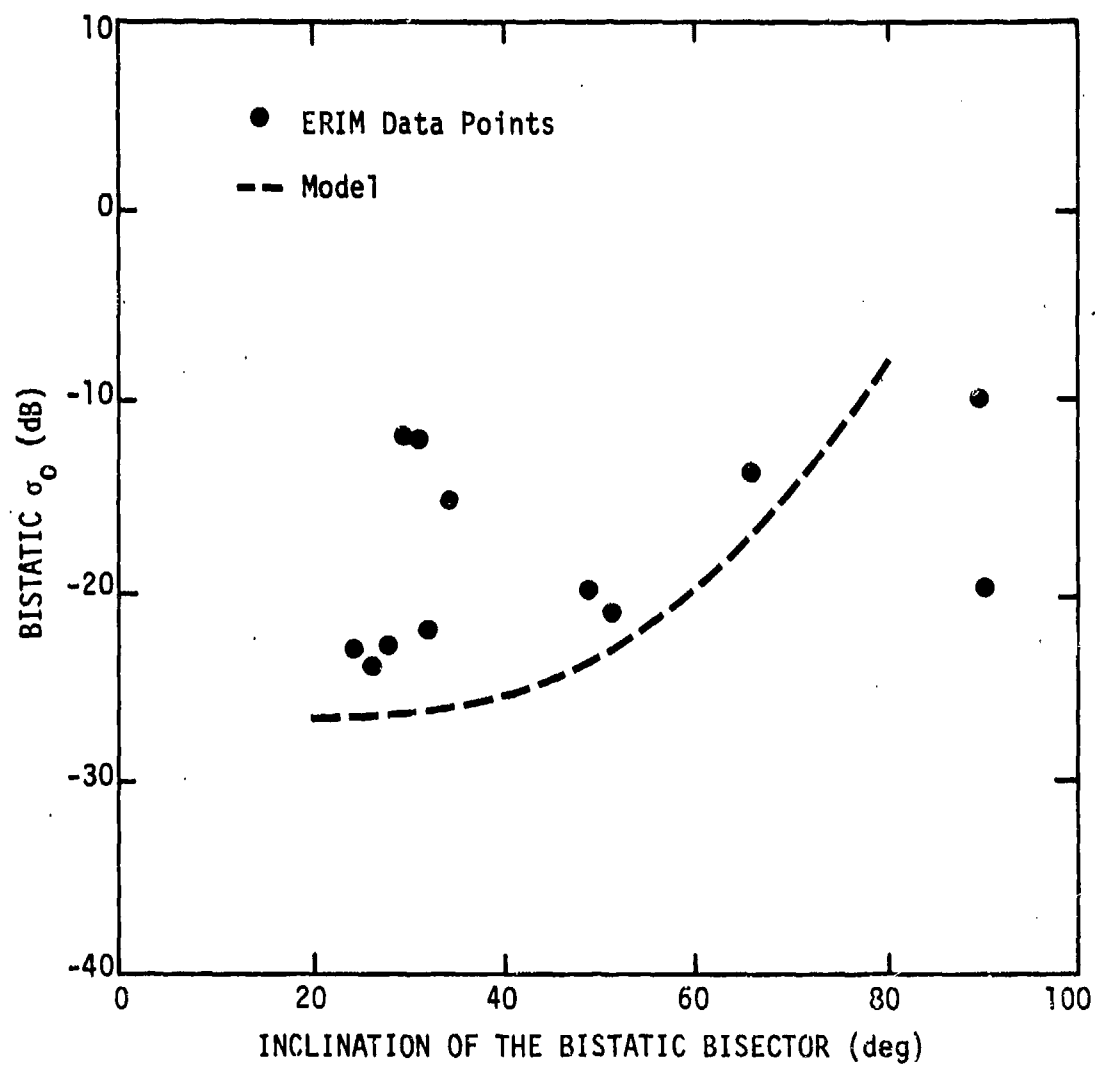


Figure 4-12. L-Band Principal Polarization (HH) Bistatic σ_0 Data of 19 February 1978 (All Passes) for a Snow Covered Field

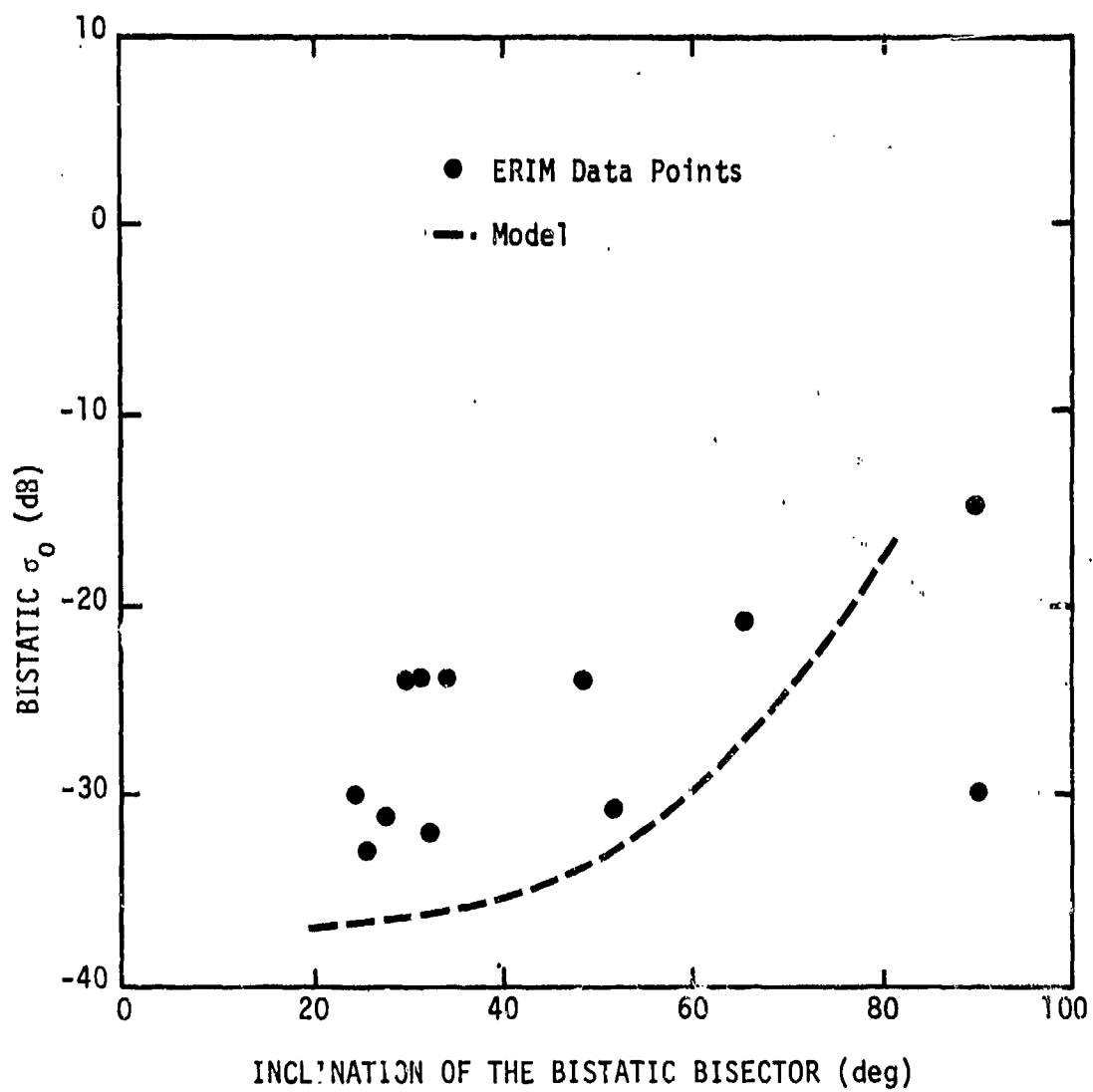


Figure 4-13. L-Band Orthogonal Polarization (HV) Bistatic σ_0 Data of 19 February 1978 (All Passes) for a Snow Covered Field

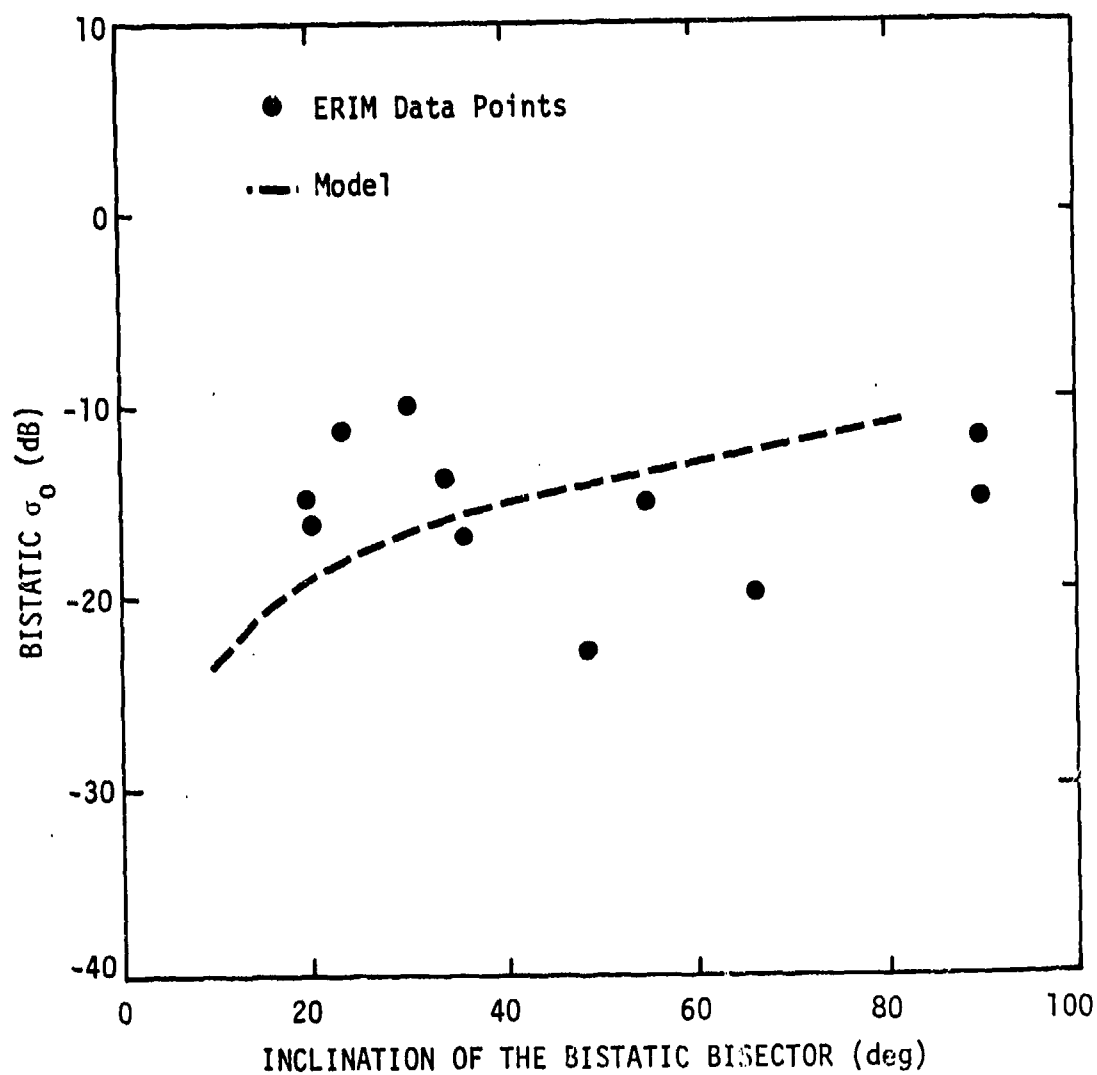


Figure 4-14. L-Band Principal Polarization (HH) Bistatic σ_0 Data of 17 March 1978 (All Passes) for Wooded Terrain

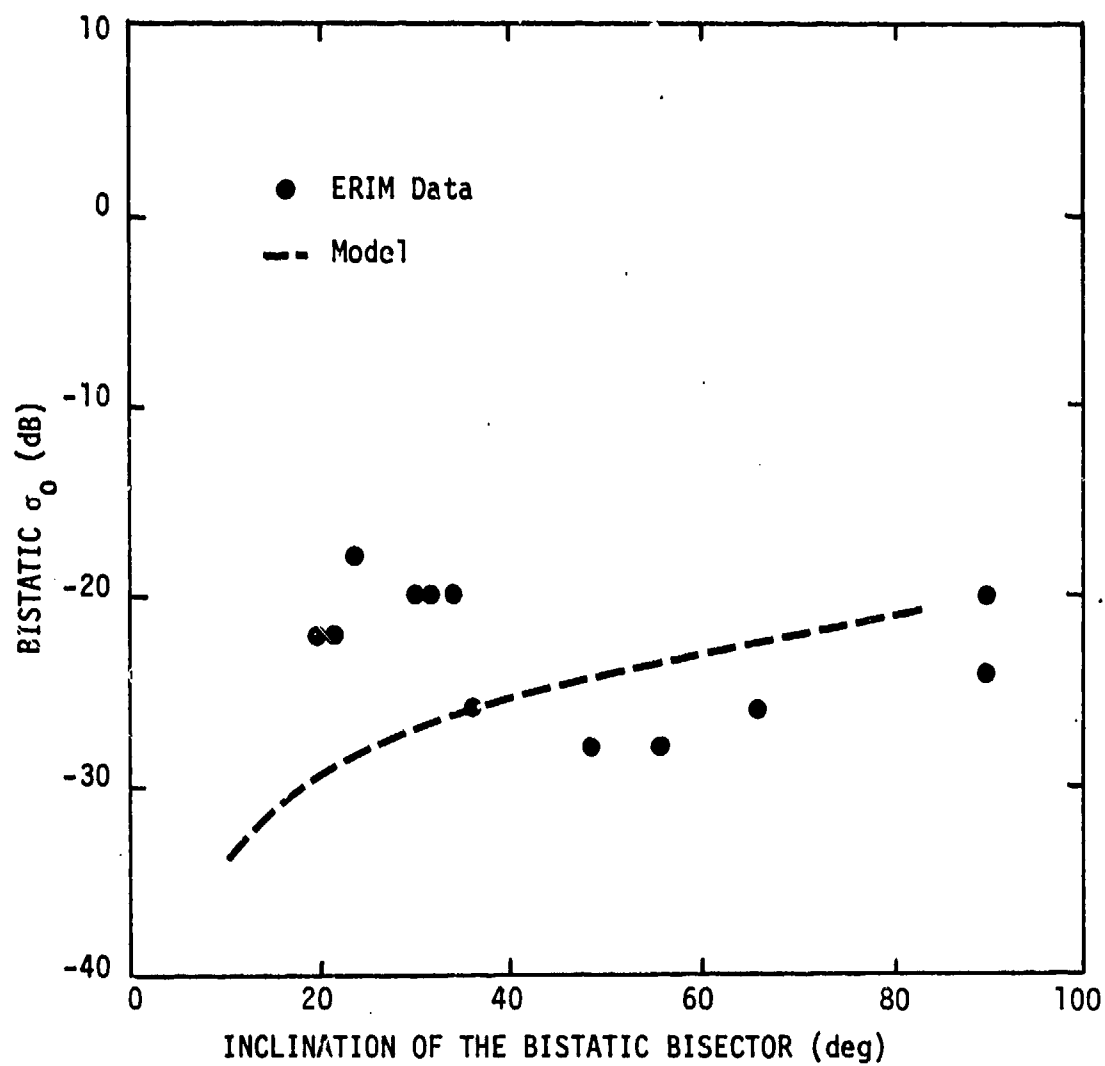


Figure 4-15. L-Band Orthogonal Polarization (HV) Bistatic σ_0 Data of 17 March 1978 (All Passes) for Wooded Terrain

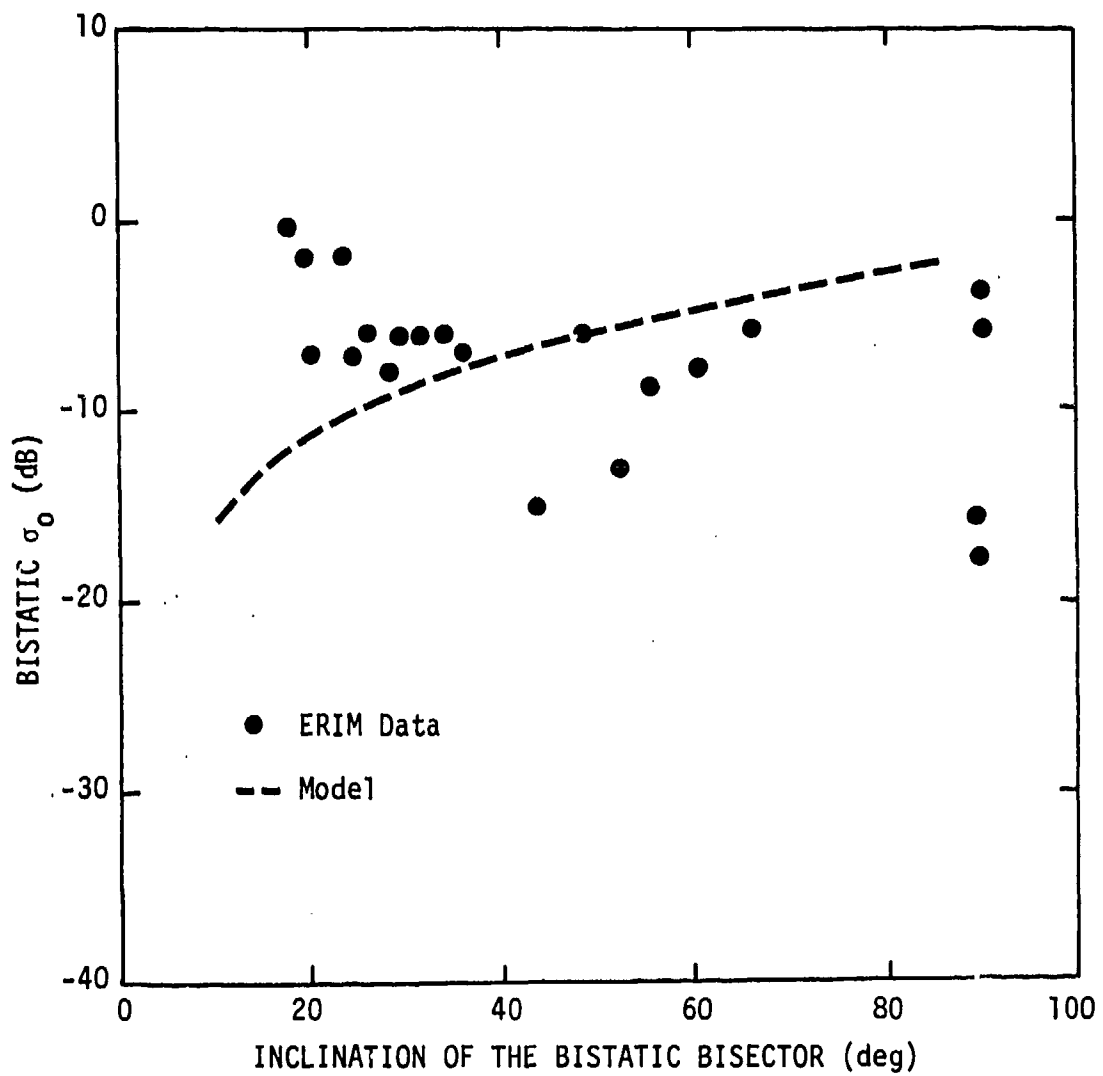


Figure 4-16. X-Band Principal Polarization (HH) Bistatic σ_0 data of 17 March 1978 (All Passes) for Wooded⁰ Terrain

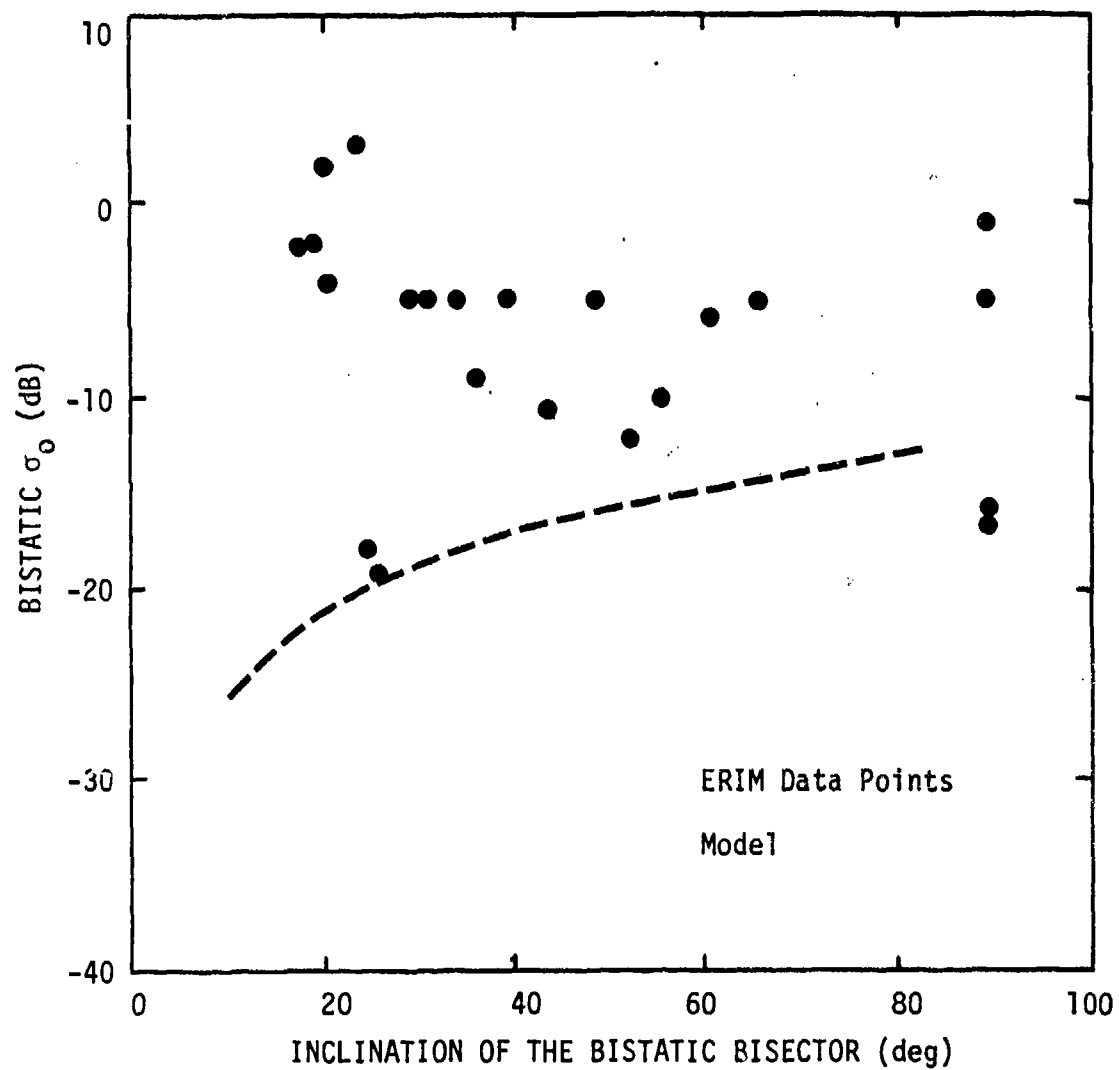


Figure 4-17. X-Band Orthogonal Polarization (HV) Bistatic σ_0 Data of 17 March 1978 (All Passes) for Wooded Terrain

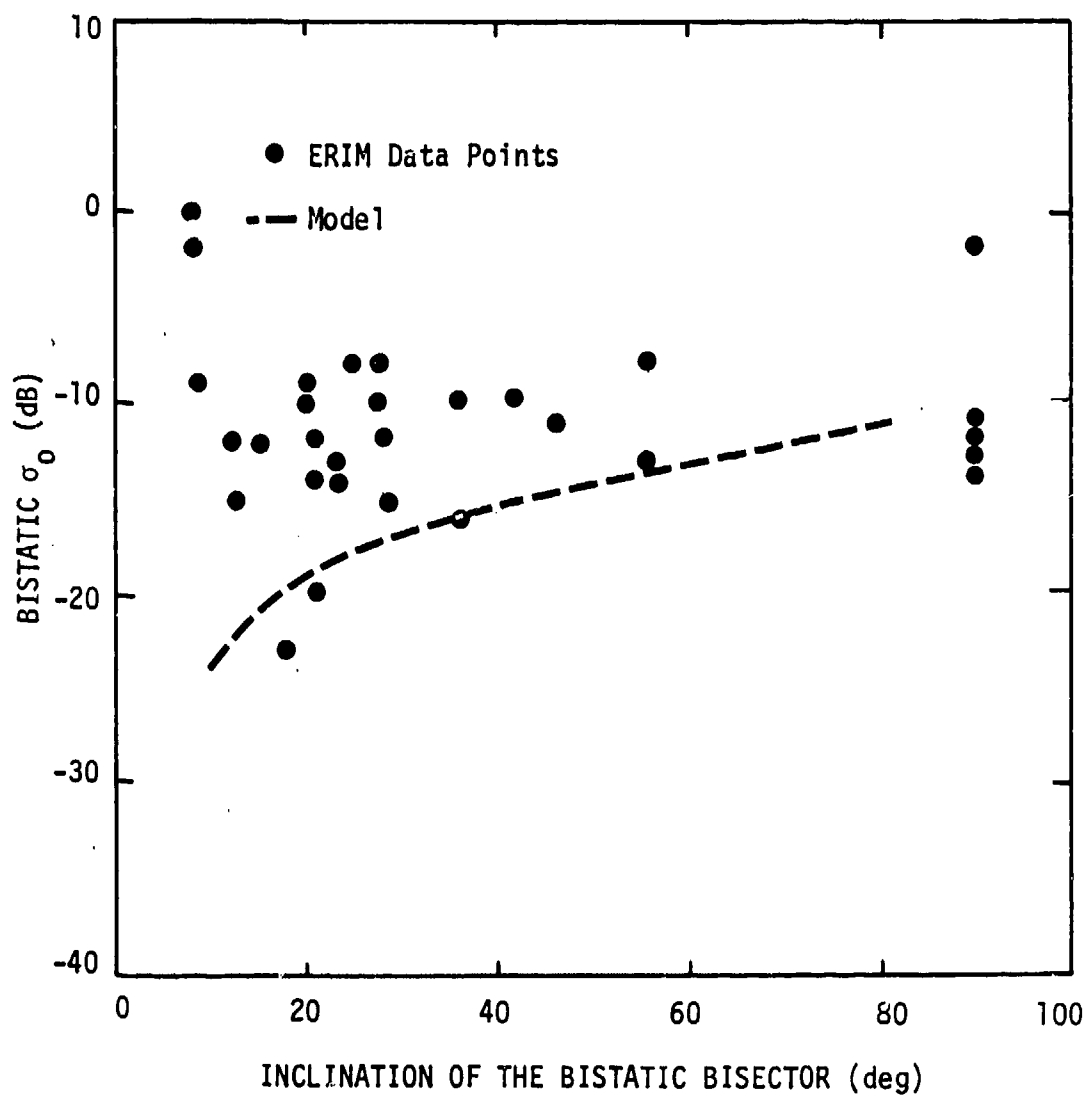


Figure 4-18. L-Band Principal Polarization (HH) Bistatic σ_0 Data of 18 March 1978 (All Passes) for Wooded Terrain

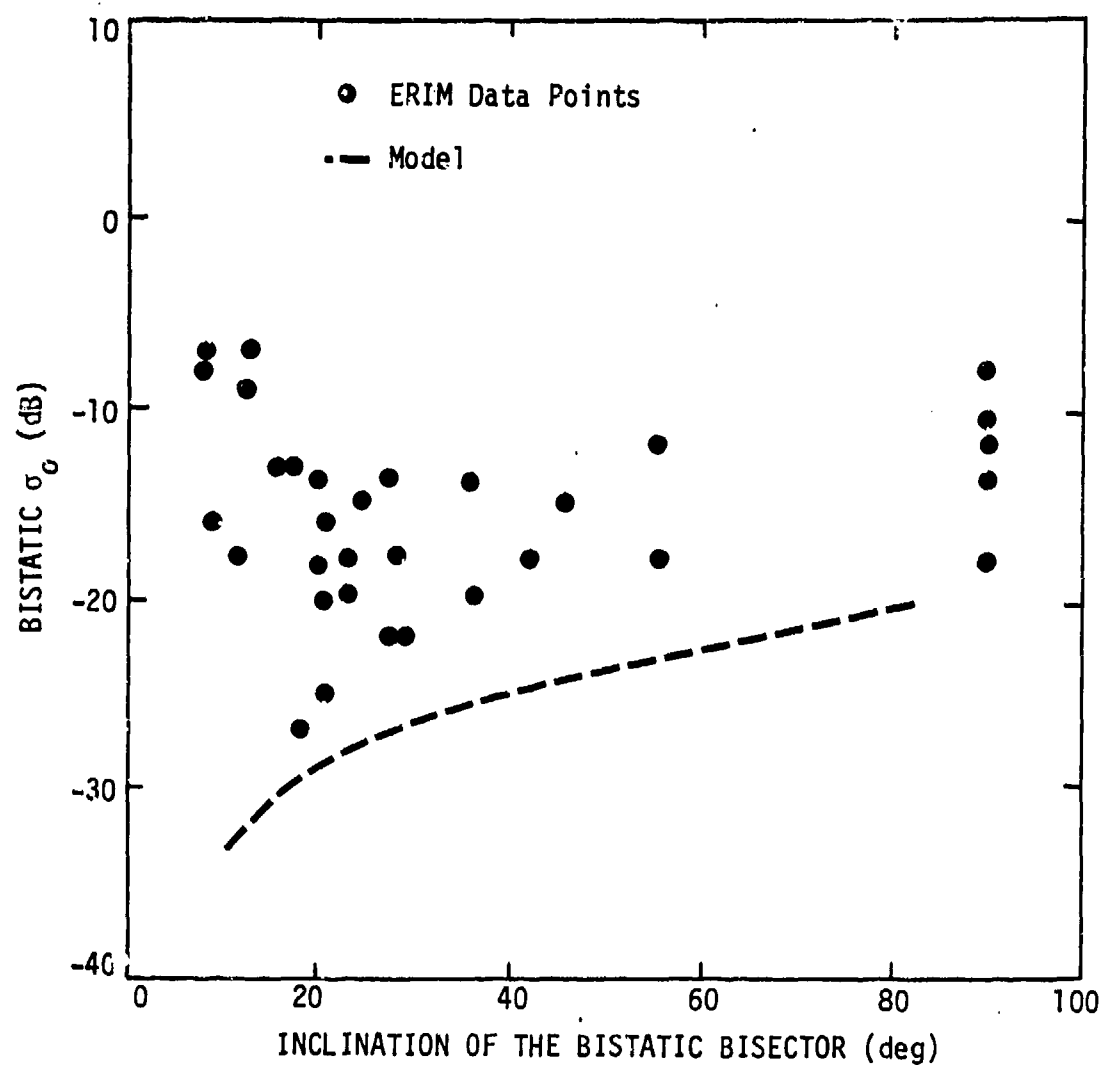
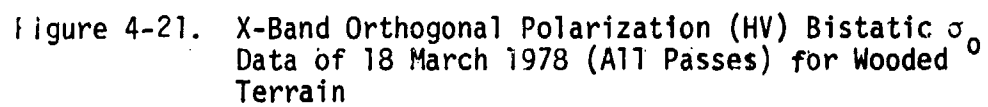


Figure 4-19. L-Band Orthogonal Polarization (HV) Bistatic σ_0 Data of 18 March 1978 (All Passes) for Wooded Terrain



4.4 CONCLUSIONS

In their report concerning the 1978 data,¹ ERIM drew the following conclusions with regard to the agreement of their most recent data and earlier data:

The σ_0 results obtained from the processed data appear to be in general agreement with other available data. A few comparisons with reported results from appropriate backscatter measurements using horizontal-horizontal polarization have been made. Results reported by Linell² show the average X-band σ_0 value for forests to be -11 dB for low depression angles. For similar conditions, Hayes et al.³ report σ_0 values ranging from -14.2 to -3.6 dB. Results of Katz and Spetner⁴ report average X-band σ_0 values of -16 dB for $\theta_S = 130^\circ$ (10° depression angle), $\sigma_0 = -11$ dB for $\theta_S = 70^\circ$, and $\sigma_0 = -10$ dB for $\theta_S = 60^\circ$. Ament et al.⁵ report median L-band σ_0 values of -21 dB for $\theta_S = 80^\circ$, -22 dB for $\theta_S = 70^\circ$, and -17 dB for $\theta_S = 60^\circ$. These values compare favorably with the results obtained from the March 1978 measurements of the orchard-forest scene.

DSA is in substantial disagreement with ERIM's conclusions. The Linell reference ERIM cites contains data for snow-covered cultivated terrain for which σ_0 is -39 dB for a 5° grazing angle. This is in substantial disagreement with the February data collected at Site II most of which is higher than the Linell data by 10 dB or more.

¹R. Larson et al., Measurements of Bistatic Clutter Cross Section at 23 cm and 3 cm Wavelength, Environmental Research Institute of Michigan, Final Technical Report to the Defense Advanced Research Projects Agency, Contract No. F30602-77-C-0145, August 1978.

²T. Linell, "An Experimental Investigation of the Amplitude Distribution of Radar Terrain Returns," 6th Conference of the Swedish National Committee on Scientific Radio, March 13, 1963.

³R. Hayes et al., op. cit.

⁴I. Katz and L. Spetner, "Polarization and Depression Angle Dependence of Radar Terrain Return," Journal of Res. NBS, Vol. 64D, No. 5, September 1960.

⁵W. Ament et al., op. cit.

The Hayes et al. data which ERIM cites was for rough wooded terrain where the incidence angle has no meaning and one must assume that the radar return is dominated by echos from areas for which the grazing angle is large. Indeed, σ_0 in the range -3.6 to -14.2 is in good agreement with the model used to evaluate the March data. DSA's evaluation showed little agreement between the data and the model. In many cases the data ranges 10 to 20 dB from the model. The terrain at Site III is wooded but not rough, so the Hayes data is not appropriate data to compare with the ERIM Site III data.

The Katz and Spetner data which ERIM cites is appropriate data to compare with their March or Site III data. In fact, the Katz and Spetner data, identical to that in Ament et al., constitute the DSA model for Site III. As we stated earlier the Site III data and this model disagreed by 10 to 20 dB.

Because of the lack of agreement between the ERIM data and the data previously collected and because of numerous discrepancies in the ERIM data, DSA urged ERIM to examine their data acquisition and processing procedure for sources of error. While this report was in preparation, ERIM reprocessed much of the February and March 1978 data and supplied DSA with a second data set. It was not feasible for DSA to perform a complete evaluation of this data; but, for the purpose of comparison, DSA generated a plot of the newly submitted L-band data of 18 March 1978. That plot, shown in Fig. 4-22, exhibits (just as the earlier plots did) a strong and clear tendency for σ_0 to rise abruptly at low values of the inclination of the bistatic bisector where the geometry is such that scattering is nearly monostatic,* and inclination of the bistatic bisector can be read as a grazing angle. This tendency is not observed in the monostatic or bistatic data of others, as represented by the curve labeled "model" in the figure. The tendency is

* In the range of inclination of the bistatic bisector of 0° to 20° , 60% of the data points correspond to bistatic angles of from 15° to 30° .

stated as being strong because the rise is in excess of 15 dB and is stated as being clear because there is little scatter in the data at low inclination angles, while there is considerable scatter in the data at larger values of inclination of the bistatic bisector.

While one may quarrel with DSA's use of monostatic data and the bistatic theorem to generate a model with which to compare the ERIM data, one can hardly quarrel with the comparison of a body of monostatic data with ERIM's data for measurement geometries that are essentially monostatic. This latter comparison shows a substantial lack of agreement.

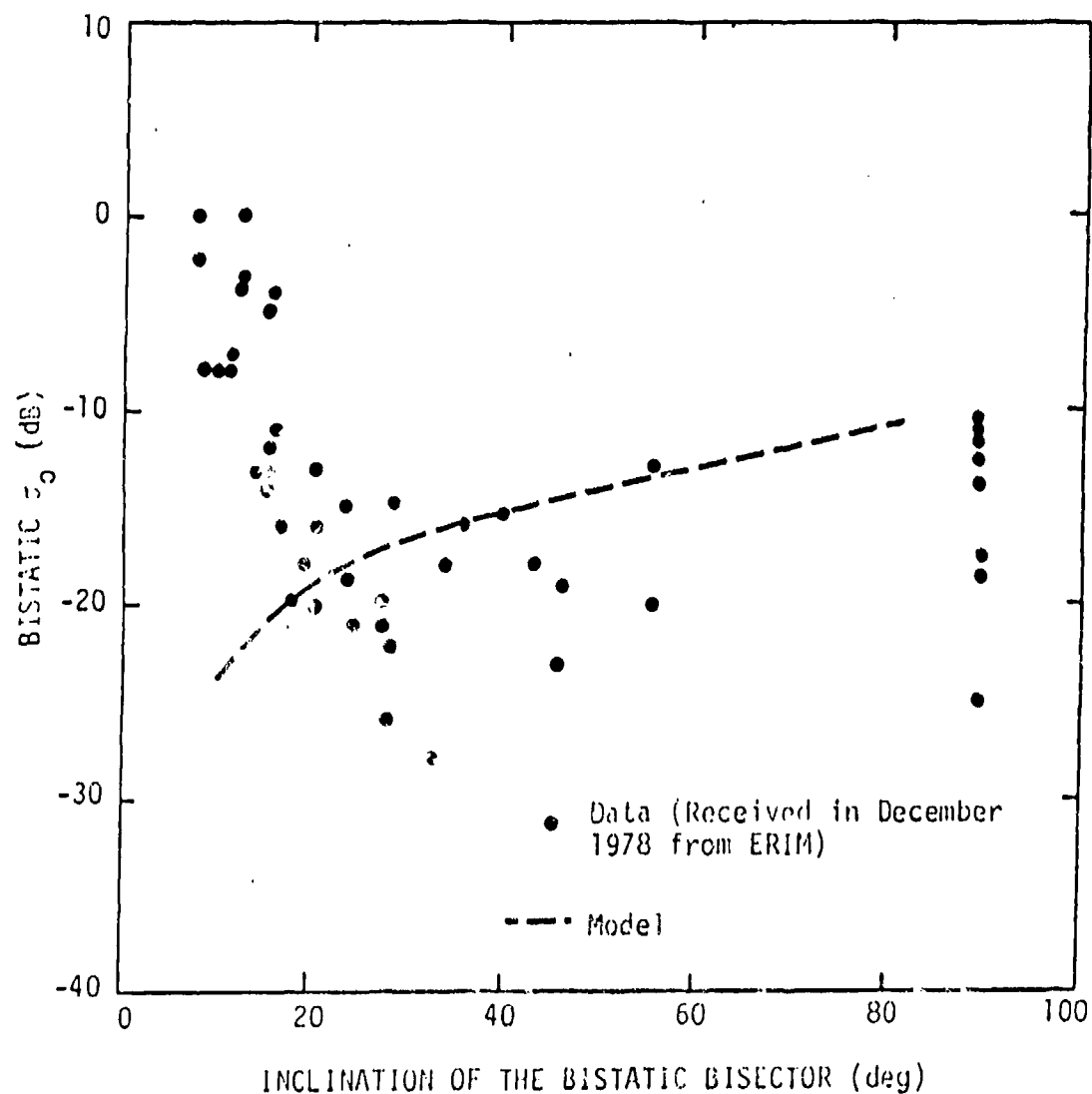


Figure 4-22. L-Band Principal Polarization (HH) Bistatic σ_0 Data of 10 March 1978 (All Passes)

APPENDIX A

TEST EQUIPMENT PARAMETERS

The relevant parameters of the transmitters, receivers, and antennas used in the bistatic terrain reflectivity tests are shown in Tables A-1 and A-2.

At the receiver site, calibrated and time-referenced analog tape records were made of the received power in the X- and L-band HH and HV channels and other parameters including the azimuth to the aircraft and the pointing azimuth of the receiver antennas. On the aircraft, a time-referenced flight path was established by vertical photography, and time referenced records were made of the transmitted power and the pointing azimuth of the transmitter antennas. Using this recorded data, the scattering geometry and antenna pattern factors on the ground could be calculated.

TABLE A-1
TRANSMITTER AND TRANSMITTING ANTENNA CHARACTERISTICS

Platform: ERIM C-46 Aircraft

Transmitter parameters:

	L-Band	X-Band
Center frequency	1.315 GHz	9.450 GHz
Bandwidth	>100 MHz	>100 MHz
Peak power	5 kW	0.5 kW
Average power	1.8 W	0.14 W
Pulse width	90 nsec	70 nsec
PRF	4000	4000
Losses	0.5 dB	1.9 dB

Transmitter antenna parameters:

	H	H
Polarization	H	H
Cross-polarization isolation	>20 dB	>25 dB
Center frequency	1.315 GHz	9.450 GHz
Maximum bandwidth (3 dB)	100 MHz	100 MHz
Horizontal beamwidth (3 dB)	12°	12°
Vertical beamwidth (3 dB)	90°	13°
Peak antenna gain (referred to as isotropic)	16 dB	22.2 dB

TABLE A-2
RECEIVER AND RECEIVING ANTENNA PARAMETERS

Receiver

	<u>L-Band</u>	<u>X-Band</u>
Type	Coherent	Coherent
Channels	2 (V & H)	2 (V & H)
Bandwidth (3 dB)	30 MHz	30 MHz
Noise figure	4 dB	5 dB
Losses	2 dB	2 dB
Range-gate width	1.6 μ sec	1.6 μ sec
Minimum detectable signal	-78 dBmW	-75 dBmW

Receiving Antenna:

Polarization	V & H	V & H
Cross-polarization isolation	>31 dB	>27 dB
Center frequency	1.315 GHz	9.450 GHz
Maximum bandwidth (3 dB)	100 MHz	100 MHz
Beamwidth (3 dB; horizontal and vertical)	5°	5°
Peak gain	30 dB	31 dB
Aperture diameter	3.1 m	46 cm
Gain (sidelobe region)	0 dB	0 dB
Highest sidelobe	<-25 dB	<-25 dB
Mount	Inverted elevation over azimuth	
Minimum scanning speed	25°/sec	25°/sec
Time to reach speed	\approx 2 sec	\approx 2 sec
Position readout accuracy	<1°	<1°
Azimuth scan angle	0-360° (in segments)	
Elevation scan angle	0-90°	0-90°
Maximum safe wind loading during operation	10 mph	10 mph

APPENDIX B
DATA OF 17 MARCH AND 18 MARCH PROCESSED BY DSA

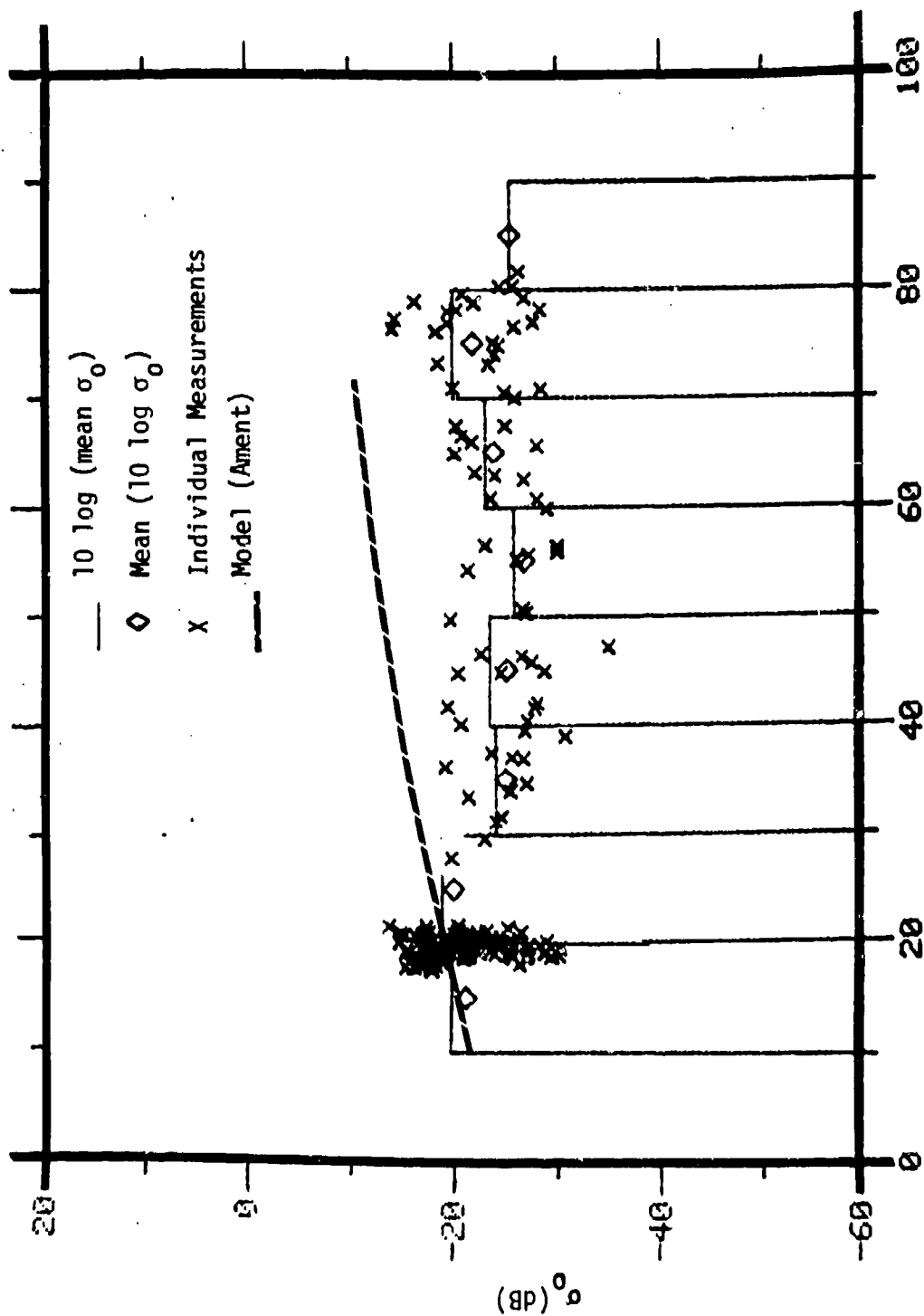
The disagreement between the most recent ERIM data and past data appeared to be greatest for the March 1978 data, and for that reason DSA processed some of that data completely to make an independent check of ERIM's processing. Passes 3 and 10 of 17 March and passes 3 and 10 of 18 March were chosen for this check.

The received power levels were converted to σ_0 using first the lower and then the higher ranges of the calibration curve as discussed in Subsection 3.4. The results associated with the higher range for L-band and the lower range for X-band appeared the more appropriate. Data were edited out based on the transmitter illumination test described in Subsection 3.5. The results of this processing appear in the Figs. B-1 through B-6. The X's indicate the individual data points; the bar indicates a linear average over a 10° interval of inclination of the bistatic bisector; and the diamond indicates a dB average over a 10° interval of inclination of the bistatic bisector.

DSA, in editing and processing the data obtained on passes 3 and 10 of 17 March and 18 March, turned up very little additional information from the raw data. Because of the editing, there appears to be less scatter in the data, but the relationship between σ_0 and the inclination of the bistatic bisector that runs counter to earlier data is in these plots as well as those plots generated from ERIM-processed data.

Both the L-band and the X-band on both principal and orthogonal polarization data show a σ_0 decreasing with increasing inclination of the bistatic bisector. DSA is not aware of any theoretical argument or data to support this trend.

No significant X-band data were collected on passes 3 and 10 of 18 March 1978.



INCLINATION OF THE BISTATIC BISECTOR (deg)

Figure B-1. L-Band Principal Polarization (HH) Bistatic σ_0 Data of 17 March 1978
(Passes 3 and 10, $\theta_s = 80^\circ$, $\theta_i = 60^\circ$) for Wooded Terrain

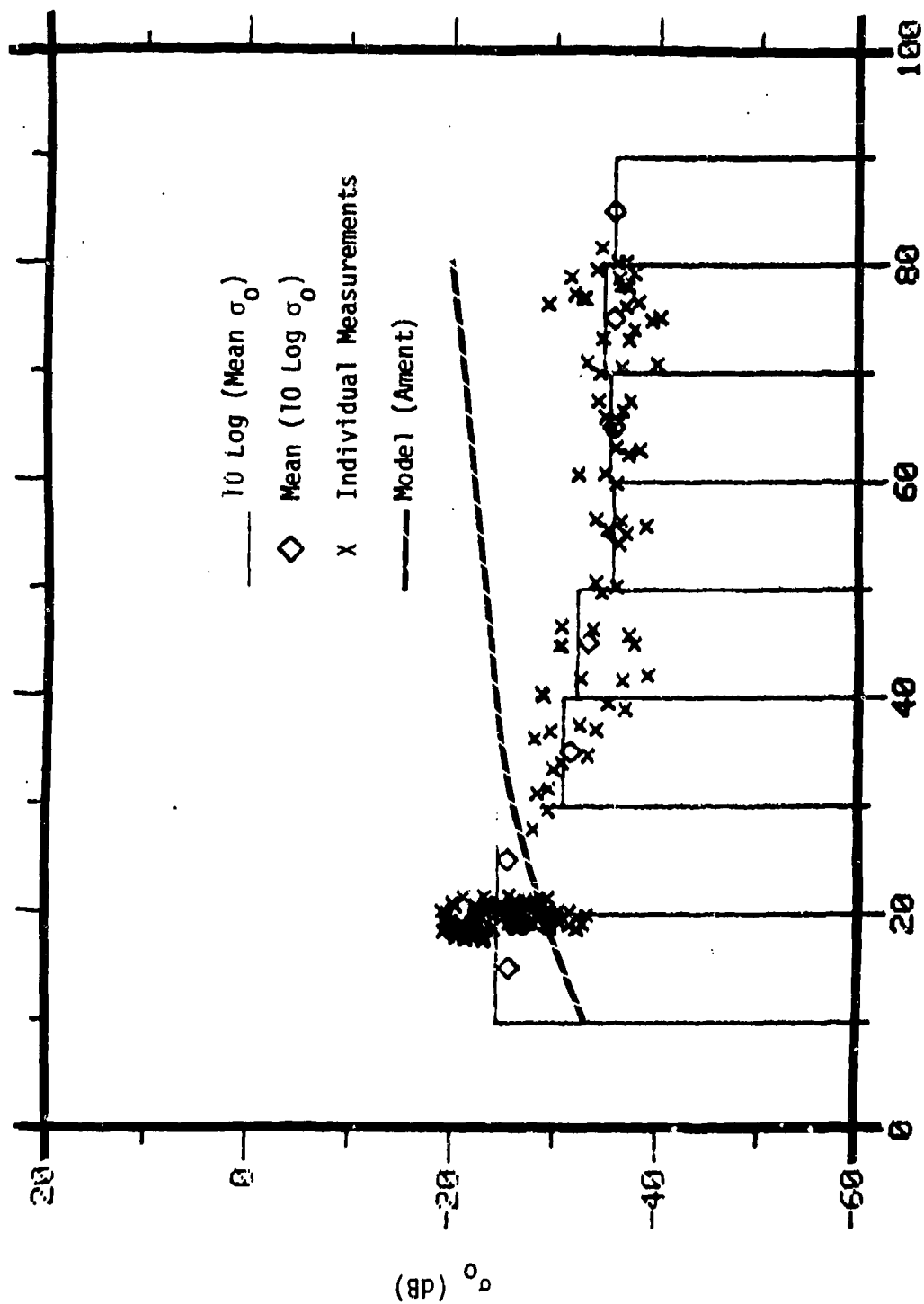


Figure B-2. L-Band Orthogonal Polarization (HV) Bistatic σ_0 Data of 17 March 1978
(Passes 3 and 10, $\theta_s = 80^\circ$, $\theta_i = 60^\circ$) for Wooded Terrain

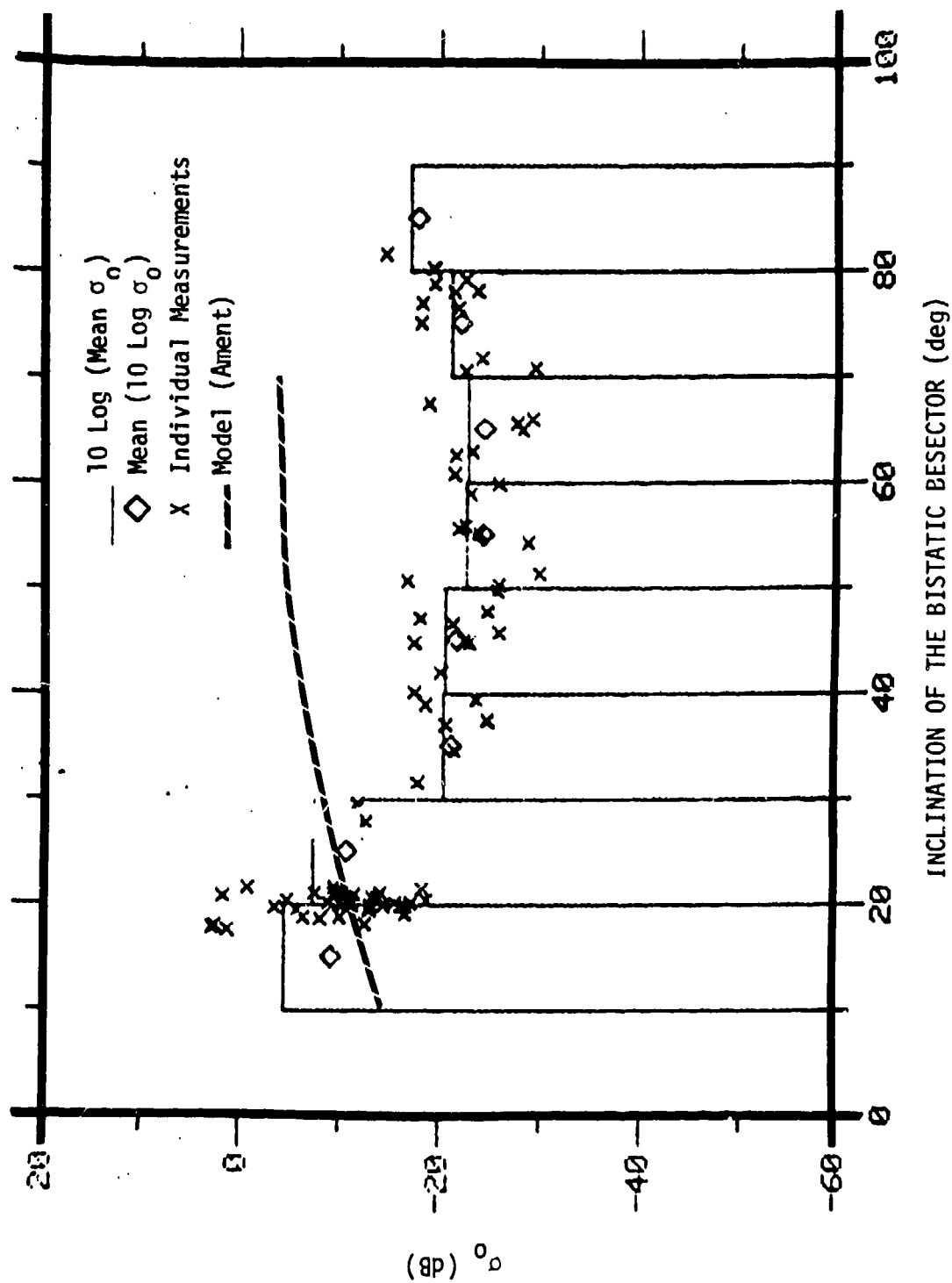


Figure B-3. X-Band Principal Polarization (HH) Bistatic σ_c Data of 17 March 1978
(Passes 3 and 10, $\theta_s = 80^\circ$, $\theta_i = 60^\circ$) for Wooded Terrain

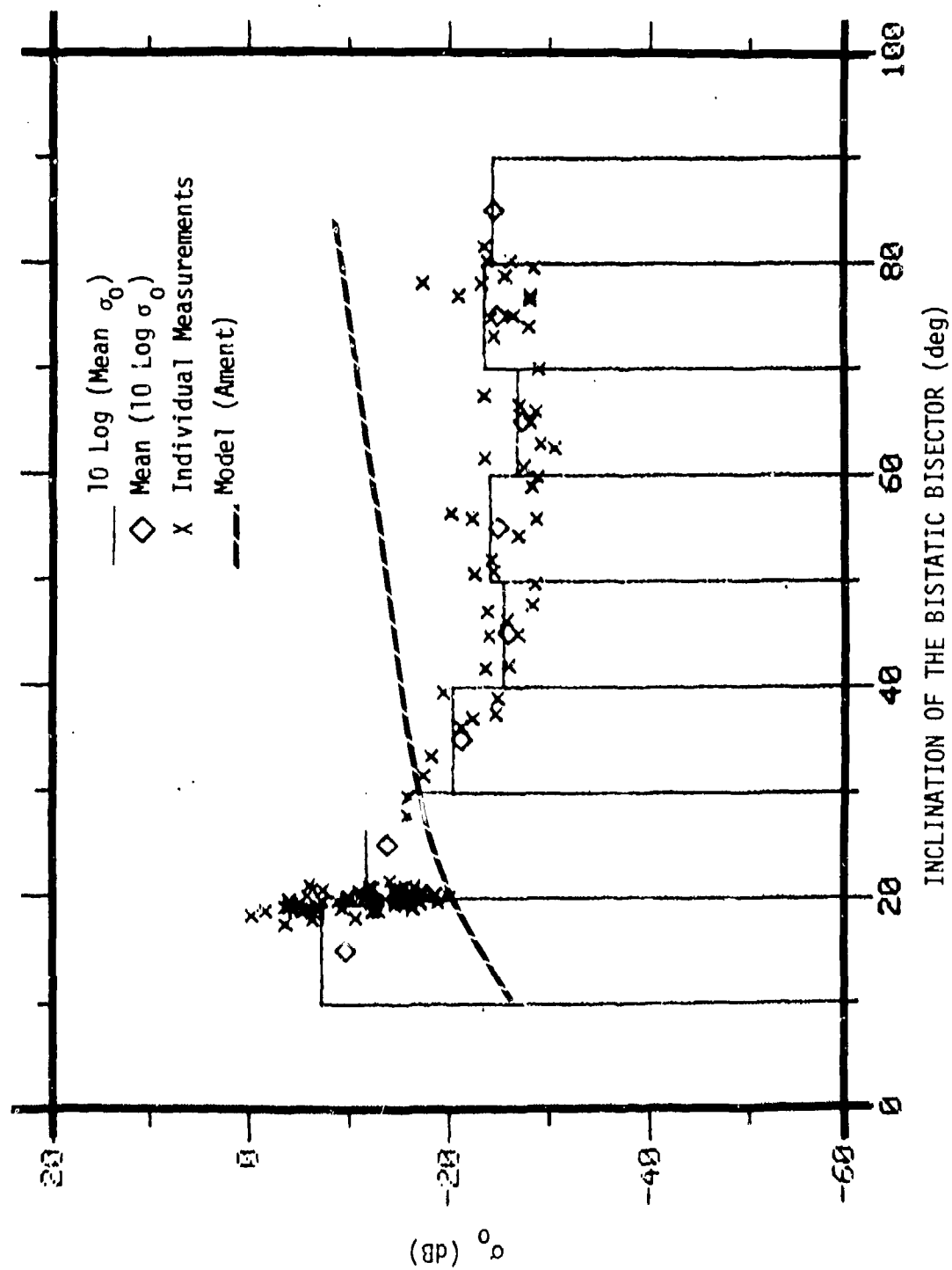


Figure B-4. X-Band Orthogonal Polarization (HV) Bistatic σ_0 Data of 17 March 1978 (Passes 3 and 10, $\theta_s = 80^\circ$, $\theta_i = 60^\circ$) for Wooded Terrain

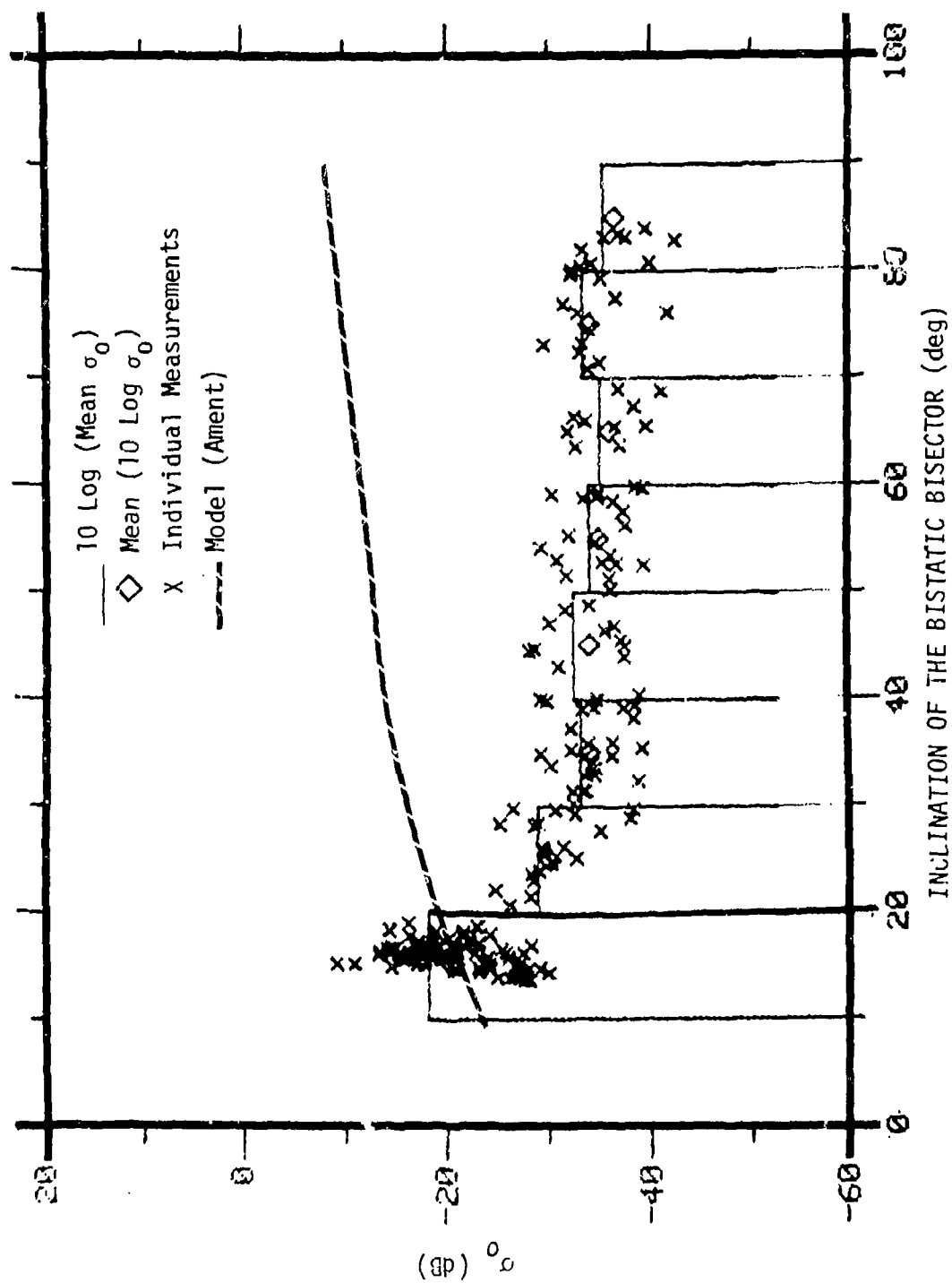


Figure B-5. L-Band Principal Polarization (HH) Bistatic σ_0 Data of 18 March 1978 (Passes 3 and 10, $\theta_s = 80^\circ$, $\theta_i = 70^\circ$) for Wooded Terrain

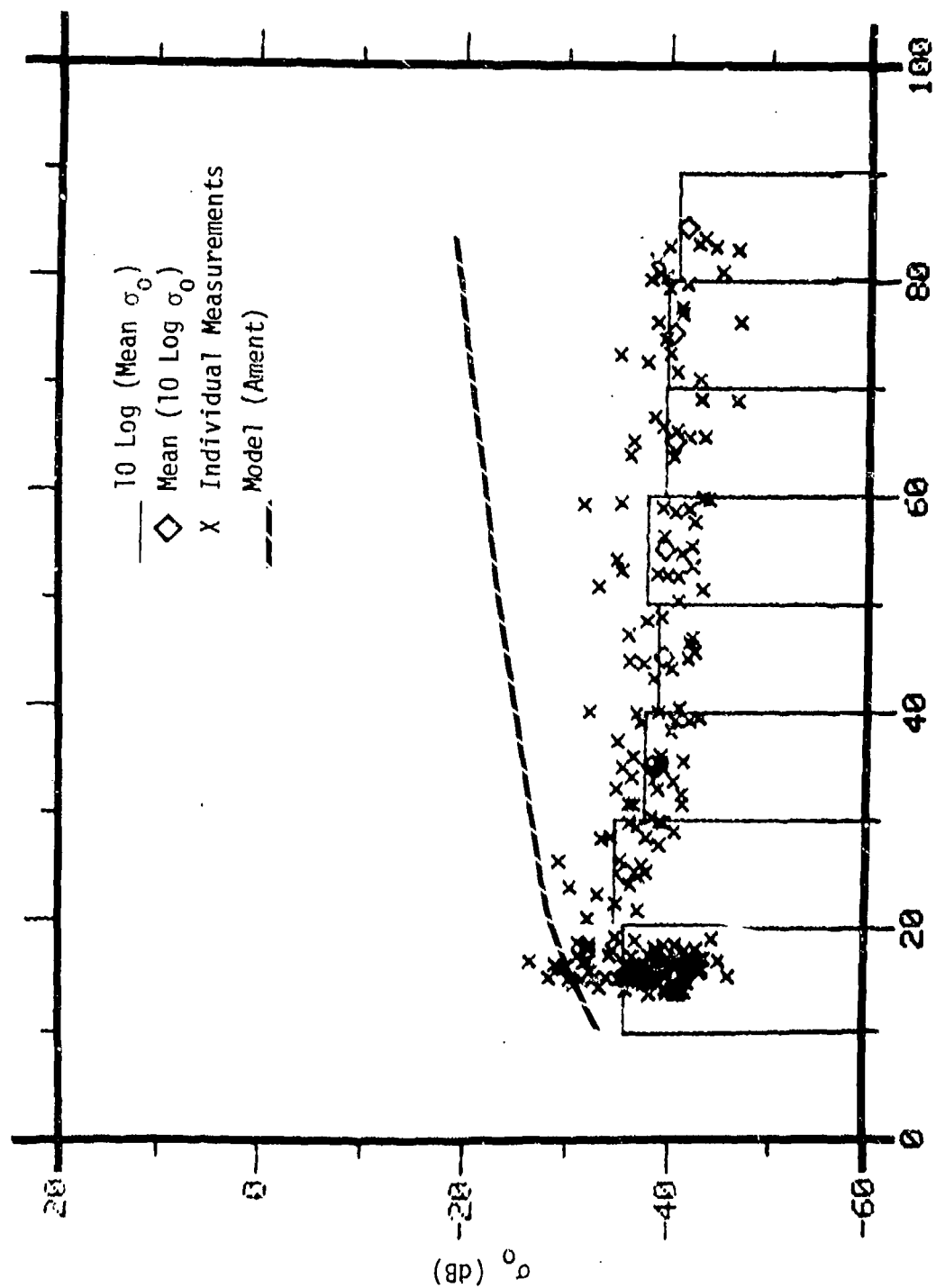
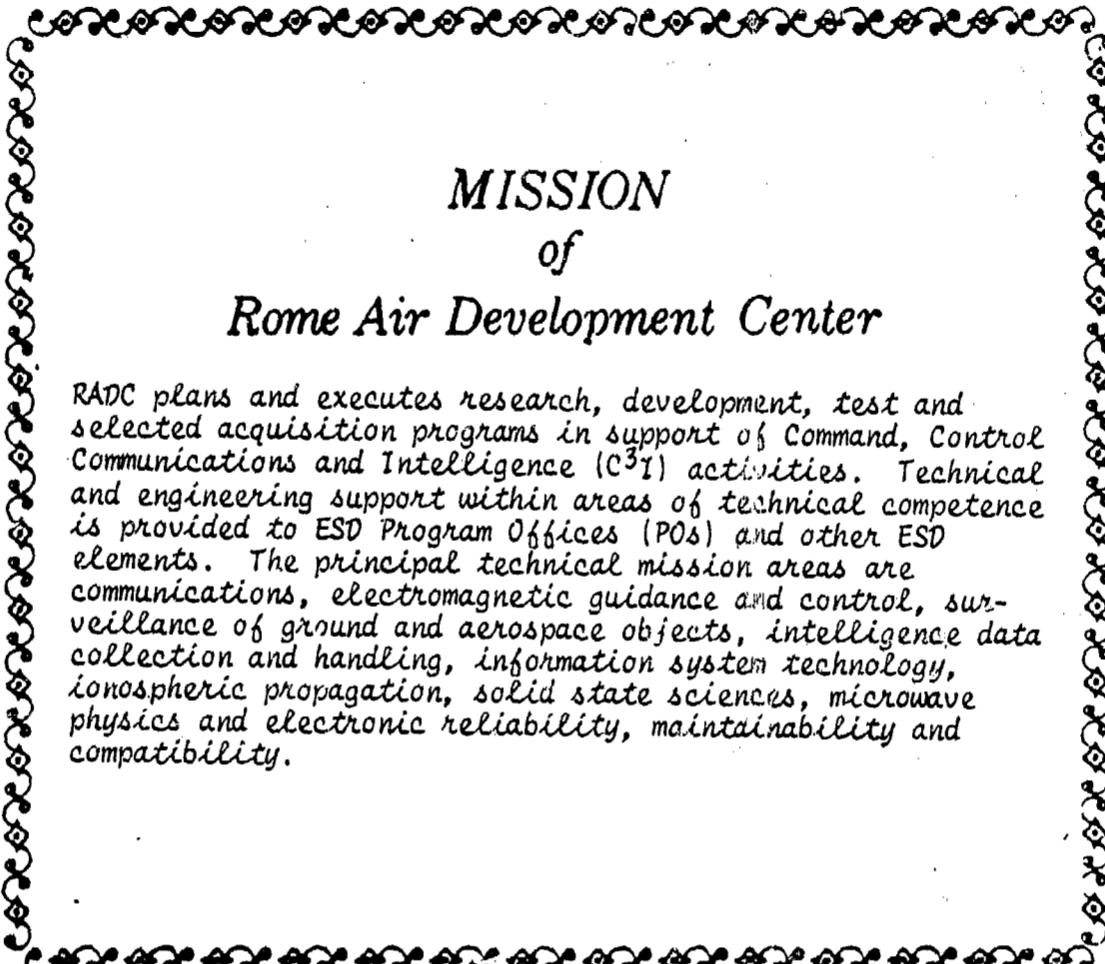


Figure B-6. L-Band Orthogonal Polarization (HV) Bistatic σ_0 Data of 18 March 1978 (Passes 3 and 10, $\theta_S = 80^\circ$, $\theta_S = 70^\circ$) for Wooded Terrain



MISSION
of
Rome Air Development Center

RADC plans and executes research, development, test and selected acquisition programs in support of Command, Control Communications and Intelligence (C³I) activities. Technical and engineering support within areas of technical competence is provided to ESD Program Offices (POs) and other ESD elements. The principal technical mission areas are communications, electromagnetic guidance and control, surveillance of ground and aerospace objects, intelligence data collection and handling, information system technology, ionospheric propagation, solid state sciences, microwave physics and electronic reliability, maintainability and compatibility.